New Approaches to Thermodynamics-based Predictive Modelling of Gas Chromatography and
Comprehensive Two-dimensional Gas Chromatography

by

Keisean Ackeim Jamaro Michael Stevenson

A thesis submitted in partial fulfillment of the requirements for the degree of

Doctor of Philosophy

Department of Chemistry
University of Alberta

Abstract

Thermodynamics-based predictive models of retention in gas chromatography and comprehensive two-dimensional gas chromatography have been demonstrated to provide high prediction accuracy across a wide range of separation conditions. They generally predict better than retention index-based models and can be more readily applied to comprehensive two-dimensional gas chromatography. However, no large or readily accessible databases of these parameters exist yet. The parameters generated from thermodynamic models are also suitable for use in creating Quantitative Structure-Retention Relationship models. Despite these benefits, thermodynamic parameters obtained using a column of a particular geometry and housed in a given instrument often lead to poor predictions of separation on another column of the same phase chemistry but differing in geometry and the system in which it is installed. As a result of this, the act of creating a database of thermodynamic parameters that can be used by experimenters to reliably model retention on their specific systems has been hindered. This thesis is aimed at investigating new and innovative approaches to improve the predictive capabilities (speed, accuracy and reliability) of thermodynamic models for predicting retention in gas chromatography and comprehensive two-dimensional gas chromatography (particularly across systems and column geometries). This is carried out by the design of a novel Quasi-Newton based optimization algorithm for the estimation of thermodynamic and geometric parameters that allow accurate cross-column and cross-system retention time prediction and transfer. A less time-consuming experimental approach for acquiring and using these parameters accompanies the computational design. The initial stages of the creation of a database of parameters are also presented. Then, parameters obtained using the new algorithm are applied to an innovative method for accurately and quickly predicting peak widths across geometries and systems without

the need for additional experimentation. A new approach to estimating additional contributions to band broadening is also explored. Lastly, these thermodynamic parameters are used to calculate characteristic parameters by way of a distribution-centric approach to thermodynamic modelling. The mapping and predictive capabilities of the calculated characteristic parameters are then investigated through a series of thermally modulated comprehensive two-dimensional gas chromatography experiments on different combinations of stationary phase chemistries and geometries.

Preface

(Mandatory due to collaborative work)

Portions of Chapter 2 have been previously published in three articles in the Journal of Separation Science. The publications include:

1) "A simple, fast, and accurate thermodynamic-based approach for transfer and prediction of gas chromatography retention times between columns and instruments Part I: Estimation of reference column geometry and thermodynamic parameters", S. Hou, K.A.J.M. Stevenson, J.J. Harynuk, Volume 41 (2018), 2544-2552.

2) "A simple, fast, and accurate thermodynamic-based approach for transfer and prediction of gas chromatography retention times between columns and instruments Part II: Estimation of target column geometry", S. Hou, K.A.J.M. Stevenson, J.J. Harynuk, Volume 41 (2018), 2553-2558.

3) "A simple, fast, and accurate thermodynamic-based approach for transfer and prediction of gas chromatography retention times between columns and instruments Part III: Retention time prediction on target column", S. Hou, K.A.J.M. Stevenson, J.J. Harynuk, Volume 41 (2018), 2559-2564.

For each paper, I was responsible for planning, designing and executing all experiments. I was also responsible for processing, analysing and performing calculations on experimental data as well as interpreting the results of said calculations and experiments. I provided insight into chromatographic and thermodynamic theory that advised the equations used in creating the code and was responsible for various writing sections of the introduction, experimental, and results and discussion portions (especially portions related to chromatography and thermodynamics) of

each paper. I also proofread and edited sections written by S. Hou. S. Hou was responsible for deriving the equations associated with the optimization algorithm, carrying out higher-level mathematical calculations (e.g.matrix and vector calculus), writing and testing the code that performs the optimization and predictions, and performing calculations on data from experiments. He wrote various sections of the introduction, experimental, and results and discussion sections (especially portions related to the algorithm) and proofread portions written by me. J.J. Harynuk was the supervisory author and was involved with concept formation, manuscript composition and edits.

Dedication

To anyone with a struggle they've yet to win…

…Use that pride in our hearts

To lift us up to tomorrow

'Cause just to sit still

Would be a sin

-Queen Latifa. "I Know Where I've Been." Hairspray: Soundtrack to the Motion Picture.
By Marc Shaiman and Scott Wittman. 2007

Acknowledgements

A great number of people made an impact on this thesis, in one way or another. They contributed significantly to making this work and its completion possible, and for that, I am grateful.

To my supervisor, Dr. James Harynuk, thank you for the guidance, support, travel opportunities and mentorship you provided. Thank you, also, for being an understanding supervisor.

Thank you, Dr. Gabriel Hanna and Dr. Mark McDermott, for serving as my Supervisory Committee members and for your continued interest in my progress.

To my fellow Harynuk group members, past and present, thank you for creating an encouraging, entertaining, welcoming, and supportive work environment. Thanks for all your assistance, for teaching me, and for giving me a chance to teach you.

Thank you, to my undergraduate students - Rachel, Grace, Christian, Yanwen, Fahim and Caleb. Without your time and talents, this work would not have progressed as quickly as it did. Thank you for presenting me with opportunities to be a teacher and mentor.

To my collaborators, Dr. Siyuan Hou and Dr. Leonid Blumberg, thank you for the lessons taught and the honour of working alongside such exceptional minds.

To the technical, administrative and support staff of the Department of Chemistry, thank you for your warm and friendly brand of professionalism, and for your skills and services that helped make this work possible.

To Jason Murray and Rebecca Ponting, thank you for guiding me to the tools I needed to succeed, that no lab or classroom could supply. Thank you both for your ability to strengthen and equip others.

To Paulina, thank you for listening, having faith in me, and your ability to maintain and share a bright, positive and hopeful outlook.

To Seo Lin, thank you for your sense of humour and for being able to induce laughter and raise spirits with just a look or a few words.

To Robin, thank you for your knowledge and insight, and for your ability to manage somehow to say so much yet listen so well.

To Michael, thank you for your kindness and thoughtfulness, and for being able to perceive and respond to the needs of others.

To Lawrence, thank you for your honest and giving nature, and your ability to be fair and critical without being cruel.

Juan and Carson, thank you for friendship, laughter, listening ears, chauffeuring hands and for being great roommates and friends. Thanks for creating a home to which I am happy to return at the day's end.

Bryan, thank you for coffee, clever conversation and confidence in my ability to succeed. Thank you for being so caring.

Joel, thank you for being an all-round good friend, for Game of Thrones and for Mr. Robot. Thank you for your ability to be cheerful, understanding and available.

To Mom (Celia), for raising me to be an independent, considerate, kind and resourceful man, thank you. Thank you for being caring, encouraging and supportive, and for being my biggest fan. Thank you for teaching me that although life doesn't make us guarantees or promises, things can and often do work in our favour. For believing in me and for a mother's love, thank you.

Nicholas, thank you for patience, reassurance, precociousness and for never doubting that I was capable of getting through this. For being a listening ear, and a source of joy, strength, comfort and peace amidst the chaos, thank you. Thank you for your ability to carry as Mercy, even after she is nerfed.

I am sure I've left out some names but to everyone who has helped in making this possible, I say "Thank you."

Thank you all.

Table of Contents

List of Tables

List of Figures

List of Abbreviations

FID   -   Flame ionization detector

GC   -   Gas chromatography

GC×GC   -   Comprehensive two-dimensional gas chromatography

NIST   -   National Institute of Standards and Technology

PAH   -   Polyaromatic hydrocarbon/polycyclic aromatic hydrocarbon

QSRR   -   Quantitative Structure Retention Relationship

SSE   -   Sum of squared errors of prediction

List of Symbols

$^1T_{e,theo}$	-	Theoretical primary elution temperature
^1t_M	-	Primary void time
^1t_R	-	Primary retention time
$^1\beta$	-	Primary column phase ratio
^2t_M	-	Secondary void time
^2t_R	-	Secondary retention time
$^2t_{Rtheo}$	-	Theoretical secondary retention times
$^2\beta$	-	Secondary column phase ratio
c_M	-	Concentration of solute in the mobile phase
c_S	-	Concentration of solute in the stationary phase
d_c	-	Column inner diameter
d_f	-	Stationary phase film thickness
D_G	-	Diffusion coefficient in the mobile phase
D_L	-	Diffusion coefficient in the stationary phase
H	-	Height equivalent to a theoretical plate / Plate height
K	-	Partition coefficient
k	-	Retention factor

L -   Column length

M_R -   Modulation ratio

N -   Efficiency

P -   Ratio of inlet pressure to outlet pressure

$P_i \, or \, P_{in}$ -   Inlet pressure

P_M -   Modulation period

$P_o \, or \, P_{out}$ -   Outlet pressure

P_x -   Pressure at point x

R -   Gas constant

r_c -   Column inner radius

R_S -   Resolution

T -   Absolute temperature

T_0 -   Reference temperature

T_{char} -   Characteristic temperature

T_e -   Elution temperature

t_M -   Void time

t_R -   Retention time

T_{ref} -   Reference temperature (T-centric model)

T_{Ref} -   Reference temperature (K-centric model)

t_S	-	Time solute spends in stationary phase / Adjusted retention time (t_R')
$^t t_M$	-	Transfer line void time
u	-	Carrier gas velocity
u_x	-	Velocity at point x
w_b	-	Width at baseline
w_h	-	Width at half-height
x	-	Position along the column
α	-	Selectivity factor / separation factor
β	-	Column phase ratio
ΔC_p	-	Change in heat capacity at constant pressure of phase transition
ΔG	-	Change in Gibbs energy
ΔH	-	Change in enthalpy of phase transition
ΔS	-	Change in entropy of phase transition
η	-	Carrier gas viscosity
θ	-	Thermal constant of analyte-column interaction
θ_{char}	-	Characteristic thermal constant
σ^2	-	Peak variance
$\sigma_{c,L}{}^2$	-	Peak variance in space (distance units)

$\sigma_{c,t}^{2}$ -   Peak variance in time

σ_{extra}^{2} -   Variance cause by extra-column band broadening

σ_{t}^{2} -   Total peak variance

$\varPhi$ -   Column coating efficiency

Chapter 1: Introduction

1.1 Chromatography

The responsibility of the analytical chemist may be loosely described as taking Sample X then, through some chemical and/or physical process, determining whether chemical Species Y is/are present and (often), if present, in what quantities. Carrying out this responsibility typically comes with several challenges; common among these is overcoming the fact that many samples are mixtures consisting of a few to thousands (or more) of chemical species. Therefore, the task of identifying then quantifying Species Y in Sample X evolves into the more complex task of efficiently separating Species Y from the rest of Sample X in order to confirm its presence (or absence) and determine its abundance.

Fortunately, the field of separation science offers many processes/techniques for performing this task on a wide range of samples containing even wider ranges of chemical entities. Chromatography is the most commonly used and powerful approach to separating mixtures of chemical compounds. Since Russian-Italian botanist Mikhail Tsvet first used the technique in the early 1900s to separate chlorophylls and carotenoids [1], chromatography has grown to encompass a variety of techniques. Today, common chromatographic techniques include (but are certainly not limited to) gas, liquid, thin-layer and supercritical fluid chromatography, and is an $8.02B market [2]. The choice of chromatographic process depends largely on the nature of the sample and the properties of the species of interest while also depending on the specific social, economical and scientific motives and restrictions surrounding the analytical problem being addressed [3]. The chromatographic process involves the partitioning of analytes between two phases, one of which

is flowing while the other is stationary. The separation arises due to differences in the partitioning between the two phases exhibited by different analytes. The work presented in this thesis is centered specifically around gas chromatography (GC) so this technique will form the entirety of the remaining discussion.

1.2 Gas Chromatography

1.2.1 Overview

As mentioned above, chromatographic techniques rely on analytes partitioning between two phases. During a gas chromatography (GC) experiment, gaseous analytes travel in an inert carrier gas (e.g. He, H_2, N_2) along the length of a column that is packed or coated with a highly viscous liquid-like polymer. The analytes partition between the inert carrier gas (the mobile phase) and the polymer (the stationary phase) as they migrate along the length of the column under pressure and temperature conditions set by the experimenter. As they migrate, they are separated from each other on the basis of the chemical properties of the stationary phase and the analyte at the temperature(s) of the experiment. Analytes then elute from the column at different times (termed retention time, t_R) and are detected at the end of the column using a variety of detectors. Gas chromatography is very efficient and is an ideal technique for the separation and analysis of volatile and semi-volatile molecules, making it an extremely common analytical tool in academic, government and industry labs.

Archer John Porter Martin and Anthony T. James first presented gas chromatography in 1952 in a *Biochemical Journal* article describing their use of the technique for separating volatile fatty acids [4]. Detailed insight into the history of the technique spanning nearly fifty years of development has been well documented [5-7]. Nowadays, gas chromatography finds

implementation as a powerful separation tool across areas of energy (petroleum and its derivatives) [8], healthcare (pharmaceuticals, metabolites) [9], food, flavour and fragrance [10-12], natural products [13], environment [14], and forensic fields [15]. The capabilities of this technique for performing efficient separations can be better understood with a brief foray into the instrumentation and theories behind it.

1.2.2 Basic Instrumentation

At its most basic level, the gas chromatograph consists of a sample introduction site (inlet) that is connected to a carrier gas supply and is usually heated to initiate (or maintain) sample volatilization. The sample, once volatilized, is carried by the carrier gas from the inlet onto the chromatographic column, which is housed in an oven. In most modern day applications, this column is a very narrow (0.1 – 0.53 mm inner diameter, 0.4-0.8 mm outer diameter) fused-silica column coated externally with polyimide. Its length for use in a typical GC experiment is about 30 m but can range from ~15 to >100 m in some applications. The walls of the column are coated with the stationary phase polymer to form a film with thicknesses varying from about 0.08 to 5 μm. Stationary phases are designed to span a wide range of polarities and can be selective for (i.e. have a stronger affinity towards) molecules across a range of chemistries. Stationary phases used in my research include: the non-polar 5 % diphenyl 95 % dimethyl polysiloxane phase, the mid-polar phases trifluoropropylmethyl polysiloxane and 50 % diphenyl 50 % dimethyl polysiloxane-"like", and the polar polyethylene glycol phase. As the sample migrates along the length of the column, its components partition between the mobile phase and the stationary phase and are separated in accordance with their relative volatilities and/or their interactions with the stationary phase. The column outlet is connected to a detector, which responds to the presence of analytes as they elute from the column. Detectors vary in their

function and utility; the responses of some are selective for particular atoms or functional groups (e.g. nitrogen-phosphorus detectors - NPD) while others simply respond to the presence of nearly any (typically organic) molecules (e.g. flame ionization detectors - FID, mass spectrometers - MS). Some detectors such as MS and vacuum ultraviolet detectors (VUV) also provide structural information, which aids the analyst in inferring the identity of the detected species. The experimental work presented in this thesis employed the use of the FID – a mass sensitive, ubiquitous GC detector. This detector, although destructive and incapable of providing structural information for compound identification, is widely used because of its high sensitivity, wide dynamic range, robustness and ability to respond to nearly all carbon containing molecules. Briefly, molecules entering the FID are combusted in a H_2/air flame. Carbon moieties of molecules generate ions and electrons then the latter are collected by a collector electrode resulting in an electronic signal [16]. More in-depth descriptions of each of these components, including details about their inner workings and/or design, may be found in many textbooks such as *Modern Practice of Gas Chromatography* by R.L. Grob and E.F. Barry [16].

1.2.3 Basic theory

The two main theories used to describe the chromatographic process are Rate Theory and Plate Theory – both valid and useful for different reasons. Before their details and their importance to the modelling of GC separations can be discussed, it is important to understand some more fundamental concepts in partition chromatography.

1.2.3.1 Overview of chromatographic nomenclature

The chromatographic process in which analytes partition between the mobile and stationary phase in a column can be viewed as an equilibrium processes in which an analyte, Y is distributed between the two phases according to its equilibrium constant, K.

$$Y_{(mobile\ phase)} \leftrightharpoons Y_{(stationary\ phase)}$$
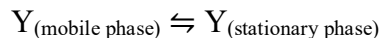
The equilibrium constant, K for this processes can be described relatively simply as the ratio of the concentration of Y in the stationary phase (c_S) to its concentration in the mobile phase (c_M).

$$K = \frac{c_S}{c_M} \tag{1-1}$$

This value, for a given analyte, governs the outcome of the separation. In practice we do not usually measure K because doing so is not convenient and is rarely necessary. Generally speaking, for a given set of conditions, a molecule with a larger K will elute from the column later than a molecule with a smaller K. Therefore, we instead measure the retention time of the analyte, t_R, which is the time it takes for the analyte to travel through the entire length of the column from introduction (injection) to detection. The analyte travels along the length of the column, when partitioned into the mobile phase, at the speed of the mobile phase. However, because it experiences retention in the stationary phase, its retention time, t_R, is the sum of the time it spends in both phases. We can therefore describe it as:

$$t_R = t_S + t_M \tag{1-2}$$

Here, t_S and t_M are the times spent in the stationary and mobile phases respectively. Given that it is more practical to measure retention times, we can define another parameter that is proportional

to the equilibrium constant, also called the partition coefficient, K, and can be expressed as a function of time. This parameter is the retention factor, k (older references might call it the capacity factor, k'), and it is the ratio of the time a compound spends in the stationary phase to the time it spends in the mobile phase.

$$k = \frac{t_S}{t_M} = \frac{t_R - t_M}{t_M} \qquad (1\text{-}3)$$

Recall that migration along the length of the column (longitudinally) can only occur in the mobile phase, so t_M is also the time it takes for the mobile phase (or an unretained analyte contained in it) to travel the length of the column. This time, t_M, is commonly referred to as the column void time or dead time. The average linear velocity of the mobile phase, u, can therefore be defined as:

$$u = \frac{L}{t_M} \qquad (1\text{-}4)$$

where L is the length of the column. This velocity has units of distance per unit time and has an impact on the retention time of analytes undergoing chromatography. The speed of the mobile phase through the column can also be described in units of volume per unit time and is termed the flow rate, F.

As mentioned previously, each capillary column has a certain inner diameter, d_c and the stationary phase is coated along its interior walls to a certain thickness, d_f. These two factors can be used to describe the ratio of volume of the mobile phase to the stationary phase, the phase ratio, β. It is commonly approximated by:

$$\beta = \frac{d_c}{4d_f} \qquad (1\text{-}5)$$

This phase ratio plays a role in governing the retention time of an analyte and this role can be seen through its relation to K.

$$K = k\beta \qquad (1\text{-}6)$$

The aim of chromatography is to separate the analyte(s) of interest from other components of a sample. It is therefore useful to define a term that can reflect this separation between pairs of compounds. The selectivity factor (or separation factor), α, describes the relative retention of a pair of compounds (A and B), where A elutes before B (i.e. $t_{R,A} \leq t_{R,B}$; $\alpha \geq 1$).

$$\alpha = \frac{k_B}{k_A} = \frac{t_{R,B}}{t_{R,A}} \qquad (1\text{-}7)$$

1.2.3.2 Plate Theory

A chromatographic column may be treated (in a mathematical sense) as being analogous to a distillation column consisting of discreet plates/layers (these plates, although discreet, touch each other). Martin and Synge in 1941, termed these plates "theoretical plates" [17]. Migration of an analyte along the length of a column can be visualised as the transfer of analyte, equilibrated in the mobile phase, from one successive plate to another. The more plates there are in a given length of column the more efficient the separation will be; this means that for two columns of equal length, the column with the higher number of plates (therefore smaller plates) will be more efficient. The equation describing this is:

$$N = \frac{L}{H} \qquad (1\text{-}8)$$

N is the number of theoretical plates (or efficiency), L is the column length and H is the height equivalent to a theoretical plate (or plate height).

While migrating, the analyte is subject to diffusion, which results in a broadening of the analyte in space. This diffusion causes band broadening and results in analyte molecules acquiring a Gaussian distribution (seen as a Gaussian-shaped peak upon detection). The plate height, H can be described in terms of this variance as the length of column, x, that contains a fraction of analyte that lies between L (the column length) and $L - \sigma$ [18].

$$H = \frac{\sigma^2}{x} \tag{1-9}$$

What is most important to take from this is that plate theory provides a way for us to explain the Gaussian shape of chromatographic peaks and their band broadening that is crucial in allowing their peak widths to be modelled (as I illustrate in Chapter 3 of this thesis). The width of a chromatographic peak at its base, w_b, is based on the distance between the two points where tangents to the peak at its inflection points cross the baseline. In terms of variance, σ^2, this is given by:

$$\sigma^2 = \frac{w_b}{4} \tag{1-10}$$

Combining Equations (1-8), (1-9) and (1-10) gives equation (1-11) below for a peak eluting from a column (i.e. when $x = L$) [19]:

$$N = \frac{16L^2}{w_b^2} \tag{1-11}$$

which, in units of time, corresponds to:

$$N = \frac{16t_R^2}{w_b^2} = \frac{t_R^2}{\sigma^2} \tag{1-12}$$

Plate theory, on its own, does not factor in the kinetics of mass transfer. It provides a way of explaining the observed band broadening but does not describe the mechanics of it very well;

such a description is fundamental for modelling GC separations (particularly peak widths). This is where the Rate Theory, which borrows nomenclature from the Plate Theory, comes in.

1.2.3.3 Rate Theory

As mentioned earlier, chromatographic bands broaden and become Gaussian in shape because of diffusion. The rate theory describes this behaviour in terms of the rates of mass transfer between phases, rates of diffusion along the column and carrier gas flow rates (and fluid dynamics) [16].

An analyte band migrating in a chromatographic column can broaden as a result of: 1) the multiple random pathways its molecules take to travel the length of the column, 2) longitudinal diffusion in the mobile phase and 3) resistance to mass-transfer in the mobile and stationary phases (radial diffusion). Contribution 1) will not be discussed further here as it applies to packed columns and all experiments done in this thesis were carried out using wall-coated open-tubular columns (as is common for most modern GC analyses). Lacking packing, there is only one path for analytes to follow, and thus the multiple pathway effect does not apply. The extent of the contribution of longitudinal band broadening to the shape of a peak depends primarily on its diffusion coefficient in the mobile phase, D_G, and the time, t, it spends in that phase.

$$\sigma^2 = 2D_G t \qquad (1\text{-}13)$$

If an analyte migrates a distance, x, in a column at a rate of u_x distance per unit time, then the time it spends in the column, t is given by x/u_x. Thus, according to equation (1-13)

$$\sigma^2 = \left(\frac{2D_G}{u_x}\right)x \qquad (1\text{-}14)$$

Combining equations (1-9) and (1-14) we see that for a given distance of column, x,

$$H = \frac{2D_G}{u_x} \qquad (1\text{-}15)$$

Equation (1-15) summarises the contribution of longitudinal diffusion to plate height and band broadening. It is not the only contributor to plate height; we can call $2D_G$ in equation (1-15), B – the contribution caused by longitudinal diffusion.

In order to partition between phases, the molecules of an analyte must travel radially (towards the walls of the column) through the mobile phase and into the stationary phase. Then, diffuse radially away from the column walls out of the stationary phase and into the mobile phase so they can proceed down the column. The resistance to this process contributes to band broadening and depends on the retention factor of the analyte, its diffusion coefficient in both phases and the geometric properties of the column d_c and d_f, introduced earlier. These terms are well defined for open-tubular GC. In the mobile phase, the mass transfer term, C_M is

$$C_M = \frac{11k^2 + 6k + 1}{96(1+k)^2} \frac{d_c^2}{D_G} \qquad (1\text{-}16)$$

and the stationary phase mass transfer term C_S is

$$C_S = \frac{2k}{3(1+k)^2} \frac{d_f^2}{D_S} \qquad (1\text{-}17)$$

Both of these contributions increase with faster carrier gas rates. Combining all contributions together and summing over the length of a column we get:

$$H = \frac{B}{u} + C_M u + C_S u \qquad (1\text{-}18)$$

Equation 1-18, a modified version of the van Deemter equation [19,20], provides a kinetic and mechanistic description of band broadening and is central to the rate theory and the modelling of peak width employed in this work.

1.2.3.4 Resolution

Recall that the aim of chromatography is efficient separation of analytes molecules from the rest of the sample (matrix). Earlier, the selectivity factor, α, efficiency, N, and retention factor, k, were introduced. These three terms connect through a term called resolution, R_S, which is a measure of a column's overall ability to permit good separation (well-spaced, clearly distinguishable peaks) between two neighbouring analytes. Optimizing this parameter is very important when building a GC method, making it one of the reasons behind the addition of peak width prediction to the models shown in this thesis. For two adjacent peaks to be considered baseline resolved, the resolution between them R_S should be at least 1.5 (greater R_S means greater resolution). Once again, considering two adjacent peaks A and B, the resolution between them can be calculated using

$$R_S = 2\frac{t_{R,B}-t_{R,A}}{w_{b,B}+w_{b,A}}$$
(1-19)

When analytes A and B have very similar partition coefficients, the equation used to optimize the resolution between them (by choosing a column with sufficient properties to enable their separation) is

$$R_S = \frac{\sqrt{N}}{4}\frac{k_B}{1+k_B}\frac{\alpha-1}{\alpha}$$
(1-20)

Rearrangement of equation (1-20) allows the calculation of the column efficiency, N, needed to achieve a desired resolution. Equations (1-8) and (1-5) to (1-20) show that reducing H increases N and that H (and/or N) can be improved by the manipulation of column properties such as inner diameter, length and film thickness, as well as carrier gas flow rates (or linear velocities). The choice of carrier gas (properties such as viscosity and molecular size), although not discussed here since all experiments in this work were done using helium, is also crucial to manipulating H as this also affects the diffusion coefficients of analytes. However, it is not quite common in practice (outside of fundamental research) to switch carrier gases in an attempt to improve efficiency. Regardless, method translation tools exist to allow switches to be performed with relative ease (with regards to method development, not the physical logistics associated with changing gases).

These terms and theories described above are brief descriptions of the foundational concepts that govern and guide GC separation, including the experiments carried out in this thesis. Together they allow the design of methods for separating thousands of analytes in a variety of samples using this technique. When coupled with a detection method that provides structural information such as MS, a new dimension of separating power is added to the technique. Some samples, however, possess such great molecular complexity that even with detectors such as MS and VUV, their analytes often require an additional separation mechanism to permit confident identification and quantification.

1.3 Multidimensional Gas Chromatography

1.3.1 Overview

Mulitidimensional gas chromatography, as the name suggests, involves subjecting a sample (or portion of a sample) to GC separation by at least two different chromatographic phases. It usually takes one of two approaches. In one approach, called heart-cutting, a portion of the sample is sent to a secondary column upon eluting from the primary (first) GC column. Both columns separate by different mechanisms. This approach, is normally represented as GC-GC or 2D-GC, in writing. No heart-cutting is carried out in this work so it is not discussed further here. J.V. Seeley discusses it in moderate but insightful detail in a review article in *Journal of Chromatography A* [21]. The other approach is comprehensive two-dimensional gas chromatography, denoted as GC×GC [22]. This technique features heavily in Chapter 4 of this work.

Recently demonstrated, but not in common usage is comprehensive three-dimensional gas chromatography [23,24].

1.3.2 Comprehensive two-dimensional gas chromatography, GC×GC

The technique, GC×GC, is relatively young as it was not until 1991 that the first GC×GC separation was demonstrated, by Liu and Phillips [25]. Much of the theory surrounding its development, although older than its first demonstration, is also quite young – pioneered primarily by Giddings through his publications on concepts in multidimensional separations in 1984, 1987 and 1995 [26-28]. In one of his works he set out the criteria required for a multidimensional separation technique to be considered comprehensive. Two very important

criteria must be met; they are as follows. 1) The entire sample (or a representative fraction thereof) must be subjected to two or more separation techniques each of which varies in separation mechanism/selectivity. 2) Separation from a given dimension must be maintained in subsequent dimensions (i.e. no recombination of already separated analytes should occur) [27]. The second criterion means that the sampling rate and separation speed of a given dimension must be sufficiently fast to maintain the separation profile obtained on previous dimensions.

The instrumentation required to perform GC×GC separations, at its most basic level, is not vastly different from that required to perform a one-dimensional GC separation with regards to major components. GC×GC calls for a second column, a device for introducing effluent from the primary column to the secondary column in a manner that ensures criterion number 2) above is met, and a detector with a fast enough sampling rate to generate well-defined peaks (which are typically much narrower in GC×GC than in GC) [29]. It is not uncommon to also include a secondary oven that houses the secondary column at some temperature offset above the primary oven to allow the chromatographer more control over retention on that column.

The device that enables criterion number 2) to be met is the modulator. It has two jobs to perform: it needs to trap/sample the effluent from the primary column, and then at regular time intervals, introduce/inject the trapped effluent into the secondary column as a narrow band. For reasons discussed briefly in Chapter 3, the time intervals are normally set such that 3-5 portions/slices of each peak leaving the first column are sampled and introduced [30,31]. Also important to meeting criterion 2) is that the second dimension separation be completed before the modulator introduces a subsequent sample. Usually this is achieved by using very short second dimension columns (0.3 to 5 m, depending on the type of modulation used) and/or very fast carrier gas flow rates in the second-dimension (up to 20 mL min^{-1}). The result of this is

separations on the order of about 1 to 5 s. The introduction of the analytes to column 2 as a narrow band, coupled with the very fast separation speed, results in very narrow but tall peaks which in turn requires fast detectors. These design elements, however, do not completely eliminate cases of wrap-around, the phenomenon that occurs when an analyte does not elute from the secondary column by the end of one modulation period.

Modulation can be performed in a number of ways including thermal modulation and pneumatic (flow) modulation. The latter, although increasing in usage throughout academia and industry is not as widely employed and was not used for the work presented in this thesis. I encourage the interested reader to consult the referenced articles which describe the design, development and application of this approach to modulation [21,32-35].

Thermal modulators, like the one used in Chapter 4, collect and introduce analytes using a mechanism that induces a change in temperature, and therefore retention, of the analyte band. One commonly used and readily available type of thermal modulator on the market is the dual-stage modulator. With this modulator, modulation occurs on the first few cm of the second-dimension column using four jets. The process takes place in the following steps:

1) Primary column effluent is carried onto the first few centimeters of secondary column by carrier gas.

2) After a few centimeters the contents of the effluent are slowed down and trapped by the stage 1 cold jet (which blasts the column with a spray of cold gas, usually N_2 or air).

3) Soon after, the stage 1 hot jet sprays the same region of column with a blast of "hot" (modulator temperature, ~ 3-5 °C above primary oven) gas, releasing the trapped analyte.

4) A few centimeters farther along the column, the stage 2 cold jet traps the recently released band again, focusing it into a narrow zone and preventing it from combining with the previously modulated effluent (preventing break-through).

5) The stage 2 hot jet releases the trapped band to the remainder of the secondary column for separation.

An illustration of this process is available in a review article by P.Q. Tranchida and coworkers [36].

The advantages of thermal modulators include their ability to be operated at very short or very long modulation periods, the refocusing of bands (in the case of dual stage devices), and their ability to trap a wide range of analytes (systems that use $N_2(g)$ from pressurized liquid nitrogen dewars are excellent at trapping even very volatile analytes). The first advantage means that peaks having a wide range of widths can be well modulated while the second helps in preventing loss of first-dimension separation and enables higher sensitivity. The last of these advantages is a double-edged sword as many modulators require the usage (and therefore continued purchase) of large quantities of coolants (such as liquid nitrogen), some however are designed to be consumable free and can use air but must compromise on the ability to trap very volatile species. The presence of three heated zones (primary oven, secondary oven and modulator) along with the fact that modulation takes place on the secondary column makes the modelling of systems like these challenging. This often results in simplification of the process to enable modelling [37]. Dual-stage thermal modulation is used exclusively for the work shown in Chapter 4.

As a result of the way in which data from a GC×GC experiment is acquired, the first dimension retention time is quantized to the modulation period. This is because the effluent of the primary column is not detected. Instead, what is detected are the slices of said eluent as they elute from

the second-dimension. The modulator is connected to the data collection system (a computer) and what is recorded (apart from the signal from the peaks leaving the second-dimension) is the beginning of each modulation period. The result is a one-dimensional chromatogram containing modulated peaks which is folded to create a two-dimensional contour plot. The primary retention time of the contour peak is the nearest multiple of the modulation period of the base peak (the largest "slice" of a modulated primary column effluent peak). This adds another layer of challenges when modelling GC×GC separations and the effect of this challenge is discussed further in Chapter 4. A description of the data handling is well described and illustrated in Chapter 4 of an online Comprehensive Analytical Chemistry handbook on GC×GC, consisting of a collection review articles, edited by L. Ramos [38].

Overall, GC×GC, by adding another separation dimension increases the peak capacity of the separation space and allows the analysis of complex samples containing analytes which would have otherwise coeluted under one-dimension GC conditions. This added separation power, however, results in a system in which the optimization of parameters becomes a complicated endeavour as altering one parameter often causes changes (for better or worse) in two or more other parameters [39]. This makes it even more important to develop an accurate, fast and reliable computational means of simulating GC×GC separations thereby easing the challenges associated with method development and optimization for new and/or complex samples.

1.4 Predictive Modelling of Retention in GC and GC×GC

1.4.1 Overview

The processes of developing and optimizing GC and GC×GC methods are necessary but often complicated tasks, especially for newer or uncommon types of samples. For targeted analyses,

the challenge comes with devising a method that effectively separates your analyte(s) of interest from the rest of the sample matrix. For untargeted exploratory analyses (analyses in which a large profile of the molecular components of the sample is required or it is not yet known which analytes are relevant for addressing a particular research question), the challenge comes from creating a method that permits as complete a separation of as many species as possible. Typically, chromatographers make an educated guess (based on an understanding of the terms and equations discussed in section 1.2.3) at which columns and instrumental conditions would achieve their desired separation. Following this, through trial and error, they adjust conditions and perform separations until the results are satisfactory. The time required for this process can take anywhere from a few hours to weeks depending on the complexity of the sample and the chromatographer's experience. Therefore, a tool that permits the rapid, accurate and reliable prediction of retention times and peak widths of compounds would be an invaluable asset for speeding up method development and optimization in GC and GC×GC. This is where predictive modelling of separations comes in.

Predictive models take a variety of forms but at their core, they all involve relating some physical property of analytes to some indicator of retention such as retention indices or retention times. These models may be based on relatively simple properties such as boiling point, as within a given homologous series, on very non-polar stationary phases, elution order is largely dictated by boiling point [40-44]. Other predictive models are built on somewhat more descriptive properties such as relative retention (retention indices) [45-49], entropy and enthalpy changes (thermodynamic parameters) [37,50-64], or molecular descriptors of structure and interaction (quantitative-structure retention relationships, QSRR) [65-69] or some combination thereof.

Retention indices are commonly used because the data required to calculate them is easy to generate, their calculation is simple to implement and databases containing them are relatively large and easy to access (e.g. NIST [70]). They can allow the experimenter to roughly estimate elution order and tentatively identify an unknown analyte peak. They do not, however, readily lend themselves to accurate predictive modelling of GC and less so for GC×GC. Their values depend on the experimental conditions under which the data used in their determination was obtained, making them unreliable for producing accurate predictions on other systems or under other conditions. Additionally, the acquisition of retention indices on the second dimension column requires the creation of isovolatility curves through a series of technically challenging experiments [71].

QSRR models have been used extensively throughout the literature with varying degrees of success. A recent review on these approaches by R. Amos and coworkers covers their use across several areas of chromatography [72]. Essentially, these models work by using molecular descriptors of various physicochemical and structural properties of compounds and correlating them with different retention properties (such as retention indices and retention times) or with other parameters related to retention (e.g. thermodynamic parameters). They have the advantage of requiring little or no experimentation to generate, as usually all that is required is an optimized structure of the molecules in question to generate descriptors, and some database (usually already existing) of the parameters to which one wishes to relate those descriptors. Usually the challenges associated with QSRR methods surround the quality of the data used to build them as well as the selection of the most appropriate features for correlation to retention through some variable selection algorithm. QSRR models are, however, a powerful complement to and

enhancement of, the predictive capabilities of other models. The work in this thesis is centred around thermodynamic based models so these will be discussed here in greater detail.

1.4.2 Thermodynamics-based predictive modelling

A GC separation can be viewed through a thermodynamic lens by considering the entropic and enthalpic changes involved in the partitioning of the analyte between mobile and stationary phases. As shown in equation (1-1), this partitioning is an equilibrium process with equilibrium constant, K, the partition coefficient.

This equilibrium can be expressed in relation to changes in Gibbs energy associated with the partitioning process.

$$\Delta G = -RT \ln K = \Delta H - T\Delta S \tag{1-21}$$

Here ΔG is the change in Gibbs energy, R is the molar gas constant, and ΔH and ΔS are the changes in enthalphy and entropy, respectively, for a molecule partitioning between the mobile and stationary phases.

Rearrangement of this equation gives a two-parameter thermodynamic model relating an analyte's K to its temperature.

$$\ln K = \frac{\Delta S}{T} - \frac{\Delta H}{RT} \tag{1-22}$$

This equation, however, assumes that ΔH and ΔS are not temperature dependent, which is not the case over the temperature ranges typically covered in GC experiments. This means that while this model may be descriptive, thermodynamic parameters derived using it do not predict retention very well [73]. However, Clarke and Glew [74] laid the ground work for a three-parameter

model which takes into account the temperature dependence of thermodynamic parameters and also incorporates changes in heat capacity at constant pressure, ΔC_p, as molecules partition between mobile and stationary phases.

$$ln\,K = A + \frac{B}{T} + C\,ln\,T \tag{1-23}$$

where

$$A = \frac{\Delta S(T_0) - \Delta C_p(1 + ln\,T_0)}{R} \tag{1-24}$$

$$B = -\frac{\Delta H(T_0) - \Delta C_p T_0}{R} \tag{1-25}$$

$$C = \frac{\Delta C_p}{R} \tag{1-26}$$

$\Delta S(T_0)$ and $\Delta H(T_0)$ are the entropy and enthalpy changes at a reference temperature, T_0. This model was adapted for GC in 1990 by Castells and coworkers [50] and has been the model of choice for thermodynamic prediction methods for several researchers [37,55,59,61,75-77].

This approach to predictive modelling has advantages over the use of retention indices as thermodynamic parameters depend on the stationary phase chemistry and the choice of carrier gas and do not shift greatly when changes in temperature or pneumatic conditions come into play. They also readily lend themselves to use in GC×GC modelling as thermodynamic parameters acquired from one-dimensional separations can be applied to GC×GC predictions [58]. These parameters can also be used for relating molecular properties of analytes to retention related parameters as is used in QSRR modelling. The acquisition of thermodynamic parameters is experimentally more demanding than that of retention indices but strides have been made recently to improve the speed and ease of the process, some of which are discussed in Chapter 2

of this thesis. The lack of a large and readily accessible database of thermodynamic parameters is also a hindrance to their usage. Despite these challenges, the predictive accuracy provided by thermodynamics-based models is worth the investment in research time and effort.

1.5 Thesis overview

This thesis is a presentation and discussion of work carried out towards the enhancement of the predictive capabilities of thermodynamic retention models and the creation of innovative approaches to modelling GC and GC×GC separations. Chapter 2 describes the use of a new numerical optimization algorithm and experimental design for acquiring thermodynamic parameters which enable fast and accurate retention time predictions to be made across column geometries and GC systems (for a given stationary phase). It also highlights the first steps towards creating a library of thermodynamic parameters. The integration of peak width prediction capabilities into the methods described in Chapter 2 is discussed in Chapter 3 as well as a convenient and innovative way of accounting for additional band broadening contributions. Chapter 4 presents a new approach to mapping distribution and relative retention in GC×GC through the use of characteristic thermodynamic parameters obtained from distribution-centric models. It also describes the first steps towards a means of predicting retention times in GC×GC using these parameters. Each aspect of the work in this thesis is performed with the goal of moving towards a thermodynamics-based tool for optimizing GC and GC×GC method development.

Chapter 2: Fast and accurate transfer and prediction of GC retention times across column geometries and instruments[1]

2.1 Introduction

Analytical chemists often need to analyse mixtures that contain molecular species ranging from a few to a few thousand in number. Some mixtures, by virtue of their composition prove simple to separate and analyse; others, however, pose great challenges for even the experienced chromatographer. Complex samples can include petroleum, biofluid extracts, foods, fragrances, soil, freshwater, seawater, air, etc. and span a wide variety of sources and matrices. Fortunately, for samples of this nature, many of the analytes of interest they contain are small volatile molecules that lend themselves well to separation and analysis by GC.

Even when this is the case, developing and optimizing a GC method to separate such analyte(s) of interest from the rest of a sample matrix, is often a difficult and/or time-consuming endeavour of educated guesses and trial and error. Such an approach to selecting stationary phase chemistry, column geometry, carrier gas pneumatics, and oven conditions for a successful separation (whether the goal is speed, capacity and/or resolution) is inefficient and diverts bench time away from the actual analysis of samples. With this in mind, several researchers have worked on creating methods for predicting retention times in GC. These methods share the goal of reducing the amount of experimental work needed to optimize a separation but differ in the approach taken to accomplish this goal. Some make use of retention indices [78-82], others, such as

---

quantitative structure retention relationship models (QSRR), utilize structural molecular descriptors [65,69,83-98], while some rely on thermodynamic parameters [37,50-53,55,56,58,59,61-64,75-77,99-103]. A few of the aforementioned references rely on some combination of the three approaches.

Among the various approaches, thermodynamics-based predictive models have attracted a great deal of attention in recent years. This is largely due to their tendency to better account for changes in experimental conditions, particularly, temperature and temperature program rates, resulting in better accuracy compared to retention index based methods [58]. They are also better suited to modelling GC×GC separations compared to the isovolatility curve generation methods needed to use retention indices in the second dimension [58,71].

Despite these benefits, a few improvements to thermodynamics-based models were required to make them more viable for common use as method development and optimization tools. First, there was a need to demonstrate that thermodynamic parameters could be quickly transferred across GC systems and still give very accurate predictions without requiring a great deal of experimentation on the part of the user. That is to say that thermodynamic parameters could be acquired on a given GC instrument, using a given capillary column (henceforth called the reference system) and used to very accurately predict retention times on another column of the same stationary phase chemistry (but possibly different geometry) installed in a different GC instrument (the target system). Second, whereas retention index databases are plentiful there did not exist a database/library of thermodynamic parameters that users could access to make predictions. My work in this area was aimed at addressing these two challenges.

Our group previously carried out investigations into the first challenge. Dr. Teague McGinitie, then a doctoral student, worked on and published an approach to calibrating thermodynamic data

for predicting retention time in GC [76]. This work relied on measuring the length of columns either by direct measurement of an uncoiled column or by measuring the diameter of the column coils and counting the number of coils of the column on the column cage. The former is accurate but inconvenient and requires access to an undisturbed space that can accommodate the entire 30-100 m of column. The latter is less accurate and dependant on careful counting, accurate diameter measurement and quality column wrapping. Some manufacturers' columns, while well wrapped, do not readily submit themselves to ring counting or uncoiling. It was also necessary to determine the column inner diameter, d_c, as the nominal inner diameter (provided by the manufacturer) is not accurate enough for the purposes of thermodynamic parameter transfer. This was done, following the measurement of column length, by measuring the column dead time via manual injections of methane (as a dead time marker) and calculating the inner radius of the column, r, using Poiseuille fluid dynamics for compressible fluids[76].

$$r_c = \sqrt{\left(\frac{32\bar{u}\eta L}{3}\right) \times \frac{(P_i^3 - P_o^3)}{(P_i^2 - P_o^2)^2}} \qquad (2\text{-}1)$$

In the above equation, $\bar{u}$ is the carrier gas velocity calculated by dividing the length, L by the dead time measured at constant pressure using methane. η is the carrier gas viscosity at the oven temperature used for measurement and P_i and P_o are the inlet and outlet pressures, respectively. Although simple in principle, this approach requires that the column length be accurately known and requires precise replicate measurements of dead time, t_M (which, when determined via manual injection depends largely on the skill and experience of the experimenter and when done by autosampler requires an elaborate set-up). Other methods exist but are often detector-specific. Lastly, a Nelder-Mead Simplex optimization, *fminsearch* in MATLAB (MathWorks, Natick, MA)), was used to acquire thermodynamic parameters and the estimated film thickness of the

target column (from Grob Mix retention data) [59,76]. That work demonstrated that good prediction of retention time (average error of 1.6 s) on columns of the same stationary phase as the reference column but of different column geometry could be achieved [76]. However, those experiments were performed using a single instrument (i.e. the target column was installed in the same instrument as the reference column). When we tried to apply the same approach to data from an inter-laboratory trial aimed at validating the transferability of the methods between laboratories, we encountered some problems. The thermodynamic parameters determined in a given lab could be used to make accurate predictions in the same lab on the same system used to obtain the thermodynamic parameters (with errors < 2%). Unfortunately, when these parameters were used to make predictions on systems in other labs, unacceptably large prediction errors were encountered (up to 51%) [104]. Further investigations revealed that the *fminsearch* function was producing different estimates of thermodynamic parameters each time it started from a different initial guess. While it is not quite clear why this is the case, it has been reported in the literature that if the objective function curve with respect to the parameters being optimized is almost flat, the Nelder-Mead simplex algorithm may not find a true minimum [105,106].

This chapter presents the experimental details and findings of our investigations aimed at solving the problems mentioned above. It describes how changes made to the manner in which reference and target column geometries are determined, as well as a new numerical optimization algorithm based on the quasi-Newton method allowed us to accurately transfer thermodynamic parameters across systems for accurate retention time prediction. Also included in this chapter are the results of extensive preliminary work I (with the aid of three dedicated, hardworking volunteers) carried out over the course of two semesters, towards building a library of thermodynamic parameters. Currently thermodynamic parameters for ~115-180 compounds on four different stationary phase

chemistries have been calculated. These phases include the low polarity 5% diphenyl 95% polydimethylsiloxane phase, the mid polarity trifluoropropylmethyl polysiloxane and (50% phenyl)-methylpolysiloxane-like phases, and the high polarity polyethylene glycol phase.

The approach taken here is based on the three-parameter thermodynamic model which relates the partition coefficient of a molecule, K, at a given temperature, T, to three thermodynamic parameters [50,56,59]. Briefly, from chromatographic rate theory, an analyte travelling down a column in a carrier gas will strive to maintain equilibrium between the stationary phase and the mobile phase. The partition coefficient, K (the ratio of the concentration of the analyte in the stationary phase, c_S, to its concentration in the mobile phase, c_M), governs this equilibrium and by extension governs the separation. K can be expressed in terms of retention factor, k:

$$K = \beta k \tag{2-2}$$

where β is the phase ratio of the column (the ratio of mobile phase volume to stationary phase volume).

Furthermore, K, in terms of thermodynamic parameters is given by,

$$K = e^{A+\frac{B}{T}+C \ln T} \tag{2-3}$$

or more conveniently,

$$\ln K = A + \frac{B}{T} + C \ln T \tag{2-4}$$

where T is the absolute temperature and A, B, and C are three thermodynamics-based parameters described below.

$$A = \frac{\Delta S(T_0)-\Delta C_p(1+\ln T_0)}{R} \tag{2-5}$$

$$B = -\frac{\Delta H(T_0)-\Delta C_p T_0}{R} \tag{2-6}$$

$$C = \frac{\Delta C_p}{R} \tag{2-7}$$

$\Delta S(T_0)$ and $\Delta H(T_0)$ are the entropy and enthalpy changes associated with a molecule moving from the mobile phase to the stationary phase at some reference temperature, T_0. ΔC_p is the change in heat capacity at constant pressure, and R is the gas constant.

While K governs the partitioning of an analyte between the stationary and mobile phases of a column, the analyte's movement down the column while in the mobile phase is governed by fluid dynamics as described by Poiseuille's equation for the flow of a compressible fluid. From this equation, the velocity of the mobile phase at some point x, along a column can be obtained by,

$$u_x = \frac{d_c^2}{32} \frac{P_{in}^2 - P_{out}^2}{2\eta L} \frac{1}{\sqrt{\left(P_{in}^2 - \left(\frac{x}{L}\right)\left(P_{in}^2 - P_{out}^2\right)\right)}} \tag{2-8}$$

d_c is the column inner diameter while P_{in} and P_{out} are the inlet and outlet pressures, respectively. L is the column length, and x is the position along the column length under consideration (usually the analyte position). η is the viscosity of the mobile phase in poise (g cm^{-1} s^{-1}) which, as a function of temperature, for helium, is given by equation (2-9) [107].

$$\eta = 3.923 \times 10^{-5} + 5.954 \times 10^{-7}T - 2.151 \times 10^{-10}\, T^2 \tag{2-9}$$

By considering, both retention in the stationary phase and movement in the mobile phase, the distance, Δx, an analyte travels down a capillary column in a time increment, Δt can be modelled as,

$$\Delta x = u_x \frac{1}{1+k} \Delta t \tag{2-10}$$

Equations (2-2), (2-3) and (2-8) can be substituted into (2-10). Doing so (along with some rearrangement) yields equation (2-11) below.

$$\Delta x = \frac{d_c^2}{32} \frac{P_{in}^2 - P_{out}^2}{2\eta} \frac{1}{\sqrt{\left(P_{in}^2(L^2 - Lx) + LxP_{out}^2\right)}} \frac{1}{1 + \frac{1}{\beta}e^{A + \frac{B}{T} + C\ln T}} \Delta t \tag{2-11}$$

With equation (2-11), the motion of an analyte can be modelled given its thermodynamics-based parameters (A, B and C), the column geometry, inlet and outlet pressures, mobile phase viscosity and temperature. By considering an infinitesimally small distance, dx, travelled in an infinitesimally small time, dt, equation (2-11) becomes,

$$dx = \frac{d_c^2}{32} \frac{P_{in}^2 - P_{out}^2}{2\eta} \frac{1}{\sqrt{\left(P_{in}^2 (L^2 - Lx) + LxP_{out}^2\right)}} \frac{1}{1 + \frac{1}{\beta} e^{A + \frac{B}{T} + C \ln T}} \, dt \qquad (2-12)$$

Integrating both sides of equation (2-12) should provide an expression for x with respect to t. Unfortunately, this equation is rather complex and difficult to integrate especially given the fact that T and P_{in} change with time and η changes with temperature. Riemann integration [108] can be used, however, to give a close approximation of x. In short, the integration interval ($[0, t]$) can be divided into 10,000 partitions, the area under the integrand curve for each partition calculated, then all areas summed.

Equation (2-12) serves as the base of our mathematical models for estimating d_c of the reference and target columns, β of the target column, and A, B and C of the analytes. By extension, it allows the prediction of retention times of analytes, whose thermodynamics-based parameters have been estimated, on columns with optimized geometries. Inspection of equation (2-12) shows that, although there are five unknowns (A, B, C, d_c, β), β cannot be isolated from the A term. Therefore, β for the reference column can be assumed to be equal to its nominal value and any actual deviation from this value will be captured by the optimized A term. This leaves four unknowns to be optimized as all the other terms in the equation are known (i.e. they are set by the experimenter or are known constants). Our model for optimizing these unknowns is based on the least-squares method [109] and so is aimed at minimizing the sum of squares of the errors between the retention times from actual experiments and from the thermodynamic model shown

in equation (2-12). The objective function, therefore, can be expressed as:

$$min \, S = \sum_h^g \sum_{i=1}^n \left[(t_R)_{hi} - \sum_{j=i}^{m_i} \Delta t_{hij} \right]^2 \tag{2-13}$$

The subscripts in Equation (2-13) are as follows, g is the total number of analytes tested, h is the index for a given analyte, n is the total number of experiments from which retention data is obtained, i is the index of a given experiment, m_i is the total number of partitions in the Riemann integration, and j is the index of a given partition. With a well-defined objective function we can rearrange (2-12) and replace dx with Δx to obtain an equation for Δt_{hij}.

$$\Delta t_{hij} = \frac{64 \, \eta_{hij} \sqrt{P_{in_{hij}}^2 (L^2 - Lx_{hij}) + Lx_{hij} - P_{out}^2} \left(1 + \frac{1}{\beta} e^{A_h + \frac{B_h}{T_{hij}} + C_h \ln T_{hij}} \right)}{d_c^2 \left(P_{in_{hij}}^2 - P_{out}^2 \right)} \Delta x \tag{2-14}$$

The last important step is to design an optimization algorithm that is fast and effective at finding solutions for the unknown parameters in equation (2-14). As mentioned earlier, we hypothesised that the Nelder-Mead simplex algorithm struggled to find consistent solutions because the optimization surface is very flat, causing it to stop before reaching the true minimum, or resulting in the simplex oscillating about the minimum without ever settling on it. Thus, we opted for a gradient-based method, which would evaluate the slope of the surface at each point, and travel downhill until the slope was below a certain threshold. We opted for a quasi-Newton optimization, the mathematical details of which are quite heavy but can be found in the supplemental information sections of the published work [62-64]. Here I briefly describe the important steps involved in the overall process, with minimal mathematical detail.

The optimization algorithm searches for the minimum of the objective function (equation (2-13)) starting with some initial guess at each of the unknowns. When a minimum is reached, the first order partial derivatives of the function with respect to the parameters being optimized will be

zero. The vector of these partial derivatives is called the gradient vector, ∇S and its elements are an assessment of the steepness of the function at every point searched by the algorithm. At a minimum,

$$\nabla S = 0 \tag{2-14}$$

The gradient vector is analogous to the first derivative of a function of one variable at some point x_0, $f'(x_0)$. The algorithm also needs to determine the direction in which to search for the minimum. This is achieved through the calculation of the Hessian matrix, $\mathbf{H}$, which is a square matrix of second-order partial derivatives of the function, and its elements provide information on the local curvature of the function, guiding the algorithm "downward" towards a minimum. It is analogous to the second derivative of a function of one variable at some point x_0, $f''(x_0)$. More accurately, the inverse of the Hessain matrix, $\mathbf{H}^{-1}$, allows the calculation of the search direction. Given the complexity of the gradient vector for this problem, $\mathbf{H}$, proved very difficult and impractical to calculate; we therefore used an approximation to the Hessian matrix, $\tilde{\mathbf{H}}$[62]. With a gradient vector, ∇S and a search direction, $\tilde{\mathbf{H}}^{-1}$ in hand we can calculate the iterative update (i.e. the next approximation of min S). If $\mathbf{v}_k$ is a vector containing the parameters to be optimized, the next iteration in the search for min S, $\mathbf{v}_{k+1}$ is given by,

$$\mathbf{v}_{k+1} = \mathbf{v}_k - \alpha_k \tilde{\mathbf{H}}_k^{-1} \nabla S_k \tag{2-15}$$

where α_k is a modifier between 0 and 1 that controls the step size towards the next iteration. Our iterative update continues until equation (2-14) is near-satisfied and all elements of ∇S are less than 1×10^{-8}.

Overall, our new approach may be described in three major parts:

1. Optimize the inner diameter of the reference column, d_c, and the thermodynamics-based parameters, A, B, C of a set of probe molecules (henceforth called a calibration mix) using retention data gathered on said column.

2. Optimize d_c and the phase ratio, β, of the target column (the column for which separations will be predicted) using retention data for the calibration mix gathered on the target column and the optimized A, B, C terms for said molecules.

3. Optimize A, B and C for new analytes of interest using their retention data on the now geometrically calibrated reference column and predict their retention times on the now geometrically calibrated target column.

2.2 Experimental

2.2.1 Standards and Samples

An in-house mixture (henceforth called the calibration mix) comprised of five non-coeluting compounds representing a few different types of chemistries/functionalities as well as a range of retention times, at concentrations of approximately 500 - 2000 µg mL^{-1} in dichloromethane (Sigma Aldrich, St. Loius, MO), was prepared and separated on the reference and target systems described below. The retention time data from this mixture allows the optimization of the inner diameter of both columns and enables the transfer of the thermodynamics-based parameters optimized on the reference system to the target system, permitting prediction on the latter. The compounds chosen were: 2-octanone (Matheson Coleman and Bell, Cincinnati, OH), n-decane (ACROS Organics, Geel, Belgium), 1-octanol (Fisher Scientific Company, Fair Lawn, NJ), 2,4-dimethylphenol (Eastman Organic Chemicals, Rochester, NY) and 2,6-dimethylaniline.

A Programmed Test Mix (Sigma-Aldrich, Oakville, ON) (based on the Grob mixture) containing 2,3-butanediol, decane, 1-octanol, undecane, nonanal, 2,6-dimethylphenol, 2-ethylhexanoic acid, 2,6-dimethylaniline, methyl decanoate, dicyclohexylamine and methyl laurate at varying concentrations (280 – 530 μg mL^{-1}) in dichloromethane was selected as the "sample" to be predicted on the target column. The mixture was diluted approximately 1:5 in dichloromethane (Sigma-Aldrich) and analysed on the geometry optimized reference system (to acquire thermodynamics-based parameters) and on the geometry optimized target system. The latter runs were done to produce experimental retention times to which the predictions of this system may be compared.

2.2.2 Instrumentation

An HP 6890 gas chromatograph (Agilent Technologies, Mississauga, ON) equipped with a split/splitless injector and flame ionization detector was used as our reference system. Injections (1 μL) were performed in split mode using a split ratio of 50:1, an inlet temperature of 275 °C, and He carrier gas (5.0 grade; Praxair, Edmonton, AB). The inlet pressure was programmed from 11.47 psi to 25.13 psi at rates of 0.24, 0.39, 0.49, 0.78 and 0.98 psi min^{-1} with no hold times. The pressure programming conditions were selected to give a flow rate of about 2.6 mL min^{-1} throughout the separations, translating to approximate speed-optimized flow conditions for the column used. Separations of the calibration mix and the Programmed Test Mix (Sigma-Aldrich) were carried out using linear oven temperature programs of 40 °C to 320 °C at ramp rates of 5, 8, 10, 16 and 20 °C min^{-1} with no hold times. All separations were performed on a RESTEK Rtx-5 column (Restek Corperation, Bellefonte, PA) (nominal geometry: 30 m × 0.32 mm; 0.5 μm d$_f$; 5% diphenyl 95% dimethyl polysiloxane). The column length was calibrated after installation by the injection of methane (as a dead time marker) and by using the column calibration tool

included with Chemstation (version A.08.03; Agilent Technologies). This approach provided a calibrated column length of 30.9 m which was used in all calculations that followed. The exact column length is unknown but this estimate is easy to obtain and is adequate for the purposes of this study.

An Agilent 7890A gas chromatograph (Agilent Technologies, Mississauga, ON) equipped with a split/splitless injector and flame ionization detector was used as our target system. Injections (1 µL) were performed in split mode using a split ratio of 50:1, an inlet temperature of 275 °C, and He carrier gas (5.0 grade; Praxiar, Edmonton, AB). The inlet pressure was programmed from 17.858 psi to 37.108 psi at rates of 0.344, 0.550, 0.688, 1.100 and 1.375 psi min^{-1} with no hold times. The pressure programming conditions were selected to give a flow rate of about 2.0 mL min^{-1} throughout the separations, translating to approximate speed-optimized flow conditions for the column used. Separations of both mixtures were carried out using linear oven temperature programs of 40 °C to 320 °C at ramp rates of 5, 8, 10, 16 and 20 °C min^{-1} with no hold times. All separations were performed on a RESTEK Rtx-5 column (Restek Corperation, Bellefonte, PA) (nominal geometry: 30 m × 0.25 mm; 0.25 µm d_f; 5% diphenyl 95% dimethyl polysiloxane). The column length was calibrated after installation into the instrument by the injection of methane (as a dead time marker) and by using the column calibration tool included with Chemstation (version B.04.03; Agilent Technologies). This approach provided a calibrated column length of 26.51 m. The exact column length is unknown but this estimate is adequate for the purposes of this study.

2.2.3 Inter-laboratory data analysis

A subset of the data collected in 2013 during an inter-laboratory study was used to compare the cross-laboratory predictive capabilities of our group's previous Nelder-Mead simplex based predictive methods [59,76] to the current quasi-Newton method [62-64]. An HP 6980 (Agilent Technologies) system, installed in our group's lab in Edmonton, AB, was used as the reference system. The reference column was an Rxi-1MS (RESTEK) (nominal geometry, 30 m × 0.25 mm; 0.25 µm d_f 100 % dimethyl polysiloxane) measure to be 29.89 m. The target system was an Agilent 7890 GC located in a lab of the Restek Corporation, Bellefonte, PA. It housed an Rxi-1MS column (RESTEK) from a different production batch than the column in the reference system (nominal geometry, 30 m × 0.25 mm; 0.25 µm d_f 100 % dimethyl polysiloxane). The calibration mixture was a Grob Test Mix (RESTEK). For the sample, retention data from an 8270 Calibration Mix #1 (RESTEK) (a 19 component mixture of substituted phenols), separated on both systems, was used. Column geometry calibration, thermodynamics-based parameter estimation and retention time prediction were performed using both methods.

2.3 Results and Discussion

2.3.1 Calibration of the reference column

Five separations of the calibration mix on the reference system were carried out under the experimental conditions described above (Section 2.2.2). The retention times of the mixture components are given in Table 2-1. The five compounds are well separated in all chromatograms and the elution order does not change.

Table 2-1 Retention times (in seconds) of the five components of the calibration mixture on the reference column

Oven ramp rate (°C min^{-1})	2-octanone	n-decane	1-octanol	2,4-dimethylphenol	2,6-dimethylaniline
5	595.24	610.49	736.17	872.41	908.42
8	458.20	467.88	548.69	636.89	663.52
10	403.26	410.94	476.19	547.88	570.91
16	307.76	312.49	354.08	400.48	417.02
20	270.61	274.35	307.90	345.60	359.57

These retention times (along with the experimental parameters) were input into the quasi-Newton optimization algorithm with the column length set to 30.9 m and the phase ratio was set to 160. The optimized d_c was determined to be 0.314_7 mm and the estimated parameters thermodynamic based parameters are shown in Table 2-2. It is worth noting that the estimated inner diameter captures any error in the fixed length, such that the ratio of L-to-d_c is accurate. Additionally, the A term captures both the thermodynamic information and any differences between the nominal and actual phase ratio.

Table 2-2 Estimated thermodynamic parameters of calibration mixture components

	2-octanone	n-decane	1-octanol	2,4-dimethylphenol	2,6-dimethylaniline
Term A (mol)	-44.3601	-43.0001	-64.6718	-83.1000	-59.5755
Term B (mol K)	7132.4427	7127.1451	8612.4020	9865.2138	8403.0093
Term C (mol)	5.2136	4.9951	8.0621	10.6961	7.4122

Table 2-3 shows the fit of the experimental data and the goodness of said fit is shown with the residuals in Table 2-4. From these data, it is apparent that the experimental data fit the model well. The sum of squared residuals is $0.23_1 \, \text{s}^2$ and both positive and negative errors appear.

Table 2-3 Fitted retention times (in seconds) of the calibration mixture components from reference column data

Oven ramp rate (°C min^{-1})	2-octanone	n-decane	1-octanol	2,4-dimethylphenol	2,6-dimethylaniline
5	595.24	610.50	736.19	872.43	908.42
8	458.15	467.80	548.56	636.75	663.44
10	403.35	411.06	476.36	548.07	571.05
16	307.67	312.40	354.00	400.37	416.88
20	270.66	274.39	307.93	345.64	359.64

Table 2-4 Differences between experimental data and the fitted data of the calibration mixture on the reference column (residuals, in seconds)

Oven ramp rate (°C min^{-1})	2-octanone	n-decane	1-octanol	2,4-dimethylphenol	2,6-dimethylaniline
5	0.00	-0.01	-0.02	-0.02	-0.01
8	0.05	0.08	0.13	0.14	0.08
10	-0.09	-0.12	-0.17	-0.19	-0.14
16	0.10	0.09	0.08	0.11	0.14
20	-0.06	-0.04	-0.03	-0.04	-0.08

2.3.2 Calibration of the target column

It is important that the concept of effective column geometry be introduced here. The optimized parameters pertaining to column geometry, d_c and β, provide values that are often close to their true physical values, but will differ in order to mathematically account for fluctuations in column geometry as well as instrument-to-instrument variations (precise calibrations of pressures and temperatures which vary from one physical sensor to another, etc). We refer to column geometry described by these optimized parameters as effective column geometry. Even if the determined column geometric parameters differ from their true physical values, they will be accurate relative to the reference column and the determined thermodynamic parameters on the reference column. In order to achieve this accurate transfer, the thermodynamic parameters of the probe compounds determined on a reference column act as a bridge between the reference and target columns. We assume the thermodynamic parameters for a given compound on both columns are the same when both columns have the same stationary phase chemistry and the same mobile phase is used.

Therefore, the thermodynamic parameters obtained from the reference column can be used when estimating the geometric parameters of the target column.

The same calibration mixture containing five probe molecules was separated under five temperature ramps on a target column installed on an Agilent 7890A chromatograph. Their retention times under different experimental conditions are shown in Table 2-5.

Table 2-5 Retention times (in seconds) of the calibration mixture on the target column

Oven ramp rate (°C min^{-1})	2-octanone	n-decane	1-octanol	2,4-dimethylphenol	2,6-dimethylaniline
5	457.53	470.70	588.54	718.49	747.71
8	361.87	370.52	447.52	532.25	554.54
10	322.07	329.11	391.72	460.73	480.15
16	250.43	254.87	295.11	339.81	354.09
20	221.94	225.49	258.02	294.36	306.61

The optimization algorithm was applied to the retention times in Table 2-5 above along with the experimental conditions of the target system described in section 2.2.2. The column length was set to be 26.5 m and the inner diameter was optimized from the initial value of 0.25 mm. The phase ratio was set to 250. The thermodynamics-based parameters were taken as the estimated values from Table 2-2. Upon convergence, the inner diameter was estimated to be 0.243_5 mm and the optimized phase ratio was 242.2_4. Neither is very far from the nominal values provided by the manufacturer.

The fitted values are shown in Table 2-6 while residuals between the fitted and the experimental retention times are placed in Table 2-7. The sum of squared residuals is 7.80 s^2. The fitting is not as good as that in Table 2-4, as expected. The increase of the residuals is because the fitting results incorporate errors in the retention times on both the reference and target columns. Based on the principle of error propagation, the error variances on both the reference and target column will be propagated into the model fitting here and cause a larger magnitude of observed residuals. It seems there is some association with the chemical compounds because errors are somewhat all positive or negative for a single compound. Also, retention times from the first chromatogram show relatively larger residuals, indicating some association with chromatograms as well. Nevertheless, the model fitting overall is still very good.

Table 2-6 Fitted retention times in seconds of the calibration mixture components from target column data

Oven ramp rate (°C min⁻¹)	2-octanone	n-decane	1-octanol	2,4-dimethylphenol	2,6-dimethylaniline
5	456.16	470.59	589.71	719.51	747.38
8	361.00	370.41	448.08	532.52	553.88
10	321.46	329.07	392.19	460.92	479.56
16	250.26	255.06	295.54	340.00	353.74
20	221.97	225.79	258.50	294.64	306.42

Table 2-7 Differences (in seconds) between experimental data and the fitted data (residuals).

Oven ramp rate (°C min^{-1})	2-octanone	n-decane	1-octanol	2,4-dimethylphenol	2,6-dimethylaniline
5	1.36	0.11	-1.16	-1.03	0.33
8	0.88	0.11	-0.56	-0.28	0.66
10	0.61	0.04	-0.46	-0.19	0.59
16	0.17	-0.18	-0.43	-0.19	0.35
20	-0.03	-0.30	-0.48	-0.28	0.19

2.3.3 Estimation of Thermodynamics-based Parameters on Calibrated Reference Column

The Programmed Test Mix (Sigma-Aldrich) was separated on the reference system as described in section 2.2.2. It should be mentioned that not all compounds are completely separated under all conditions tested. As such, we chose seven compounds that were well separated in all runs to ensure we acquired accurate retention times. The seven compounds chosen were 2,3-butanediol (the larger of its peaks), decane, 1-octanol, undecane, 2,6-dimethylaniline, methyl decanoate and methyl laurate. The retention times of the seven chosen compounds are shown in Table 2-8. These retention times, along with the experimental conditions and the optimized reference column geometry (length 30.9 m, d_c 0.314$_7$ mm and phase ratio 160) were input into the optimization algorithm to estimate the thermodynamics-based parameters, A, B, and C, for each of the chosen compounds. The estimated thermodynamic parameters for each chosen compound are listed in Table 2-9 and the fitted data are shown in Table 2-10. As prior knowledge of the thermodynamics-based parameters for each chosen compounds is unknown, we are not able to

comment on whether we have obtained accurate estimates of the thermodynamics-based parameters. However, the fitted data are very close to the experimental data, suggesting good model fitting.

Table 2-8 Experimental retention times (in seconds) of select Programmed Test Mix components on reference column

Oven ramp rate (°C min^{-1})	2,3-butane diol	decane	1-octanol	undecane	2,6-dimethyl aniline	methyl decanoate	methyl laurate
5	278.31	608.97	733.00	783.56	906.84	1157.01	1454.29
8	240.61	466.75	546.49	579.25	662.37	816.02	1003.69
10	222.97	410.16	474.68	501.24	570.15	691.82	842.61
16	188.04	311.98	353.11	370.07	416.49	490.52	585.67
20	172.77	273.87	306.99	320.65	359.06	417.38	493.76

Table 2-9 Estimated thermodynamic parameters of select Programmed Test Mix components on reference column

	2,3-butane-diol	decane	1-octanol	undecane	2,6-dimethyl aniline	methyl decanoate	methyl laurate
Term A (mol)	-50.02	-45.96	-64.37	-55.89	-59.50	-80.29	-100.61
Term B (mol K)	6670.88	7279.67	8586.84	8239.73	8397.66	10589.67	12646.66
Term C (mol)	6.13	5.42	8.02	6.78	7.40	10.09	12.81

Table 2-10 Differences between fitted and experimental retention times (in seconds) of select Programed Test Mix components on reference column

Oven ramp rate (°C min⁻¹)	2,3-butane diol	decane	1-octanol	undecane	2,6-dimethyl aniline	methyl decanoate	methyl laurate
5	0.00	0.00	-0.02	-0.01	-0.01	-0.02	-0.01
8	0.00	0.00	0.02	0.02	0.02	0.04	0.02
10	0.02	0.05	0.04	0.04	0.04	0.03	0.05
16	-0.05	-0.13	-0.15	-0.15	-0.18	-0.18	-0.21
20	0.03	0.09	0.11	0.10	0.12	0.13	0.15

2.3.4 Prediction of Retention Times on the Target Column

Once the thermodynamics-based parameters of the chosen compounds were determined on the reference column, the next step involved making predictions of their retention times on the now calibrated target column. The actual effective geometry of the target column is: 26.5 m × 0.243$_5$ mm with a phase ratio of 242.2$_4$. This effective geometry as well as the optimized *A*, *B* and *C* terms were used with our model to make retention time predictions on the target column. In order to assess the accuracy of the predictive model, the Programmed Test Mix (Sigma Aldrich) was separated on the target column under the conditions predicted. The experimental retention times are shown in Table 2-11 while the predicted retention times are shown in Table 2-12. Table 2-13 shows the differences between the predicted and experimental retention times. In Table 2-13, we can see that the largest error is about 2.8 s. Most errors range from 0.1 s to 2.0 s and the median error is 1.29 s. The largest relative error is 1.44 % with most other relative errors ranging from 0.04 % to 0.60 % (a median relative error of 0.26 %). We observed that for this experimental data

set all errors were negative, suggesting that the errors do not follow the assumed independent and identically distributed normal distribution. The exact reasons for this consistently negative error are not clear; however, one possible explanation is that the experiments showed some systematic shifts in temperature, pressure or some unknown factors that cause the retention times to change in one direction. Despite this, overall prediction is still very good. It is also worth noting that the magnitude of the errors for a given compound show a general trend of decreasing with increasing ramp rate. A higher ramp rate corresponds to a higher elution temperature as well as a sharper, narrower peak. It is possible that more accurate experimental retention times can be acquired from peaks with smaller variances. Also noteworthy is that the compounds present in the Programmed Test Mix (Sigma-Aldrich) that were also present in the in-house mixture do not necessarily show more accurate predictions than the newly introduced compounds. Overall, very good predictive accuracy has been obtained representing an improvement in the prediction of retention times between GC columns of different geometries installed in different systems.

Table 2-11 Experimental retention times (in seconds) of select Programed Test Mix components on target column

Oven ramp rate (°C min^{-1})	2,3-butane diol	decane	1-octanol	undecane	2,6-dimethyl aniline	methyl decanoate	methyl laurate
5	195.03	470.80	589.02	635.60	747.65	1002.07	1297.03
8	174.63	370.59	447.71	478.52	554.46	712.21	899.05
10	164.36	329.10	391.81	417.04	480.05	605.60	755.93
16	142.96	254.86	295.10	311.49	353.99	431.15	526.26
20	133.17	225.47	258.00	271.29	306.52	367.62	444.11

Table 2-12 Predicted retention times (in seconds) of select Programed Test Mix components on target column

Oven ramp rate (°C min⁻¹)	2,3-butane diol	decane	1-octanol	undecane	2,6-dimethyl aniline	methyl decanoate	methyl laurate
5	192.22	469.32	586.63	634.21	745.91	1000.56	1295.42
8	172.71	369.50	446.10	477.34	552.91	710.55	896.72
10	162.93	328.30	390.58	416.06	478.76	604.02	753.65
16	142.22	254.54	294.52	310.97	353.21	430.02	524.42
20	132.70	225.37	257.68	271.00	305.99	366.74	442.57

Table 2-13 Differences between predicted and experimental retention times in seconds of select Programed Test Mix components on target column

Oven ramp rate (°C min⁻¹)	2,3-butane diol	decane	1-octanol	undecane	2,6-dimethyla niline	methyl decanoate	methyl laurate
5	-2.81	-1.49	-2.39	-1.39	-1.75	-1.51	-1.61
8	-1.92	-1.09	-1.61	-1.18	-1.55	-1.66	-2.33
10	-1.43	-0.80	-1.23	-0.98	-1.29	-1.58	-2.28
16	-0.74	-0.32	-0.58	-0.52	-0.78	-1.12	-1.85
20	-0.47	-0.10	-0.32	-0.29	-0.53	-0.88	-1.54

2.3.5 Extensive Preliminary Work towards a Thermodynamic Library

Using the experimental and computational methods described above, a library of

thermodynamics-based parameters for ~115-180 compounds (the number varies by stationary

phase chemistry) on four stationary phase chemistries was built. The four phases range from low

to mid to high polarity and include 5% diphenyl 95% polydimethylsiloxane, trifluoropropylmethyl polysiloxane, (50% phenyl)-methylpolysiloxane-like, and polyethylene glycol (RESTEK Rtx-5MS, Rtx-200, Rxi-17Sil MS and Stabilwax, respectively). This library, although seemingly just a repetition or simple use of the work carried out in this chapter, was built over the course of ~6 months of standard preparations (by myself and three undergraduate volunteers), separations (on two GC-FID systems), data analysis, and calculations (on one computer). The results of this endeavour forms the basis of the work presented in Chapter 4 and will enable the thermodynamics-based parameters to be accessible to other interested chromatographers. Tables A2-1 to A2-4 in Appendix A contain the library thus far.

2.3.6 Comparison with Previous Approach

As mentioned in this introduction to this chapter, our group's previous approach worked very well for making predictions across columns of different geometries installed in the same instrument. However, it fell short when predictions across instruments and labs were required. In a round robin study unacceptably high absolute and relative errors in prediction were quite common across labs (up to 51 %) [104]. It is important to consider that the predictions presented in this chapter were not assessed across laboratories like in the round robin. Additionally, the scope of the compounds predicted and phases investigated is smaller than that of the round robin study. However, the results of the approach implemented in this chapter represent an improvement in the accuracy of predictions across column geometries and instruments. This assessment is further supported by experiments I performed within our own lab after the results of the round robin study were evaluated but prior to the work carried out in this chapter. Briefly, I installed two Stabilwax (RESTEK) columns of different geometries each in a different instrument in our lab and proceeded to calibrate the columns, acquire thermodynamic parameters and predict retention

times in accordance with our previous methods. These experiments eliminated any inter-laboratory contributions to the errors but kept cross-instrument and cross-geometry factors. The samples consisted of even numbered C10-C28 n-alkanes, a mixture of nine substituted phenols and a mixture of 19 amines (38 compounds ran under 5 conditions each = 190 predictions). In summary, the alkanes gave absolute errors ranging from 0.32 s to 40.47 s with a median error of 13.72 s (relative errors from 0.07 % to 5.17 %, median of 2.03 %). The phenols gave absolute errors from 0.43 s to 166.42 s with a median error of 13.68 s (relative errors from 0.03 % to 8.83 %, median of 2.15 %). Lastly, the amines showed absolute prediction errors from 0.11 s to 71.74 s with a median error of 16.76 s (relative errors from 0.06 % to 6.59 %, median of 1.96%). By comparison, the approach presented in this chapter gave absolute errors from 0.10 s to 2.81 s with a median error of 1.29 s (relative errors from 0.04 % to 1.44 %, median of 0.26 %) for seven compounds across five classes under five conditions (35 predictions). Additionally, Tables A3-7 to A3-15 in Appendix A show experimental and predicted retention time data for thirteen other compounds (7 PAHs, 1 ketone, 1 alkene, 1 alcohol, 1 ester, 1 aldehyde and 1 alkane) used to assess the accuracy of a method for predicting peak width across instruments and geometries (see Chapter 3 for details). Although the data was originally obtained for predicting peak widths, I also acquired retention time data and carried out retention time predictions. In the case of the six non-PAHs, I also collected data across oven and pneumatic conditions that varied from the conditions used to collect their thermodynamics-based parameters. In summary, the seven PAHs predicted under five conditions (35 predictions) gave absolute errors from 0.01 s to 10.55 s with a median error of 1.06 s (relative errors from 0.00 s to 0.44 s, median of 0.12 %). The 10.55 s error occurred when benzo[a]pyrene (a relatively large 5-ringed molecule with a boiling point of 495 °C) was separated at 5 °C min^{-1} (a slow ramp rate). This poor prediction appears to be an

outlier as the prediction errors for this molecule under the other conditions are within the usual range seen for this method. It is possible, however, that the range of retention times covered by the calibration mixture has an impact on prediction accuracy but this will have to be investigated in the future. With that point removed, the largest absolute error was 2.79 s and median was 0.99 s (max relative error 0.28 %, median 0.12 %). The six other compounds, predicted under the usual 5, 8, 10, 16 and 20 °C min^{-1} (30 predictions) showed absolute errors of 0.34 s to 2.54 s, median of 1.16 s (0.18 % to 0.75 %, median 0.32%). When separated under four conditions that deviate (with regards to carrier gas flow rates, initial oven temperatures and/or oven ramp rates) from those under which thermodynamics-based parameters were collected (24 predictions), absolute errors ranged from 0.12 s to 2.31 s, median 0.82 s (0.02 % to 1.02 %, median 0.19 %). These 124 predictions demonstrate a significant improvement in predictive accuracy across instruments and geometries when compared to the 190 predictions made within the same lab using the Nelder-Mead simplex approach. These median and maximum errors, although much smaller with the new approach, must be compared with consideration of the fact that fewer compounds were assessed by the new approach, the classes of compounds assessed (although varied in each case) were different and the stationary phase chemistry was different. However, it is not expected that these factors will influence prediction accuracy to the extent observed here. Even with this in mind, the quasi-Newton based approach shown in this chapter provides more accurate predictions than our previous methods across instruments and column geometry.

Apart from the improvement to predictive accuracy, we must also consider the ease of use of both methods. Both required little experimental time from the user of the predictive method but the new approach required much less than the previous. With the methods described in this chapter, the user of the target column only needs to perform five fast, temperature-programmed

separations of a calibration mixture and one injection of a dead time marker to estimate the column length. Our previous approach called for the user to measure the length of their column (by counting rings or by uncoiling), perform three injections of methane at three different isothermal temperatures (nine runs) and carry out five temperature-programmed separations of a calibration mix. The work presented in this chapter improved on ease of use for the target column user.

2.3.7 Algorithmic Considerations

In the Riemann integration used to calculate the retention time in this work, the column length was divided into 10,000 partitions. This number provided a good compromise between computation time (typically < 30 s) and prediction accuracy. More partitions might theoretically result in a more accurate prediction, but would require more time to calculate.

Likewise, a balance between time (experimental and computational) and accuracy must be struck when determining the number of experiments to use for optimizing parameters (A, B, C and d_c). Mathematically speaking, with four parameters to optimize, only four experiments are required. More experiments theoretically provide more accurate estimates, but require more time. We opted for five as that was shown to give acceptable results without demanding too much time, or oven ramp rates which were inordinately slow (< 5 °C/min) or too fast for the oven to reproducibly achieve (>25 °C/min).

For work carried out after this, the Programmed Test Mix was chosen as the calibration mix as it is inexpensive, available from numerous suppliers, and commonplace in GC labs. However, some experiments carried out after the completion of this work suggested that the range of retention times covered by the components of the calibration mix has an influence on the

accuracy of the predictions. Compounds that elute long before or long after the components of the calibration mix occasionally show larger overall prediction errors at the slowest ramp rate studied (5 °C min⁻¹) than those eluting within the retention time ranges of the mix. Spiking one or two late eluting compounds into the calibration mix and making use of its earliest eluting peaks (e.g. 2,3-butanediol on a 5% diphenyl column) seems to remedy the problem (when it occurs) at the cost of requiring an extra step for the user if they wish to accurately predict very early or very late eluting compounds. More data is required to determine whether these rare observations reflect a trend or are merely outliers; a conclusive explanation for this occasional observation cannot be given yet.

2.4 Conclusions

The model and quasi-Newton optimization algorithm presented here represents an improvement in ease and accuracy of retention time predictions across column geometries and instruments. The number of experiments required to acquire thermodynamic information and to perform a prediction for a target column is greatly reduced while the accuracy of predictions is greatly improved. This approach is not only useful for predicting retention times for GC separations but, as Chapters 3 and 4 will demonstrate, is also the basis for predicting peak width in GC (thereby allowing simulation of chromatograms) as well as mapping chromatographic spaces and predicting retention times in thermally modulated GC×GC. Overall, this new approach is simple, fast and accurate and represents a major step towards creating a powerful tool for method development and optimization.

Chapter 3: The prediction of peak width

3.1 Introduction

When developing an automated approach to optimizing GC and GC×GC separations it is important to consider, in addition to the retention times of compounds, the widths of their chromatographic peaks. This is because peak widths allow the chromatographer to assess resolution of neighbouring peaks, and informs the choice of appropriate modulation periods for GC×GC separations.

Resolution, R_S is a useful measure of the efficiency of the separation between two adjacent Gaussian peaks – a higher resolution indicates a higher separation efficiency. It may be defined as:

$$R_S = \frac{2(t_{R2}-t_{R1})}{w_{b2}+w_{b1}} = \frac{1.177(t_{R2}-t_{R1})}{w_{h2}+w_{h1}} \tag{3-1}$$

where t_{R1} is the retention time of a chromatographic peak, and t_{R2} is the retention time of a later eluting adjacent peak. w_{b1} and w_{b2} are the baseline widths of the peaks 1 and 2 respectively and w_{h1} and w_{h2} are their respective half-height widths. Usually, a resolution of at least 1.5 is required in order for two peaks to be considered as baseline resolved. In situations where one peak has a very large signal intensity relative to an adjacent peak an even higher resolution (2.0 or greater) might be needed to provide clear baseline resolution.

In GC×GC separations peaks eluting from the primary column are sampled then introduced/'injected' to the secondary column by the modulator. The timeframe in which this sampling and injection occurs is called the modulation period, P_M, and is chosen by the chromatographer when the method is being made. The widths of the peaks eluting from the first

dimension guide this choice because of a parameter known as the modulation ratio, M_R, defined as:

$$M_R = \frac{w_b}{P_M} = \frac{1.699 w_h}{P_M}$$ (3-2)

In 2006, Khummueng and co-workers demonstrated that GC×GC separations aimed at precisely quantifying trace analytes should be performed with an M_R of at least 3 while an M_R of ~ *1.5* is sufficient for semiquantitative analysis of major analytes [30]. This means that the P_M chosen for a given experiment should be about $1/M_R$ times the w_b of the peak. For example, for a trace analyte with a primary peak width, w_b of 4.5 s, a modulation ratio, M_R of at last 3 is desirable. Therefore, the modulation period chosen should ideally be at most 1.5 s (i.e. $P_M = w_b/M_R = 4.5$ s/ 3). The chosen P_M ultimately influences signal intensities and limits of detection, which are crucial considerations when undertaking quantitative analysis.

Given these two reasons, we can see why it is useful to incorporate the prediction of peak width into a tool aimed at simulating/predicting retention for speedy method development and optimization. Although academic literature over the last three or so decades provides several approaches to retention time prediction, including ones based on the estimation of thermodynamic parameters [56,58,59,61,75,76,100,101,110], papers focusing on the prediction of peak width are fewer and further between. Snijders et al showed a time summation model for predicting GC retention times and peak widths under constant pressure conditions [79]. Their methods, published in 1995, relied on using thermodynamic parameters estimated from known retention indices. In the early 2000s, Lomsugarit and coworkers divided the adjusted peak width, w_R' into hold-up width, w_M' and unadjusted peak width, w_R. These properties were related through a parameter they called the width factor, p' ($p' = w_R'/w_M$). Their work also demonstrated

the relationship between p' and k and applied this to the prediction of w_R of n-alkanes, FAMES and fatty alcohols in isothermal separations [51,52]. Krisnangkura later published an improved version of this approach that included terms accounting for column geometry and carrier gas flow rate [53]. In 2009, Aldaeus et al. presented a finite element method to predict retention times and peak widths in programmed-temperature gas chromatography (PTGC). They reported prediction accuracies of <0.1% for the retention times and <10% for peak widths [55]. Then in 2012, Zhu and coworkers presented their thermodynamics-based approach to predicting retention time and peak width in GC×GC separations [57]; two years later they demonstrated its application to petroleum analysis [111]. The methods presented in these works all employed isothermally obtained thermodynamic parameters for predictions. Additionally, these papers did not address accurate transfer of thermodynamic parameters across columns installed in different instruments. Also, while some of them discussed the impact of column coating efficiency and extra column band-broadening on peak widths, they did not suggest an accurate and practical approach for estimating these parameters for a GC system one might wish to predict/simulate.

For my work, I set out to create a method for predicting peak widths in GC separations that is quick, accurate, and readily compatible with our existing approaches to retention time prediction by way of thermodynamics-based parameters. It was also important that the method would not call for additional bench time on the part of the user, preferably requiring no separations beyond the ones already performed on the calibration mixture (for optimizing column geometries, allowing transfer of parameters across column geometries and instruments). Lastly, I aimed to develop a way to acquire a fair estimate of column coating efficiency and extra-column band broadening for a given column in a given instrument (a target system), thereby improving the accuracy of peak width predictions for said system beyond the approaches presented thus far.

The work shown here introduced the prediction of peak widths to our models and integrated well with our current retention time prediction tools [62-64] in that it does not require any additional experimentation on the part of the user. The data required for attaining an accurate prediction is available from the same five PTGC separations used to generate the parameters needed to predict retention times shown in Chapter 2.

The theory and equations behind thermodynamics and fluid dynamics considerations for predicting peak width are as described in previous chapters. The estimation of thermodynamics-based parameters, and optimized reference and target column geometries used for the predictions shown here are the same as used for predicting and transferring retention times in Chapter 2. Peak width is modelled using a variation on the time summation approach described by Snijders and coworkers [79]. My approach differs in the manner in which the thermodynamic parameters (and by extension, k) are estimated, the treatment and estimation of coating efficiency and extra-column peak variance, and the use of pressure ramps (which is more applicable to modern GC programmed-temperature experiments) instead of constant pressure.

The variance of a chromatographic peak, σ_t^2, may be viewed as the sum of its on-column variance, σ_c^2, and its extra-column variance, σ_{extra}^2:

$$\sigma_t^2 = \sigma_c^2 + \sigma_{extra}^2 \tag{3-3}$$

On-column peak variance (in time) under isothermal conditions can be expressed as:

$$\sigma_{c,t}^2 = \frac{t_r^2}{N} = \frac{HL(1+k)^2}{\bar{u}^2} \tag{3-4}$$

From chromatographic plate theory, H is the column plate height while N is the plate number.

These terms have units of distance so for mathematical convenience the peak variance in time may be converted to peak variance in space, $\sigma_{c,L}{}^2$, (with distance units) by:

$$\sigma_{c,L}^2 = \frac{\sigma_{c,t}^2 \, \bar{u}^2}{(1+k)^2} \tag{3-5}$$

As an analyte travels a distance Δx along a column, its peak variance at position x may be described by:

$$\sigma_{c,x}^2 = \frac{P_{x-\Delta x}^2}{P_x^2} \, \sigma_{c,x-\Delta x} + H_x \Delta x \tag{3-6}$$

where H_x is plate height at position x, assuming uniform coating efficiency and is defined as:

$$H_x = \frac{2D_{G,x}}{u_x} + \frac{11k_x^2 + 6k_x + 1}{96(1+k_x)^2} \frac{d_c^2 \, u_x}{D_{G,x}} + \frac{2k_x d_f^2 u_x}{3(1+k_x)^2 D_{L,x}} \tag{3-7}$$

Here, $D_{G,x}$ is the binary diffusion coefficient of the analytes in the mobile phase calculated according to the empirical method developed by Fuller and co-workers [112] and $D_{L,x}$ is the diffusion coefficient in the stationary phase approximated by[79]:

$$D_{L,x} = \frac{D_{G,x}}{5 \times 10^4} \tag{3-8}$$

P_x, the pressure at position x along the column is:

$$P_x = \sqrt{P_{in}^2 - \frac{x}{L}(P_{in}^2 - P_{out}^2)} \tag{3-9}$$

The first term in equation (3-6) accounts for the compressibility of the carrier gas. The peak variance upon elution can then be calculated by summing the changes in peak variance along the entire length of the column using to equation (3-10):

$$\sigma_{c,L}^2 = \sum_{x=1}^{n} \sigma_{c,x}^2 \tag{3-10}$$

Chromatographers usually discuss peak widths in terms of time, therefore the on-column peak variance can be converted to time units by:

$$\sigma_{c,t}^2 = \frac{\sigma_{c,L}^2 (1+k_n)^2}{u_n^2} \tag{3-12}$$

So far, the equations presented here only describe on-column peak variance and thus do not account for the effect of coating efficiency of the column or extra-column variance brought about by, for example, band broadening in the injector and detector. Below I describe a rapid method for estimating these parameters. It is important to realise that this approach is not aimed at providing the exact extra-column variance for each analyte in a sample, but instead provides a value that accounts for this variance across range of analytes and separation conditions. Once determined, these parameters (column coating efficiency and extra-column band broadening) help to improve the accuracy of peak width predictions across column geometries and instruments.

By combining equations (3-3) and (3-4) the total peak variance of an analyte peak may be described as:

$$\sigma_t^2 = \frac{HL(1+k)^2}{\bar{u}^2} + \sigma_{extra}^2 \tag{3-13}$$

The first term on the right side of the equation, describing on-column variance, can be modified to include column coating efficiency, Φ:

$$\sigma_t^2 = \frac{HL(1+k)^2}{\Phi \bar{u}^2} + \sigma_{extra}^2 \tag{3-14}$$

Assuming Φ does not change appreciably along the length of the column and σ_{extra}^2 is

approximately the same for all analytes over a range of retention times, ramp rates and carrier gas velocities:

We can let $\dfrac{HL(1+k)^2}{\bar{u}^2} = \sigma^2_{c,t\ predicted}$

and $\sigma^2_t = \sigma^2_{experimental}$

Therefore,

$$\sigma^2_{expermental} = \frac{1}{\Phi}\,\sigma^2_{c,t\ predicted} + \sigma^2_{extra} \qquad (3\text{-}15)$$

The experimentally determined width of a peak is the result of contributions to band broadening caused by the column (including its coating efficiency) and extra-column considerations. Therefore, according to equation (3-15) we can express the experimental peak width as a linear function of the on-column peak width predicted assuming 100% column coating efficiency. The gradient is the inverse of coating efficiency and the y-intercept is the peak variance caused by extra-column band broadening. My approach involves the running a set of probe molecules (i.e. the calibration mix) on the target column to determine these two parameters. They can then be used in conjunction with the estimated thermodynamics-based parameters (*A*, *B* and *C*) to more accurately predict the width of other analyte peaks on that column/system.

3.2 Experimental

3.2.1 Standards and Samples

A Programmed Test Mix (Sigma-Aldrich, Oakville, ON, Canada) was diluted 1 in 4 in dichloromethane (Sigma-Aldrich) so that the concentrations of its components ranged from about 70 µg mL^{-1} to 133 µg mL^{-1}. This diluted mixture was separated as described below. It

served as the calibration mixture for transfer of thermodynamic parameters across columns and instruments.

Two different solutions were chosen as samples. An SV Calibration Mix #5/610 PAH Mix (Restek Corporation, Bellefonte, PA, USA) consisting of 11 PAHs diluted to about 100 µg mL^{-1} in dichloromethane (Sigma-Aldrich). Additionally, a mixture containing 6 compounds of various functionalities, each at approximately 100 µg mL^{-1}, was prepared in-house (henceforth referred to as Thermo. Sample Mix). It consisted of (in order of retention time) 2-heptanone (Sigma-Aldrich), trans-5-decene (Chemical Samples Co.), 2-nonanol (Sigma-Aldrich), methyl nonanoate (Eastman Organic Chemicals), undecanal (Sigma-Aldrich) and n-pentadecane (Sigma-Aldrich) dissolved in hexane (Sigma-Aldrich).

3.2.2 Instrumentation

3.2.2.1 Reference System

An HP 6890 gas chromatograph (Agilent Technologies, Mississauga, ON) equipped with a split/splitless injector and flame ionization detector housed the reference column – the column on which thermodynamics-based parameters of analytes were estimated. Injections were performed in split mode using a split ratio of 50:1, an inlet temperature of 275 ºC and He carrier gas (5.0 grade, Praxair, Edmonton, AB). The inlet pressure was programmed from 17.99 psi (gauge) to 38.04 psi (gauge) at rates of 0.35, 0.55, 0.69, 1.11 and 1.38 psi min^{-1} with 10 min hold time at 38.04 psi (gauge). The pressure programing conditions were selected to give a flow rate of about 2.0 mL min^{-1} throughout the separations (approximately speed-optimized flow). Separations were carried out using linear oven temperature programs of 40 ºC to 330 ºC at ramp rates of 5, 8, 10, 16 and 20 ºC min^{-1} with 10 min holds at 330 ºC. Separations were performed on a RESTEK

Rtx-5 column (Restek Corperation) (nominal geometry: 30 m ×0.25 mm; 0.25 µm d_f; 5% diphenyl 95% dimethyl polysiloxane). The column length was calibrated after installation into the instrument by the injection of methane (as a dead time marker) and by using the column calibration tool found in Chemstation (version A.08.03) (Agilent Technologies). This approach provided a calibrated column length of 25.7 m which was used in the calculations that follow. Some separations were performed after it became necessary to cut and reinstall the column; these include the separations of the Thermo Sample Mix and a second set of separations of the Programmed Test Mix. For these separations, a calibrated column length of 25.3 m was used for all calculations.

3.2.2 Target System

An Agilent 7890A gas chromatograph (Agilent Technologies) equipped with a split/splitless injector and flame ionization detector housed the target column. Injections were performed in split mode using a split ratio of 50:1, an inlet temperature of 275 ºC and He carrier gas (5.0 grade, Praxair, Edmonton, AB). The inlet pressure was programmed from 17.74 psi (gauge) to 37.516 psi (gauge) at rates of 0.341, 0.546, 0.682, 1.091 and 1.364 psi min^{-1} with a 10 min hold time at 37.516 psi (gauge). The pressure programing conditions were selected to give a flow rate of about 2.0 mL min^{-1} throughout the separations (approximately speed-optimized flow). Separations were carried out using linear oven temperature programs of 40 ºC to 330 ºC at ramp rates of 5, 8, 10, 16 and 20 ºC min^{-1} with 10 min hold at 330 ºC. Separations were performed on a RESTEK Rtx-5MS column (Restek Corperation) (nominal geometry: 30 m × 0.25 mm; 0.1 µm d_f ; 5% diphenyl 95% dimethyl polysiloxane). The column length was calibrated after installation into the instrument by the injection of methane (as a dead time marker) and by using the column calibration tool found in Chemstation (version B.04.03) (Agilent Technologies). This approach

provided a calibrated column length of 26.6 m which was used in the calculations that follow. In order to evaluate the performance of the model across conditions that varied from the separation conditions of the calibration mix (Programmed Test Mix), the Thermo. Sample Mix underwent four additional separations under the conditions shown in Table 3-1. The final oven temperature remained 330 °C in each case.

Table 3-1 Separations performed on the Thermo. Sample Mix on the target column under conditions that differ from the conditions under which the calibration mixture was separated

Condition Label	Desired flow rate (mL min^{-1})	Initial inlet pressure (psig)	Final inlet pressure (psig)	Pressure ramp rate (psi min^{-1})	Initial oven temperature (°C)	Oven ramp rate (°C min^{-1})
A	1.0	10.484	23.689	0.455	40	10
B	2.0	18.431	37.516	0.682	50	10
C	2.0	17.74	37.516	0.477	40	7
D	1.0	10.261	23.689	0.602	35	13

3.3 Results and Discussion

3.3.1 Calibration of reference and target columns

This time I chose as the calibration mixture, a Programmed Test Mix (Sigma-Aldrich) – based on the Grob Test Mix because it is an affordable solution, available from numerous suppliers, compatible with several stationary phase chemistries and likely to be commonplace in many GC labs. This means that users wishing to predict retention on their target systems or even for building their own internal thermodynamics based libraries should be able to implement our methods.

This mixture was separated on the aforementioned reference system (HP 6890, RESTEK Rtx-5 column (Restek Corperation), 25.7 m × 0.25 mm; 0.25 μm d_f; 5% diphenyl 95% dimethyl polysiloxane). For the separations performed after cutting and reinstalling the column, the actual length was 25.3 m. The retention times of six non-coeluting compounds of the calibration mixture, on the reference column, along with the separation conditions were input into our MATLAB code that estimates the thermodynamic parameters (*A*, *B* and *C*) of the components and the optimized inner diameter of the column (as experienced by the probe molecules of the mixture) [62] . The compounds chosen were decane, 1-octanol, undecane, 2,6-dimethylaniline, methyl decanoate and methyl laurate. The algorithm produced an optimized column inner diameter was 0.209$_4$ mm and the estimated thermodynamic parameters shown in Table 3-2.

Table 3-2 The estimated thermodynamic parameters of the 6 selected components of the Programmed Test Mix (Sigma-Aldrich) on the reference column; column length = 25.7 m

Term	Thermodynamic Parameters					
	decane	1-octanol	undecane	2,6-dimethylaniline	methyl decanoate	methyl laurate
A (mol)	279.9317	231.2608	229.6781	161.7902	173.3418	154.4987
B (mol K)	-8706.1087	-6222.3054	-6201.8262	-3004.0433	-3141.8003	-1967.8400
C (mol)	-42.4743	-35.2768	-34.9777	-24.8651	-26.5776	-23.7206

The same mixture was separated on the target system (Agilent 7980A, RESTEK Rtx-5MS

column (Restek Corporation) 26.6 m × 0.25 mm; 0.1 μm d_f ; 5% diphenyl 95% dimethyl

polysiloxane), under the conditions described above. The retention time data for the same six

components (on this system), the separation conditions and the thermodynamic parameters

shown in Table 3-2 (acquired from the reference column) were input into out MATLAB code for

optimizing the geometry of the target column [63]. This step is necessary to permit accurate

transfer of thermodynamic parameters and prediction of retention times across instruments. The

optimized column inner diameter and phase ratio were 0.241_1 and $449._8$ respectively.

3.3.2 Prediction of peak widths

The retention times and peak widths of seven select (non-co-eluting) PAHs in the SV Calibration

Mix #5/610 PAH Mix (Restek Corporation) were predicted. This chapter focuses on the

prediction of peak width so results pertaining to retention time predictions may be found in

Appendix A, Tables A3-7 to A3-15. Note that I chose to predict only non-coeluting peaks so that

I can more fairly compare my predictions to experimentally obtained peak widths. Coeluting

peaks integrated by the Agilent ChemStation (Agilent Technologies) software used often have

more inaccurately/inconsistently calculated experimental peak widths. The seven chosen PAHs

were naphthalene, acenaphthylene, acenaphthene, fluorene, fluoranthene, pyrene and

benzo[a]pyrene.

The thermodynamics-based parameters of the seven compounds used in the prediction, were

estimated using our current methods [62,64] and are shown in Table 3-3.

Table 3-3 The estimated thermodynamic parameters of the 7 selected PAHs on the reference column; column length = 25.7 m

Term	Thermodynamic Parameters						
	Naphthalene	**Acenaphthylene**	**Acenaphthene**	**Fluorene**	**Fluoranthene**	**Pyrene**	**Benzo[a]pyrene**
A (mol)	143.7983	108.5452	106.6473	102.5193	71.8331	72.7065	128.3663
B (mol K)	-2224.6318	-174.4166	-11.1973	324.5194	2535.4045	2452.1307	-845.0117
C (mol)	-22.1569	-16.8642	-16.5846	-15.9537	-11.4174	-11.5005	-19.0640

No additional experiments were required to obtain the data or parameters used in the prediction of peak width, which makes this approach complementary to the approach used in predicting retention times, and minimizes the number of experiments and bench time required to collect data.

The calculation/prediction of peak width involves the following steps. First, the on-column peak variances, σ_c^2, of the calibration mixture components are predicted for the target column assuming 100% coating efficiency, (i.e. $\Phi = 1$) and no extra-column peak variance ($\sigma_{extra}^2 = 0$). This calculation is based on the thermodynamic parameters of the calibration mix, optimized target column geometry and the known separation conditions. Second, the experimentally determined peak widths (taken directly from ChemStation (Agilent Technologies) peak tables) are converted to variances by the following equation which relates the variance of a Gaussian-peak to its width at half-height:

$$\sigma_{experimental}^2 = \left(\frac{w_h}{2.354}\right)^2 \tag{3-16}$$

This conversion assumes the peak shape is Gaussian, which is reasonable for well-behaved, non-overloaded peaks. $\sigma_{experimental}^2$ for the peaks of the calibration mixture is then plotted against their predicted on-column peak variances, σ_c^2 (with $\Phi = 1$ and $\sigma_{extra}^2 = 0$) and fitted to nonparametric linear model using a Theil-Sen estimator (ordinary least squares was not used as the errors in $\sigma_{experimental}^2$ and σ_c^2 are of similar magnitudes). This model supposes that $\sigma_{experimental}^2$ captures both the true on-column variance of a peak (including the multiplicative contribution of coating efficiency of the target column) and extra-column variance (including, but not necessarily limited to, the additive contributions of injector and detector band broadening). Equations (3-14) and (3-15) describe this fit. From these equations, $1/\Phi$ is the gradient, therefore, the inverse of

this gradient provides the coating efficiency of the target column relative to the reference column and σ_{extra}^2 is the y-intercept. Third, the empirically determined values of Φ and σ_{extra}^2 are used with the thermodynamic parameters of the sample analytes, their calculated diffusion coefficients, and the optimized target column geometry to predict their peak variances and subsequently half-height widths, under a range of separation conditions. Figure 3-1 below summarises this process and Figure 3-2 shows the linear fit via Theil-Sen estimator used in the determination of Φ and σ_{extra}^2.

The black trace in Figures 3-3A to 3-3E shows the raw experimental chromatogram (replotted in Microsoft Excel) of the PAH mixture separated at 5 °C/min. The overlapping red traces show the peaks generated using the predicted retention times and predicted peak widths. It is important to note that this chromatogram represents the most poorly predicted conditions of the PAH data set, yet all (but one) peaks investigated are visibly well modelled, as seen by the close overlap of the simulated red peaks with the experimental black peaks. Table 3-5 and Table A3-15 in Appendix A corroborate this illustration. The exception to this is benzo[a]pyrene, which shows an atypical, unacceptable prediction error (particularly in retention time). The suspected reasons for this are discussed in Chapter 2.

Table 3-4 contains the experimental and predicted peak widths of the PAH mixture components on the target column while Table 3-5 contains the errors in peak width prediction with and without the correction factors of Φ and σ_{extra}^2. In summary, the results in Table 3-5 illustrate absolute prediction errors of half-height widths for the PAHs, prior to correction for coating efficiency and extra-column variance, ranged from 0.05 s to 0.25 s (absolute relative errors from 2.21 % to 17.59 %) with a median error of 11.58 % and sum of squared errors, SSE of 0.75 s^2. After repeating the predictions with the inclusion of $\Phi = 0.78_7$ and $\sigma_{extra}^2 = 0.017_7$ s^2, errors

ranged from 0.00 s to 0.27 s (absolute relative errors from 0.10 % to 10.92 %) with a median error of 3.34 % and an SSE, of 0.21 s^2. The data shows six instances in which the prediction error, after accounting for Φ and σ_{extra}^2, was greater than or equal to the error prior to accounting for these terms. Five of these occur during the 5 °C/min run and it is not yet clear why this is the case. One possible reason is that errors in the analyte stationary phase diffusion coefficients, D_L (estimated by multiplying their mobile phase diffusion coefficient, D_G by a constant) have a greater effect on the prediction accuracy of large, highly aromatic molecules at slow oven ramps in which analytes spend more time in the stationary phase than at faster oven ramps. Despite this, there is clearly a large reduction in errors overall.

The half-height widths of the six components of the Thermo. Sample Mix were also predicted on the target column using their thermodynamic parameters acquired on the calibrated 25.3 m reference column. They were separated under the same five conditions as the PAHs as well as under the four conditions shown in Table 3-1. Their experimental peak widths, predicted peak widths and prediction errors, under the same five conditions as the PAHs are shown in Tables 3-6 and 3-7 respectively. Their thermodynamics-based parameters are shown in Table A3-1 in Appendix A. In summary, under the five conditions that matched the PAH separations, absolute prediction errors prior to correction for coating efficiency and extra-column variance ranged from 0.09 s to 0.30 s (absolute relative errors from 10.62 % to 31.74 %) with a median error of 15.62% and an SSE of 1.00 s^2. After repeating prediction with the inclusion of $\Phi = 0.78_7$ and $\sigma_{extra}^2 = 0.017_7$ s^2, errors ranged from 0.00 s to 0.10 s (absolute relative errors from 0.10 % to 11.36 %) with a median error of 1.96 % and an SSE of 0.04 s^2.

Table 3-8 summarises their prediction errors under the conditions in Table 3-1. Their experimental widths and predicted widths may be found in Tables A3-3 in Appendix A. Under

these conditions, absolute prediction errors prior to correction ranged from 0.05 s to 0.26 s (5.08 % to 20.26 %) with a median error of 12.26 % and an SSE of 0.53 s^2. After repeating prediction with the inclusion of $\Phi = 0.78_7$ and $\sigma_{extra}^2 = 0.017_7$ s^2, errors ranged from 0.00 s to 0.12 s (0.01 % to 11.29 %) with a median error of 3.69 % and an SSE of 0.07 s^2. A visual representation of the prediction accuracy is illustrated in Figures 3-4A to 3-4C that show a predicted chromatogram of Condition D, the condition most different from the five used to collect the thermodynamic parameters.

Across all three sets of data, the overall accuracy of the peak width predictions is improved. The ranges of absolute and relative errors, the median errors and the sum of squared errors are all greatly reduced by the inclusion of these additional terms and 74% of absolute relative errors were less than 5%.

Input:
Coating efficiency, $\Phi = 1$, **Extracolumn variance**, $\sigma_{extra}^2 = 0$, **Time increment**, $\Delta t = 0.01$ s
Initial time = 0 s, **Initial distance travelled along column**, $\Delta x = 0$ m

Calibration Mix experimental conditions: calibrated target column geometry (L, d_c, β), inlet and outlet pressures (P_{in}, P_{out}), oven temperatures and ramps (T, r)

Calibration Mix component properties: thermodynamics-based parameters (A, B, C), molecular mass, atomic diffusion volumes

Carrier gas properties: molecular mass, atomic diffusion volume

For each compound, at every Δt, during each separation, calculate:
increment number (i), time passed ($\Delta t \times$ i), oven temperature (T), retention factor (k), carrier gas viscosity and velocity (η, u), distance travelled along column (Δx), diffusion coefficient in mobile and stationary phase (D_G, D_L), height equivalent to a theoretical plate (H), peak variance ($\sigma_{c,x}^2$)

and sum:
Δx, $\sigma_{c,x}^2$

Has the compound eluted?

(i.e. $\sum \Delta x \geq L$?)

no

yes

Output:
On-column peak variance ($\sigma_{c,t}^2 + \sigma_{extra}^2$)
Half height width (w_h)

Figure 3-1 Flow chart and pseudocode algorithm used for the calculation of peak widths.
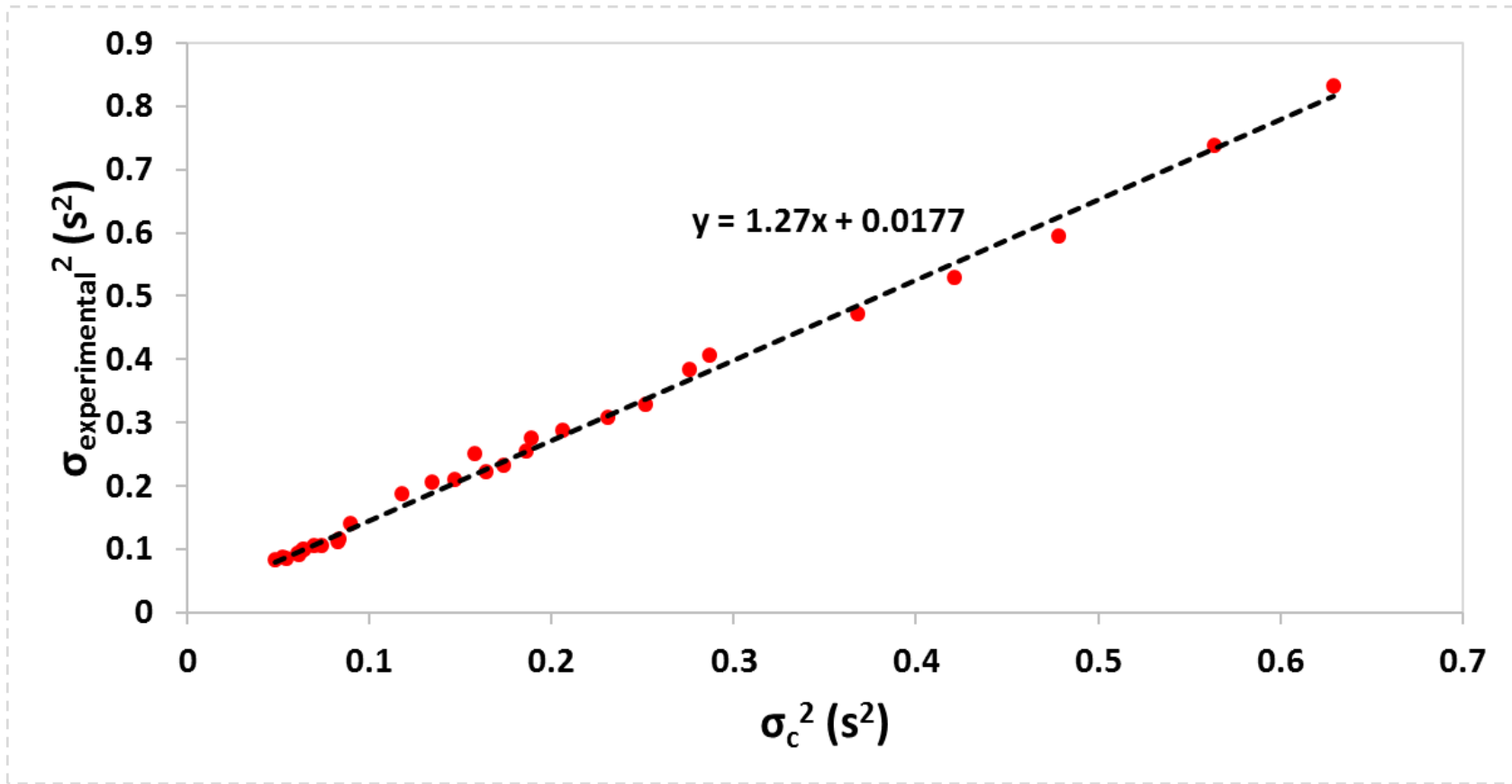
Figure 3-2 Theil-Sen Estimator used to determine Φ and σ_{extra}^2 from calibration mix. $\sigma_{experimental}^2$ are the experimental variances of each component under each separation condition while σ_c^2 are the calculated on-column variances (assuming 100% coating efficiency and no extra column variance)
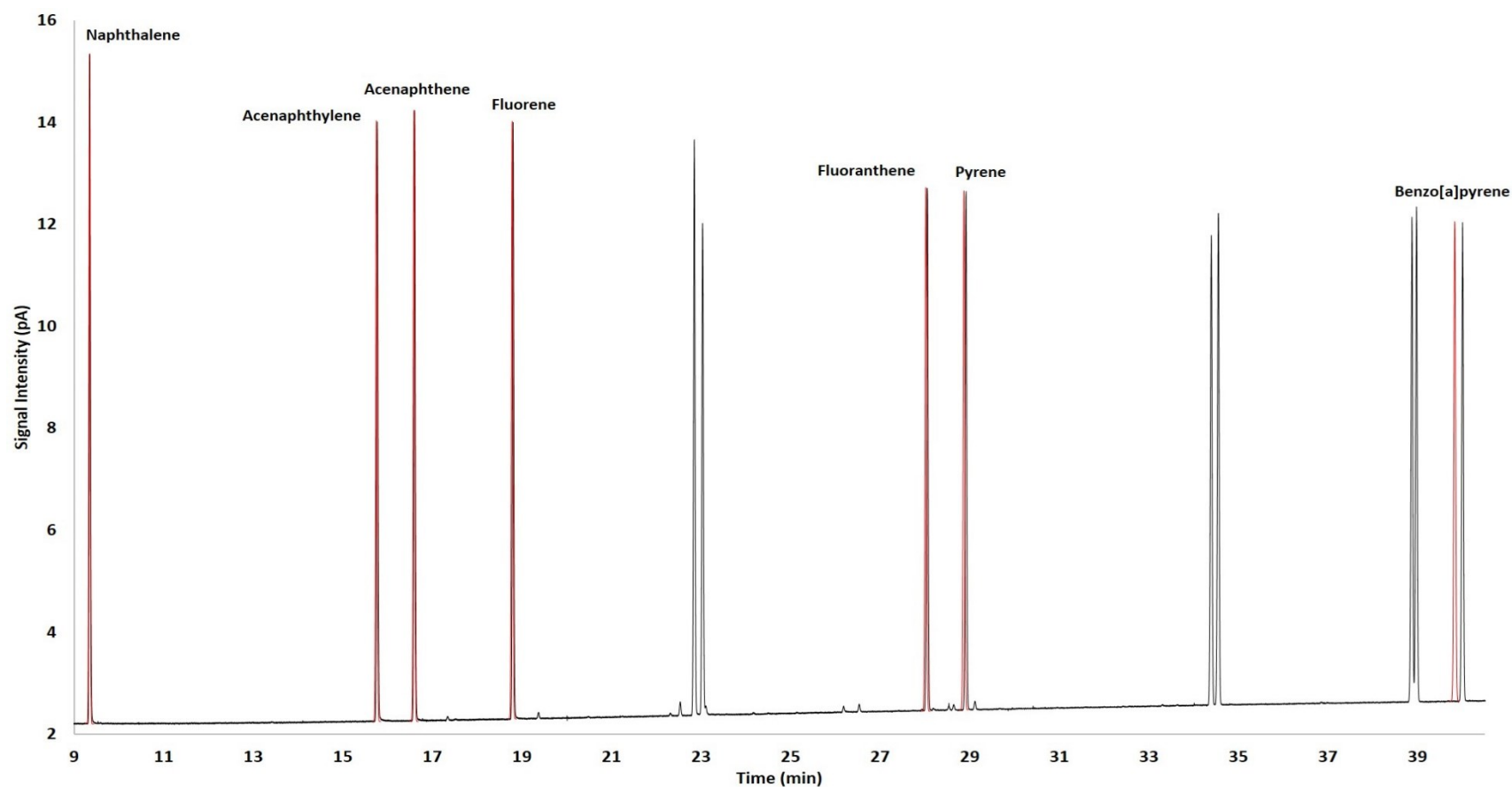
Figure 3-3A Predicted peaks (traced in red) plotted along with the experimentally obtained chromatogram of the PAH mixture separated at 5 °C/min. Red traces are modelled using their predicted (using Φ and σ_{extra}^2) peak widths and predicted retention times (as peak apexes). Both red and black traces are plotted with the same line thicknesses and peak heights of the red traces are simulated.
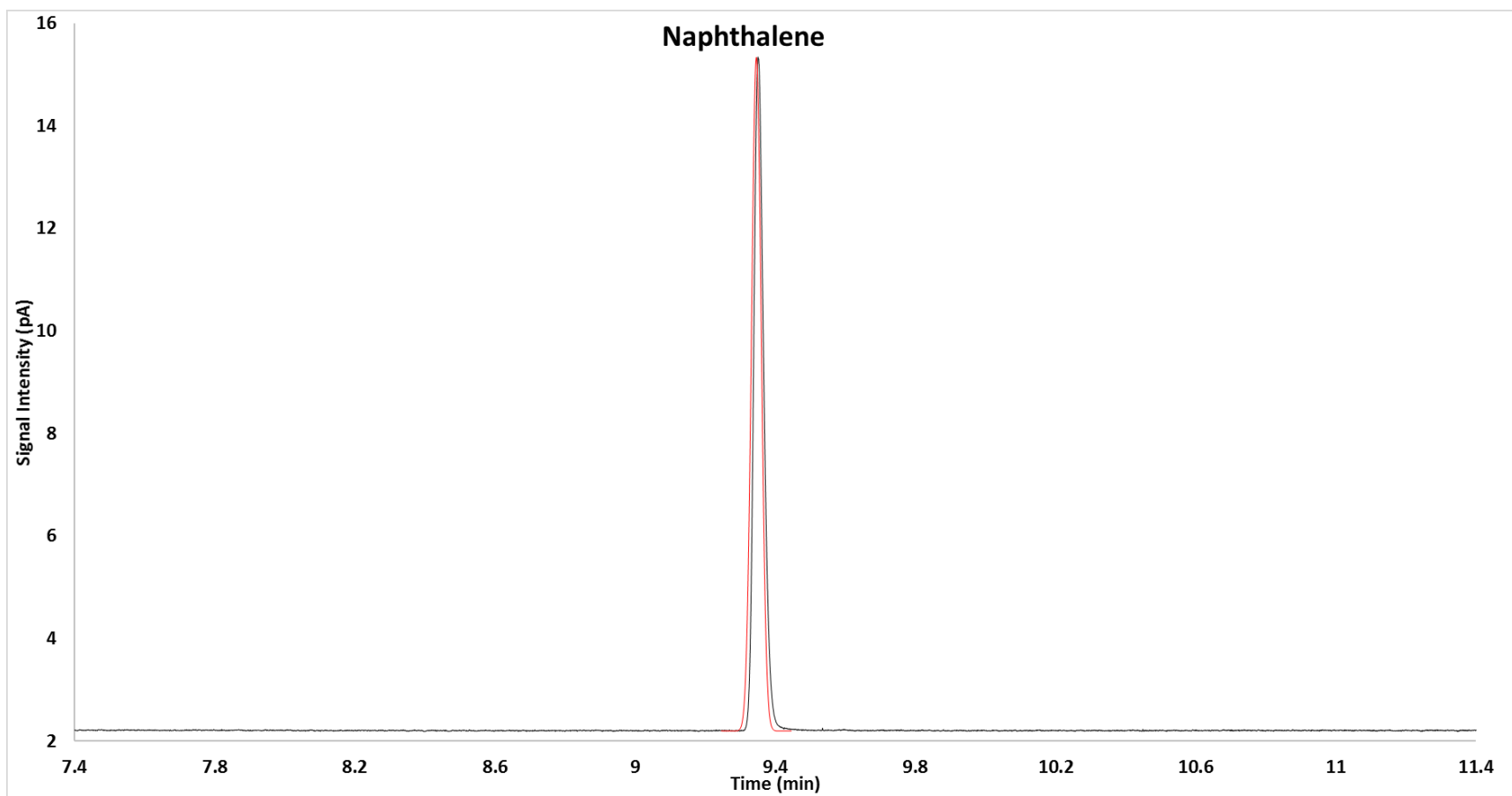
Figure 3-3B Close-up (4 minute window) view of naphthalene predicted peak (traced in red) plotted along with the experimental naphthalene peak at 5 °C/min.
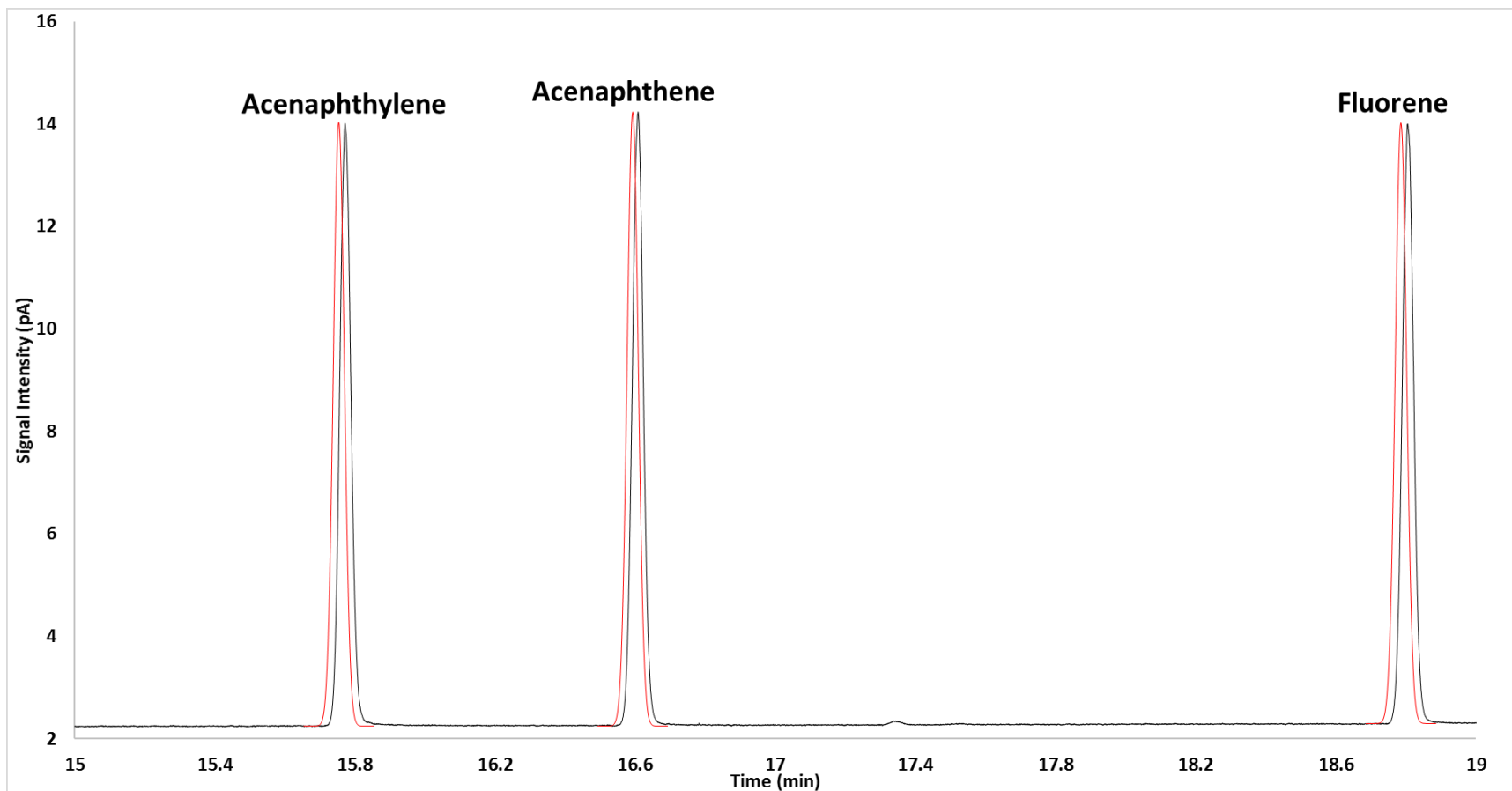
Figure 3-3C Close-up view (4 minute window) of acenaphthylene, acenaphthene and fluorene predicted peaks (traced in red) plotted along with the experimental peaks at 5 °C/min.
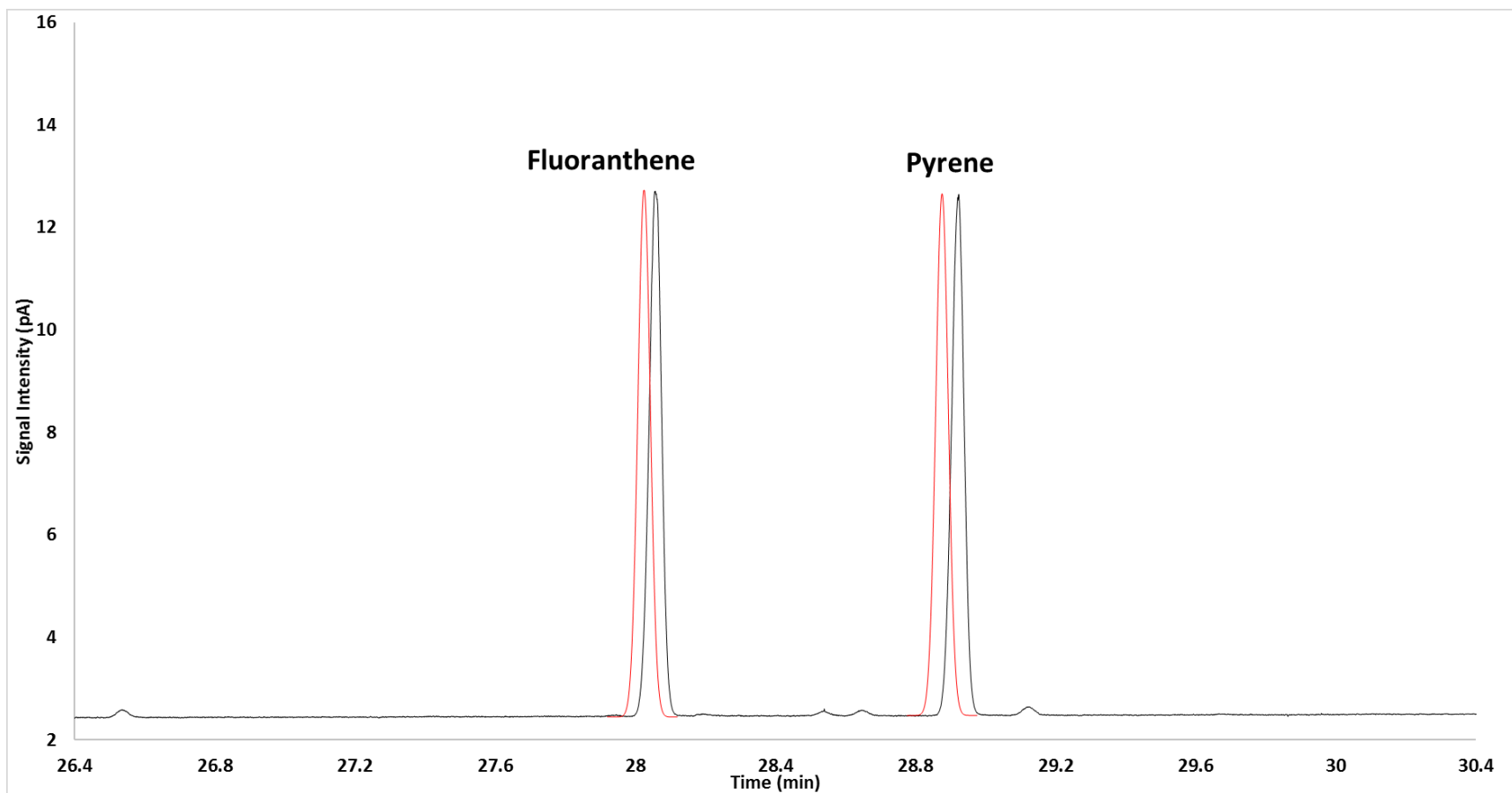
Figure 3-3D Close-up view (4 minute window) of fluoranthene and pyrene predicted peaks (traced in red) plotted along with the experimental peaks at 5 °C/min.
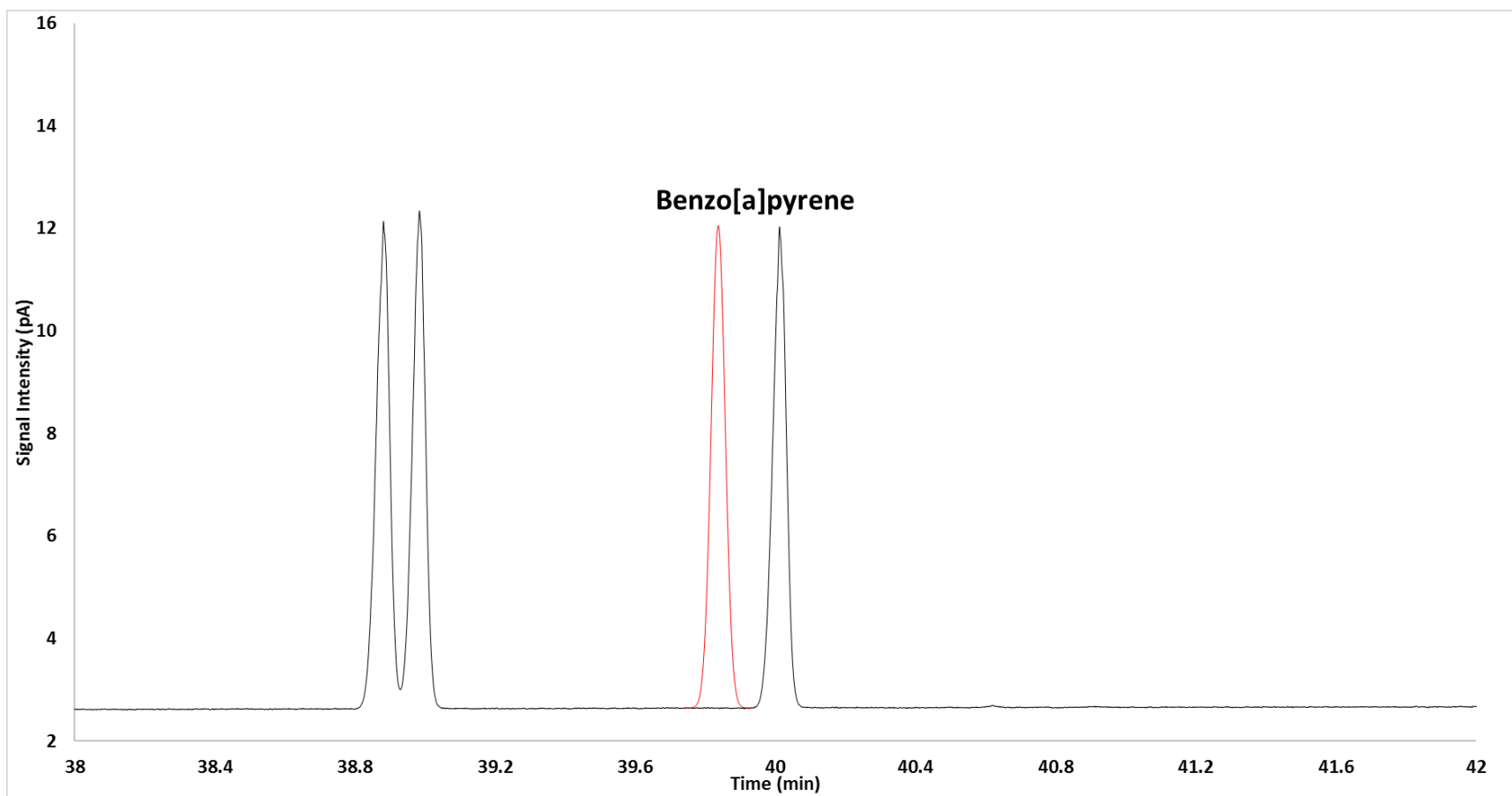
Figure 3-3E Close-up view (4 minute window) of benzo[a]pyrene predicted peak (traced in red) plotted along the experimental peak (right of predicted) at 5 °C/min.

Table 3-4 Experimental and predicted half height widths of PAHs separated on the target column. Predicted widths are in parentheses (*Italicized widths* were predicted using $\Phi = 1$, $\sigma_{extra}^2 = 0$ s^2, and ***Bold italicized widths*** were predicted using $\Phi = 0.78_7$, $\sigma_{extra}^2 = 0.017_7$ s^2)

Oven ramp rate (°C min^{-1})	Half height width (s)						
	Naphthalene	**Acenaphthyl-ene**	**Acenaphth-ene**	**Fluorene**	**Fluoranthene**	**Pyrene**	**Benzo[a]-pyrene**
5	1.82 (*1.70*, ***1.94***)	2.15 (*1.93*, ***2.19***)	2.11 (*1.95*, ***2.22***)	2.24 (*1.99*, ***2.27***)	2.32 (*2.16*, ***2.46***)	2.31 (*2.19*, ***2.48***)	2.48 (*2.42*, ***2.75***)
8	1.32 (*1.18*, ***1.36***)	1.44 (*1.30*, ***1.49***)	1.48 (*1.31*, ***1.50***)	1.46 (*1.33*, ***1.53***)	1.52 (*1.44*, ***1.65***)	1.61 (*1.46*, ***1.67***)	1.79 (*1.59*, ***1.82***)
10	1.12 (*0.99*, ***1.16***)	1.23 (*1.08*, ***1.26***)	1.24 (*1.09*, ***1.26***)	1.25 (*1.11*, ***1.29***)	1.39 (*1.20*, ***1.38***)	1.34 (*1.21*, ***1.40***)	1.47 (*1.31*, ***1.51***)
16	0.85 (*0.70*, ***0.85***)	0.89 (*0.75*, ***0.90***)	0.89 (*0.75*, ***0.91***)	0.89 (*0.76*, ***0.92***)	0.95 (*0.82*, ***0.98***)	0.94 (*0.83*, ***0.99***)	1.06 (*0.89*, ***1.05***)
20	0.72 (*0.60*, ***0.75***)	0.75 (*0.64*, ***0.79***)	0.75 (*0.64*, ***0.79***)	0.76 (*0.65*, ***0.80***)	0.83 (*0.70*, ***0.85***)	0.85 (*0.71*, ***0.86***)	0.89 (*0.74*, ***0.90***)

Table 3-5 Prediction errors of half height widths of PAHs separated on the target column. *Italicized errors* are from predictions using $\Phi = 1$, $\sigma_{extra}^2 = 0$ s^2 while ***bold italicized errors*** are from predictions using $\Phi = 0.78_7$, $\sigma_{extra}^2 = 0.17_7$ s^2

Oven ramp rate (°C min^{-1})	Prediction error in half height width (s)													
	Naphthalene		Acenaphthylene		Acenaphthene		Fluorene		Fluoranthene		Pyrene		Benzo[a]pyrene	
5	*-0.12*	***0.12***	*-0.22*	***0.05***	*-0.16*	***0.11***	*-0.25*	***0.03***	*-0.15*	***0.14***	*-0.13*	***0.17***	*-0.05*	***0.27***
8	*-0.14*	***0.04***	*-0.14*	***0.05***	*-0.17*	***0.03***	*-0.13*	***0.07***	*-0.07*	***0.14***	*-0.16*	***0.06***	*-0.20*	***0.03***
10	*-0.13*	***0.04***	*-0.15*	***0.02***	*-0.15*	***0.02***	*-0.14*	***0.03***	*-0.20*	***-0.01***	*-0.13*	***0.06***	*-0.16*	***0.04***
16	*-0.15*	***0.00***	*-0.14*	***0.01***	*-0.14*	***0.02***	*-0.12*	***0.03***	*-0.12*	***0.03***	*-0.11*	***0.05***	*-0.17*	***-0.01***
20	*-0.12*	***0.03***	*-0.11*	***0.04***	*-0.10*	***0.04***	*-0.11*	***0.04***	*-0.14*	***0.01***	*-0.14*	***0.01***	*-0.15*	***0.00***

Table 3-6 Experimental and predicted half height widths of Thermo. Sample Mix components separated on the target column under the same conditions are the PAHs. Predicted widths are in parentheses (*Italicized widths* were predicted using $\Phi = 1$, $\sigma_{extra}^2 = 0$ s^2, and ***Bold italicized widths*** were predicted using $\Phi = 0.78_7$, $\sigma_{extra}^2 = 0.017_7$ s^2)

Oven ramp rates (°C min^{-1})	Half height widths (s)					
	2-heptanone	**trans-5-decene**	**2-nonanol**	**methyl nonanoate**	**undecanal**	**n-pentadecane**
5	1.15 (*0.92*, ***1.08***)	1.44 (*1.28*, ***1.48***)	1.74 (*1.53*, ***1.75***)	1.90 (*1.70*, ***1.94***)	2.02 (*1.78*, ***2.03***)	2.20 (*1.90*, ***2.17***)
8	0.98 (*0.75*, ***0.90***)	1.12 (*0.95*, ***1.11***)	1.21 (*1.06*, ***1.24***)	1.33 (*1.15*, ***1.33***)	1.42 (*1.19*, ***1.38***)	1.47 (*1.25*, ***1.45***)
10	0.92 (*0.67*, ***0.81***)	0.97 (*0.82*, ***0.97***)	1.08 (*0.90*, ***1.06***)	1.13 (*0.96*, ***1.12***)	1.16 (*0.99*, ***1.16***)	1.21 (*1.04*, ***1.21***)
16	0.69 (*0.52*, ***0.67***)	0.74 (*0.60*, ***0.74***)	0.76 (*0.64*, ***0.78***)	0.80 (*0.66*, ***0.81***)	0.80 (*0.68*, ***0.83***)	0.83 (*0.71*, ***0.86***)
20	0.69 (*0.47*, ***0.61***)	0.63 (*0.52*, ***0.66***)	0.70 (*0.55*, ***0.69***)	0.65 (*0.57*, ***0.71***)	0.72 (*0.58*, ***0.73***)	0.76 (*0.60*, ***0.75***)

Table 3-7 Prediction errors of half height widths of Thermo. Sample Mix components separated on the target column under the same conditions are the PAHs. *Italicized errors* are from predictions using $\Phi = 1$, $\sigma_{extra}^2 = 0$ s^2 while ***bold italicized errors*** are from predictions using $\Phi = 0.78_7$, $\sigma_{extra}^2 = 0.17_7$ s^2

Oven ramp rate (°C min^{-1})	Prediction error in half height width (s)											
	2-heptanone		trans-5-decene		2-nonanol		methyl nonanoate		undecanal		n-pentadecane	
5	*-0.23*	***-0.06***	*-0.15*	***0.04***	*-0.21*	***0.01***	*-0.20*	***0.04***	*-0.24*	***0.01***	*-0.30*	***-0.03***
8	*-0.23*	***-0.08***	*-0.17*	***-0.01***	*-0.15*	***0.03***	*-0.18*	***0.00***	*-0.23*	***-0.04***	*-0.22*	***-0.03***
10	*-0.25*	***-0.10***	*-0.15*	***0.00***	*-0.18*	***-0.02***	*-0.17*	***0.00***	*-0.17*	***0.00***	*-0.18*	***-0.01***
16	*-0.17*	***-0.03***	*-0.14*	***0.00***	*-0.12*	***0.02***	*-0.13*	***0.01***	*-0.12*	***0.03***	*-0.12*	***0.03***
20	*-0.22*	***-0.07***	*-0.11*	***0.04***	*-0.15*	***0.00***	*-0.09*	***0.06***	*-0.14*	***0.00***	*-0.16*	***-0.01***

Table 3-8 Errors in predicted peak widths of Thermo. Sample Mix on the target column under the conditions in Table 3-1. *Italicized errors* are from predictions using $\Phi = 1$, $\sigma_{extra}^2 = 0$ s^2 while ***bold italicized errors*** are from predictions using $\Phi = 0.78_7$, $\sigma_{extra}^2 = 0.17_7$ s^2

Condition Label	Prediction errors (s)											
	2-heptanone		trans-5-decene		2-nonanol		methyl nonanoate		undecanal		n-pentadecane	
A	*-0.15*	***0.01***	*-0.11*	***0.06***	*-0.09*	***0.09***	*-0.11*	***0.07***	*-0.11*	***0.07***	*-0.12*	***0.06***
B	*-0.12*	***0.03***	*-0.09*	***0.07***	*-0.12*	***0.04***	*-0.13*	***0.04***	*-0.15*	***0.02***	*-0.20*	***-0.03***
C	*-0.20*	***-0.05***	*-0.16*	***0.01***	*-0.20*	***-0.01***	*-0.20*	***-0.01***	*-0.20*	***0.01***	*-0.26*	***-0.05***
D	*-0.16*	***0.00***	*-0.14*	***0.03***	*-0.12*	***0.04***	*-0.10*	***0.07***	*-0.05*	***0.12***	*-0.06*	***0.10***
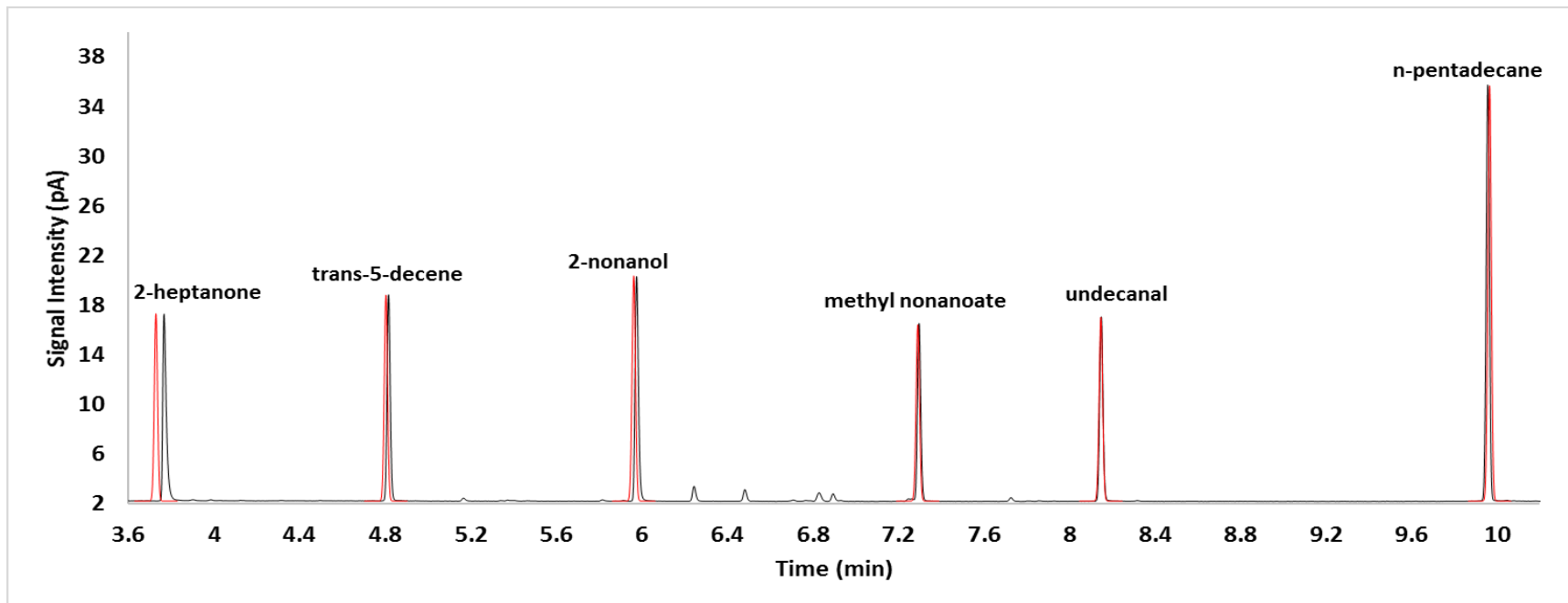
Figure 3-4A Chromatogram of the Thermo Sample Mix separated on the target system under Condition D in Table 3-1 (the conditions that most deviate from the conditions of the reference system). The black trace shows the experimental data while the red traces are predicted peaks
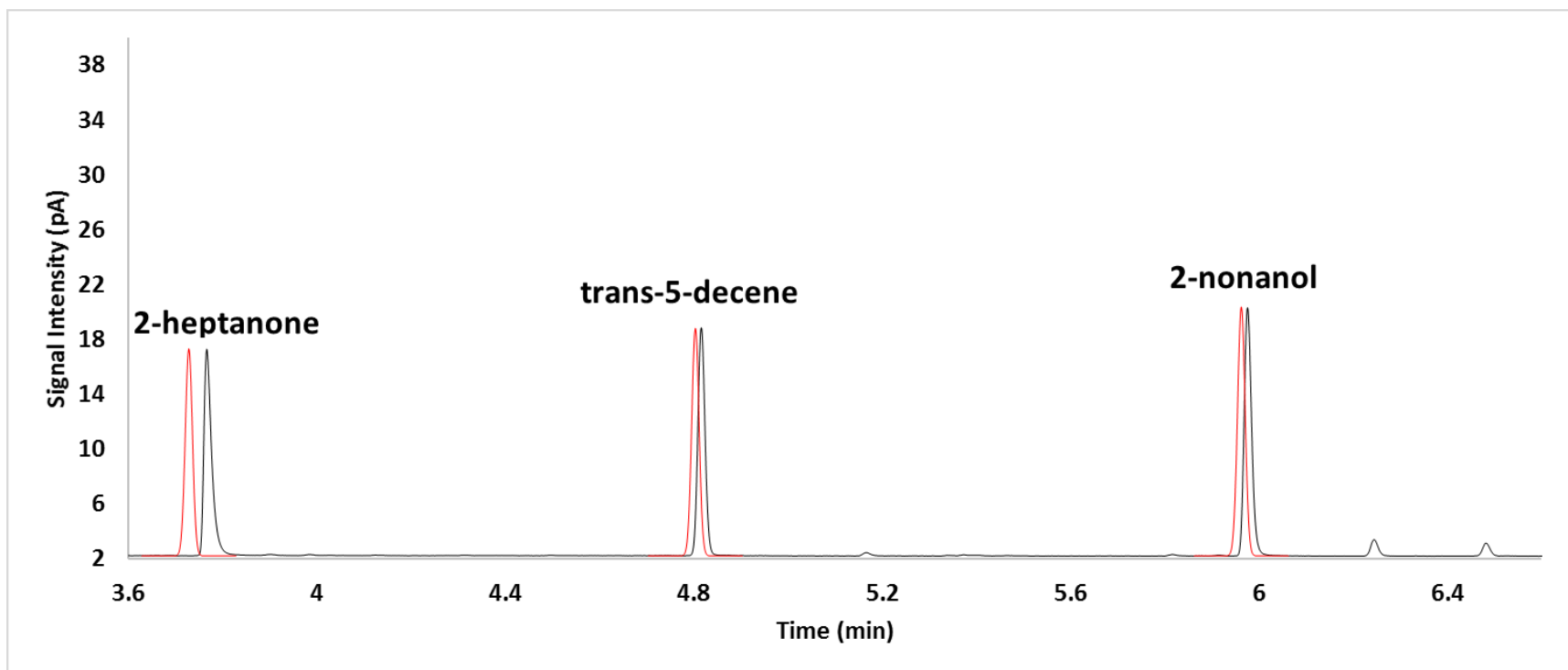
Figure 3-4B Close-up (3-minute window) of 2-heptanone, trans-5-decene and 2-nonanol separated on the target system under Condition D in Table 3-1 (the conditions that most deviate from the conditions of the reference system). The black trace shows the experimental data while the red traces are predicted peaks
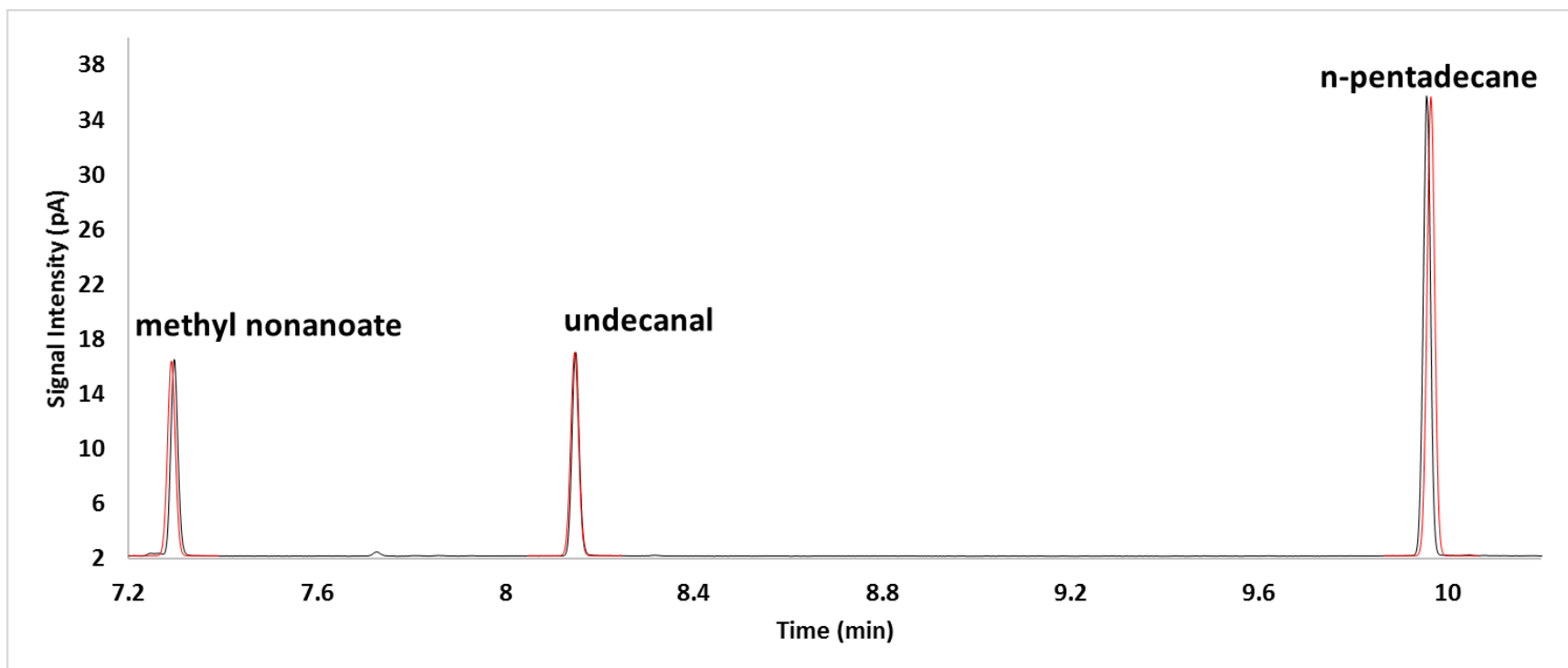
Figure 3-4C Close-up (3-minute window) of methyl nonanoate, undecanal and pentadecane separated on the target system under Condition D in Table 3-1 (the conditions that most deviate from the conditions of the reference system). The black trace shows the experimental data while the red traces are predicted peaks

3.3.3 The nature of the empirically determined $\sigma_{extra}{}^2$

As $\sigma_{extra}{}^2$ consists of all sources of extra-column peak variance it is expected to vary with factors such as total inlet flow, split vs splitless injection and detector make-up gas flow. Additionally, phenomena that might occur at the head of the column such as solvent or thermal focusing of analytes might also be captured by this term. As such, it is also expected to change with initial oven temperature and solvent polarity. With this is mind, it is important to understand that the approach used in this paper to determine the value of $\sigma_{extra}{}^2$ is not necessarily a means of finding the true extra-column peak variance for each individual peak in a separation under every feasible experimental condition. Instead, it provides a single empirical value that can serve as a practical representation of the average extra-column peak variance of a set of compounds in a separation over a range of conditions. This value, as demonstrated here, then acts as a regression parameter to permit more accurate predictions of peak width than those obtainable without the inclusion of the parameter. While there might be other approaches to calculating a value of $\sigma_{extra}{}^2$ the one presented here is demonstrated to provide acceptable prediction of peak width (typically < 5 % relative error) and complements our approach to retention time prediction, requiring minimal extra experimental effort on the part of the user. Investigations into the range of initial oven temperatures and flow rates that still produce acceptable peak width predictions remain for future study. Preliminary work shown here covers split injections over an initial temperature range of 35 °C to 50 °C and flow rates from ~1.0 mL min^{-1} to ~2.0 mL min^{-1}.

3.3.4 Errors in Φ and $\sigma_{extra}{}^2$

Φ and $\sigma_{extra}{}^2$, as calculated, in this paper rely on the use of experimentally determined peak widths and peak variances calculated under the assumption that the peaks are Gaussian. Both of

these factors introduce errors to the terms. It was observed that the value of experimentally determined peak width at half height for a given compound could change by up to 0.4 s depending on whether or not that peak was auto-integrated by GC software, manually integrated by the user or calculated using a peak finding function such as *findpeaks* in MATLAB. For this paper, we opted to use the peak widths as determined by auto-integration using ChemStation (Agilent Technologies) because it is expected that most users will auto-integrate their chromatograms (as this saves time and is usually good enough for most applications).

Although peak shapes other than Gaussian often better model chromatographic peaks, using another peak shape in the model would require users to determine (experimentally or otherwise) and input asymmetry parameters for each analyte of interest. This would add additional experiments and complexity to the model in order to account for these parameters and determine the best peak shapes to use, for little practical benefit. Even though all peaks predicted here were modelled assuming a Gaussian distribution prediction errors are still acceptable (< 5%) and generally are as good as and often better than predictions previously reported in the literature[51-53,55,57].

3.4 Conclusions

The ability to quickly and accurately predict retention times and peak widths in a GC separation is important for automated method development and optimization. The approach proposed here is fast - requiring the user of the target column to perform only five PTGC separations of a calibration mixture. It is also accurate – providing t_R prediction errors typically <1% and w_h prediction errors typically <5% even when the target column is of a different geometry and installed in a different system than the reference column. The models presented in this work, in

conjunction with our previously reported retention time prediction meet these requirements for speed and accuracy. This level of prediction accuracy in both retention time and peak width across systems, geometries and conditions meets, and in some instances surpasses, some of the best predictions noted in literature so far.

Chapter 4: Distribution-centric thermodynamics-based retention mapping of GC×GC separations

4.1 Introduction

Before developing a GC × GC method and optimizing its temperature and pneumatic parameters, the chromatographer has to answer some more fundamental questions. These include: "Which two stationary phase chemistries should I use for this analysis?" "Which phase ratios (of each chosen chemistry) would be ideal?" "Which phase should I use in which dimension?" By using distribution-centric thermodynamic parameters, we have developed a way of quickly answering these questions. The work presented in this chapter highlights the results of such efforts as well as initial attempts at predicting retention time in thermally modulated GC×GC experiments using distribution-centric parameters.

Throughout our group's history of exploring thermodynamics-based predictive modelling in GC and GC×GC [37,56,58,62-64,76,101,102,104] we have primarily relied on the use of the 3-parameter model based on the work of Clarke and Glew (Equation 3-2) [74] - an extension of the more popular 2-parameter *van't Hoff* model (Equation 4-1).

$$ln\, K = \frac{\Delta S}{R} - \frac{\Delta H}{RT} \qquad (4\text{-}1)$$

In Equation (4-1) above, the distribution coefficient of an analyte is defined with respect to temperature. R is the molar gas constant, ΔS is the entropy change associated with the partitioning of the analyte between the mobile and stationary phases and ΔH is the enthalpy associated with the same process. ΔS and ΔH, in this equation are assumed to be independent of

temperature, however this is not the case over the range of temperatures an analyte experiences in a typical GC experiment. If this assumption is made when applying the model to the prediction of retention times, the predicted times often show unacceptably large deviations from the experimentally determined values [50,56,78,113]. As such, our group, along with other researchers in the area [37,55,58,61-64,75-77,100,110,114], opt for the three-parameter model, shown below. This model has been demonstrated to provide more accurate predictions of retention than its two-parameter predecessor does.

$$ln\,K = A + \frac{B}{T} + C\,ln\,T \tag{4-2}$$

A, B and C are typically acquired through curve-fitting/numerical optimization procedures and the determination of their values is essentially all that is required to apply the model to predicting retention times and peak widths. These parameters acquire some chromatographic meaning when defined in terms of thermodynamically meaningful parameters.

$$A = \frac{\Delta S(T_0) - \Delta C_p\,ln\,T_0 - \Delta C_p}{R} \tag{4-3}$$

$$B = -\frac{\Delta H(T_0) - \Delta C_p T_0}{R} \tag{4-4}$$

$$C = \frac{\Delta C_p}{R} \tag{4-5}$$

In these equations, ΔS and ΔH are defined at some arbitrary reference temperature, T_0 (usually at about 90 °C in our group's previous work). When presented in this manner, Equation 4-2 and its parameters may be described as temperature-centric (T-centric).

Although this T-centric approach to thermodynamic modelling of retention in GC systems is useful and justified, it falls short in some regards, as discussed by L.M. Blumberg in his 2017 paper on "Distribution-centric 3-parameter thermodynamic models of partition gas chromatography" [61]. In that work, he not only discusses the limitations of the T-centric model but proposes a distribution-centric (K-centric) approach as a more meaningful alternative.

From Equations 4-3 to 4-5, one can note that the values of $\Delta S(T_0)$ and $\Delta H(T_0)$ depend on the arbitrarily chosen value of T_0. As such, when estimating these parameters for many analytes, it is often desirable and computationally efficient to select the same T_0 for each calculation. Unfortunately, at any chosen T_0 there will be analytes for which their retention factors, k, are chromatographically meaningless. If we take, for instance, a small, highly volatile molecule like butane (boiling point of about -1 °C) and inject it unto a highly polar, wall-coated ionic liquid column at 90 °C (the T_0 that we have used in previous work), butane would have a vanishingly small value for k. It would essentially pass through the column with little-to-no interaction with the stationary phase. One could not fairly describe butane's progression through the column as chromatography. On the other hand, a large heavy PAH such as benzo[a]pyrene (boiling point 495 °C) injected onto a poly(90% biscyanopropyl/10% cyanopropylphenyl siloxane) column would be expected to have a k so large at 90 °C that it would focus at the head of the column, and remain there indefinitely. Given these two common scenarios, an alternative and more meaningful approach would be to chose instead the same reference distribution coefficient, K_0 for all analytes and calculate a different T_0 for each compound such that $T_0 = T|_{K_0}$ (the temperature at which $K = K_0$). This would result in parameters that are analyte-dependent and as such are more relevant for the analyte(s) under consideration.

For the sake of clarity and out of respect for the nomenclature laid out in Dr. Blumberg's paper [61], I will be using the subscript "$_{ref}$" to denote T-centric parameters and "$_{Ref}$" to denote K-centric parameters. Going forward, $T_0 = T_{ref}$, $K_0 = K_{Ref}$ and $T|_{K0} = T_{Ref}$. The same notation applies to the thermodynamic parameters (i.e. $\Delta S(T_0) = \Delta S_{ref}$, $\Delta H(T_0) = \Delta H_{ref}$ while $\Delta S(T|_{K0}) = \Delta S_{Ref}$ and $\Delta H(T|_{K0}) = \Delta H_{Ref}$).

Using this nomenclature, combining Equations 4-2 to 4-5 then expressing them in a K-centric form results in Equation 4-6 below (see Dr. Blumberg's paper for extensive and detailed mathematical derivations [61]).

$$ln\,K = \frac{\Delta S_{Ref}}{R} - \frac{\Delta H_{Ref}}{RT} + \frac{\Delta C_p}{RT}\left(T - \frac{\Delta H_{Ref}}{\Delta S_{Ref} - R\,ln\,K_{Ref}}\right) + \frac{\Delta C_p}{R}\,ln\left(\frac{(\Delta S_{Ref} - R\,ln\,K_{Ref})T}{\Delta H_{Ref}}\right) \tag{4-6}$$

It is prudent, at this stage, to introduce another important parameter. That is the thermal constant of analyte-column interaction, θ. It is analogous to parameters such as time constants or half-lives and represents the temperature change in either direction that would cause an e-fold (Euler's number ~ 2.72) change in k in the opposite direction. It may be defined as [115,116]:

$$\theta = -\left(\frac{d\,ln\,k}{dT}\right)^{-1} \tag{4-7}$$

θ is a very convenient and versatile parameter as it represents the slope of expressions for k vs T and always has the same value regardless of how they are expressed (e.g. k vs T, $ln\,k$ vs T, $log\,k$ vs T, etc). When written as shown in Equation 4-7, it has the convenient units of temperature (°C) and is a positive quantity.

In a T-centric model, θ at any temperature can be obtained from:

$$\theta \;=\; \frac{-RT^2}{\Delta H(T_{ref}) + \Delta C_p(T - T_{ref})} \tag{4-8}$$

At T_{ref}:

$$\theta_{ref} \;=\; -\frac{RT_{ref}^2}{\Delta H_{ref}} \tag{4-9}$$

while at T_{Ref} (in a K-centric model):

$$\theta_{Ref} \;=\; -\frac{RT_{Ref}^2}{\Delta H_{Ref}} \tag{4-10}$$

Again, detailed mathematical derivations of these equations may be found in [61]. θ will prove very important in the work that follows.

Now that an argument has been put forward for using K-centric models, the question of where to set K_{Ref} when applying these models needs to be answered. For now (for mathematical simplicity), K_{Ref} can be set to a temperature, for each analyte, that results in $k = 1$. That is to say, set K_{Ref} such that at T_{Ref}, $k = k_{Ref} = 1$. Recall that,

$$K = k\beta \tag{4-11}$$

where β is the column phase ratio. Therefore when $k = 1$, $K = \beta$. Also, by combining equations 4-2 and 4-11 we can see that when $k = 1$, $ln(k) = 0$. We can therefore obtain T_{Ref} when $k = 1$ from the x-intercept of the plot of $ln(k)$ vs. T. T_{Ref} when $k = 1$ can similarly be obtained by way of the Lambert W function (used and discussed in [61]). This function, while arguably more mathematically elegant than solving a plot of $ln\ k$ vs T, is not readily accessible or intuitive to practicing chemists. As such, I will forgo any description of its details here.

When defined at $k = 1$, T_{Ref} is termed the characteristic temperature, T_{char} (i.e. $T_{char} = T_{Ref}|_{k=1}$). At T_{char}, $\theta = \theta_{char}$ and is termed the characteristic thermal constant[61,115]. Both T_{char} and θ_{char} are analyte-column-dependent K-centric thermodynamic parameters and are of fundamental importance to the work in this chapter.

How do these K-centric characteristic parameters help us map distribution in GC×GC separations? Firstly, during a single-ramp temperature-programmed GC separation, all analytes elute from the column with about the same retention factor [115,117]. Furthermore, the elution temperature of an analyte in a GC experiment, T_e is strongly correlated with its characteristic temperature, T_{char} [61] (generally, T_e increases with increasing T_{char}). For closely eluting analytes, the difference in their elution temperatures is related to their respective θ_{char} [116]. Deviations from these trends are relatively minor and previous studies have suggested that at any heating rate, analytes elute in order of increasing T_{char} [61,116]. With this in mind, I hypothesized that characteristic parameters for a given set of analytes can be used to provide a map of how analytes will distribute across the in a GC×GC separation. It might also be possible to use characteristic parameters to obtain accurate predictions of retention time in GC×GC separations, allowing for fast and easy method development and optimization for what is usually a complex technique to optimize [39].

Following many conversations with Dr. Blumberg, I designed a set of experiments aimed at evaluating whether or not a map created using my existing thermodynamics-based parameters, A, B and C, to calculate K-centric characteristic parameters, T_{char} and θ_{char} would be similar to a GC×GC chromatogram in which analytes were forced to elute with $T_e = T_{char}$. As it turns out, at a ramp rate of about 18 °C per dead time (void time) measured at 150 °C, $t_{M150°C}$, analytes typically elute with $k \approx 1$. There are, of course, some assumptions being made that guide this choice of

ramp rate, but it still served as a useful starting point for designing these experiments. In order to discuss these assumptions, it is important to introduce the concept of characteristic heating rate [115]. The temperature during single ramp temperature-programmed GC experiment can be defined as:

$$T = T_i + R_T t \tag{4-12}$$

where T_i is the initial oven temperature, R_T is the oven ramp rate (in °C min^{-1}) and t is time (min). Characteristic thermal constants may be used as basic temperature units [115] and void times may be used as basic time units [118] and together help define a characteristic heating rate:

$$R_{T,char} = \frac{\theta_{char}}{t_M} \tag{4-13}$$

The ratio $R_T/R_{T,char}$, termed the dimensionless heating rate is given by:

$$r = \frac{R_T}{R_{T,char}} \tag{4-14}$$

Data from previous studies of initially well-retained analytes (i.e. those with $k \geq 3$ at T_i), with θ_{char} ~30 °C (a typical θ_{char} for silicone based stationary phased having $\beta = 250$), show that a dimensionless heating rate of ~0.6 results in elution with $k \approx 1$ [115,118]. Plugging these values into equation 4-14 yields 18 °C t_M^{-1} as an appropriate characteristic heating rate for experimentally exploring the behaviour of these maps.

Furthermore, the retention factor of a compound at T_i, k_i, can be described by [115]:

$$ln\,(k_i) = -\frac{T_i - T_{char}}{\theta_{char}} \tag{4-15}$$

In the case of a secondary column in a GC×GC experiment, the separation is considered to be so fast that it is essentially isothermal (normally taking place in < 2 s). As such, the initial temperature of a compound entering the second dimension (eluting from the first dimension at T_{char} for the first dimension column, $^{1}T_{char}$) is $^{1}T_{char}$. We can therefore substitute T_{i} in equation 4-15 above with $^{1}T_{char}$, T_{char} with $^{2}T_{char}$ and θ_{char} with $^{2}\theta_{char}$. The resulting equation provides the retention factor of an analyte on the secondary column during a fast, effectively isothermal separation, ^{2}k:

$$ln\,(^{2}k) = -(^{1}T_{char} - {^{2}T_{char}})\,/^{2}\theta_{char} \qquad (4\text{-}16)$$

Once the similarities and differences between the maps generated from these equations and the experimental data had been evaluated, I proceeded to create similar theoretical maps for different combinations of stationary phase ratios and different configurations of stationary phases.

Following some preliminary and somewhat rudimentary investigations into these maps for one set of phase chemistries, I refined the experiments to permit the investigation of the maps' performance across other stationary phase chemistries (with difference selectivities) and over a broader range of analyte functionalities. I also experimentally investigated the effect of changing phase ratios and column configuration on the quality and usefulness of the maps.

Lastly, because GC×GC experiments do not often occur at 18 °C t_M^{-1}, I designed and executed an experiment aimed at assessing the usefulness of the characteristic parameter maps for mapping GC×GC under normal conditions and predicting accurate GC×GC retention times. Essentially, I used our existing tools to predict the first-dimension retention time under normal conditions. Then, from this predicted time, I calculated the elution temperature of each analyte from the first dimension column, $^{1}T_{e}$. Then by substituting $^{1}T_{e}$ for $^{1}T_{char}$ in equation 4-16, I calculated $ln\,(^{2}k)$.

Assuming the second dimension separation is isothermal and correcting for analyte travel through the transfer line connecting the secondary column to the detector, $^t t_M$:

$$^2 t_R \;=\; {}^2 t_M \,({}^2 k + 1) \;+\; {}^t t_M \tag{4-17}$$

The K-centric approach to thermodynamic modelling is the basis of the work presented in this chapter – the product of a conversation between Dr. Blumberg, my supervisor and myself. That conversation led to a collaborative effort towards exploring the use of a K-centric parameters in GC×GC retention mapping and prediction.

4.2 Experimental

4.2.1 Preliminary Investigations using Rtx-5 and Stabilwax

4.2.1.1 Standards

A Programmed Test Mix (Sigma-Aldrich, Oakville, ON, Canada) was diluted 1 in 4 in dichloromethane (Sigma-Aldrich) so that the concentrations of its components ranged from about 70 µg mL^{-1} to 133 µg mL^{-1}. This mixture was separated under the GC×GC conditions described below. The following compounds from this mixture were used for this study: decane, 1-octanol, undecane, 2,6-dimethylaniline, methyl decanoate and methyl dodecanoate.

A diesel range organics mixture (DRO) (Restek Corportation, Bellefonte, PA, USA) was diluted to give concentrations of about 100 µg mL^{-1} in dichloromethane (Sigma-Aldrich) and separated under the conditions described below. From this mixture, the following components were chosen for this study: dodecane, tetradecane, hexadecane, octadecane and eicosane.

Five other compounds from existing in-house solutions were chosen and diluted to about 100 µg mL^{-1} in dichloromethane. These included, 2,4-dichlorobenzyl alcohol, 4-tert-butylphenol, 2,3-

dimethylaniline. p-ethylaniline and N-ethylaniline. Each of these were separated as one component mixtures under the conditions described below.

4.2.1.2 Instrumentation

All separations were carried out using an Agilent 7890A gas chromatograph (Agilent Technologies, Mississauga, ON) equipped with a split/splitless injector, flame ionization detector and a consumable-free dual stage/quad-jet thermal modulator (Leco Corporation, St. Joseph, MI, USA). Injections of 1 μL were performed in split mode using a split ratio of 25:1, an inlet temperature of 275 ºC and He carrier gas (5.0 grade, Praxair, Edmonton, AB). The inlet was operated at a constant pressure of 25.199 psi (gauge). The primary column was an Rtx-5 (Restek Corperation) (25.2 m × 0.25 mm; 0.25 μm d_f; 5% diphenyl 95% dimethyl polysiloxane). A Stabilwax column (Restek Corperation) (0.6 m × 0.25 mm; 0.25 μm d_f; polyethylene glycol) served as the second dimension column. A transfer line made of inert fused silica (0.2 m × 0.2 mm) connected the secondary column to the detector (FID acquiring at 200 Hz). For these experiments, any compounds eluting within the first three void times (3 × t_M measured at 150 °C at the 25.199 psi (gauge)) of the column system were considered as having too little retention on the primary stationary phase at the initial temperature for the model to be applicable to them, and as such, were not to be included in calculations carried out on the data. Additionally, for mathematical simplicity, temperature ramps were programmed in a way that allowed the primary oven, modulator and secondary oven to be at about the same temperature following the initial hold of three void times. The primary oven was held at an initial temperature of 40 °C for 2.65 minutes then ramped at 20.39 °C min^{-1} (18 °C $t_M$$^{-1}$) to 250 °C where it was held for 10 minutes. The modulator and secondary oven were also ramped at the same rate to 250 °C where they were held for 10 minutes. However, their initial temperatures differed from the primary oven and from

each other because the software associated with this system demands an initial offset of at least 3 °C between the primary and secondary ovens, and at least 8 °C between the primary oven and the modulator. Therefore, the modulator was set to an initial temperature of 45 °C for 2.90 minutes and the secondary oven was set to an initial temperature of 48 °C for 3.04 minutes. This way, after 3.04 min, all three of these heated zones would be at about the same temperature (48 °C) until the end of the run. A modulation period, P_M, of 15 s was used with a hot pulse time of 3.75 s. This is an unusually large modulation period and would be unideal for the analysis of an actual sample, but was used to prevent molecules from wrapping around in the second dimension, allowing a fair comparison between the distribution of the peaks in the experimental data and the map that would be produced from the characteristic parameters.

4.2.2 Experimental exploration of other stationary phase and analyte chemistries, and the effects of changing phase ratios

4.2.2.1 Standards

A Programmed Test Mix (Sigma-Aldrich, Oakville, ON, Canada) was diluted 1 in 4 in dichloromethane (Sigma-Aldrich) so that the concentrations of its components ranged from about 70 µg mL^{-1} to 133 µg mL^{-1}. This mixture was separated under the GC×GC conditions described below. The following compounds from this mixture were used for this study: decane, 1-octanol, undecane, 2,6-dimethylaniline, methyl decanoate and methyl dodecanoate.

A diesel range organics mixture (DRO) (Restek Corportation, Bellefonte, PA, USA) was diluted to give concentrations of about 100 µg mL^{-1} in dichloromethane (Sigma-Aldrich) and separated under the conditions described below. From this mixture, the following components were chosen for this study: dodecane, tetradecane, hexadecane, octadecane and eicosane.

Twenty-eight other compounds from existing in-house solutions were chosen and diluted to about 100 µg mL^{-1} in dichloromethane. These included, 1,4-dimethylnaphthalene, 1-tetradecanol, 2,3-dimethylaniline, 2,5-dichlorophenol, 2,6-dichlorophenol, 2-decanone, 2-heptanone, 2-nonanol, 2-nonanone, 2-octanone. 2-tridecanone, 3-octanone, 3-tert-butylphenol, 4-sec-butylphenol, 4-tert-butylphenol, 5-nonanol, anthracene, bipheyl, decanal, naphthalene, N-ethylaniline, octanal, p-ethylaniline, phenanthrene, tributylphosphate, trimethylphosphate, tripropylphosphate and undecanal. Analyte chemistries represented here, which were not represented in the preliminary investigations include, polyaromatic hydrocarbons (PAHs), biphenyl, aldehydes, ketones and trialkylphosphates.

4.2.2.2 Instrumentation

All separations were carried out using an Agilent 7890A gas chromatograph (Agilent Technologies, Mississauga, ON) equipped with a split/splitless injector, flame ionization detector and a consumable-free dual stage/quad-jet thermal modulator (Leco Corporation, St. Joseph, MI, USA). Injections of 1 µL were performed in split mode using a split ratio of 25:1, an inlet temperature of 275 ºC and He carrier gas (5.0 grade, Praxair, Edmonton, AB). The inlet was operated in constant flow mode at 2.0 mL min^{-1} to assess if the model still generates good maps under pneumatic conditions similar to normal GC×GC runs. Five different stationary phase combinations were studied and are shown in Table 4-1 along with the oven ramp rates that corresponded to 18 °C t_M^{-1} for that combination. Every chromatographic column used had an inner diameter of 0.25 mm. For each combination, a fused silica transfer line of 0.18 m × 0.2 mm connected the secondary column to the detector (FID collecting at 200 Hz)

Table 4-1 Five GC×GC stationary phase configurations upon which separations were performed

Combination	1° column	2° column	1° Length (m)	2° Length (m)	1° d_f (µm)	2° d_f (µm)	Ramp rate (°C min^{-1})
A	Rtx-5MS	Rtx-200MS	30.55	0.34	0.25	0.25	16.05
B	Rtx-5MS	Rtx-200	30.55	0.34	0.25	0.50	16.05
C	Rtx-5MS	Rtx-200MS	30.55	0.35	0.50	0.25	23.26
D	Rtx-200MS	Rtx-5MS	24.7	0.35	0.25	0.25	19.30
E	Rtx-5MS	Rxi-17Sil MS	30.55	0.35	0.25	0.25	16.05

For these experiments, any compounds eluting within the first three void times ($3 \times t_M$ measured at 150 °C at 2.0 mL min^{-1}) of the column system were considered as having too little retention on the primary stationary phase at the initial temperature for the model to be applied. Thus these compounds were excluded from further analysis. Additionally, for the sake of mathematical simplicity, temperature ramps were programmed in a way that allowed the primary oven, modulator and secondary oven to be at about the same temperature following the initial hold of three void times. For each combination, the primary oven was held at an initial temperature of 40 °C for 3 void times then ramped at 18 °C t_M^{-1} to 320 °C with Rtx-200(MS) secondary columns and 330 °C with Rtx-5 or Rxi-17Sil MS secondary columns, and held for 10 minutes. The modulator and secondary oven were also ramped at the same rate to the same final temperatures °C where they were held for 10 minutes. However, their initial temperatures differed from the primary oven and from each other because the software associated with this system demands an offset of at least 3 °C between the primary and secondary ovens, and at least 8 °C between the primary oven and the modulator. Therefore, the modulator was set to an initial temperature of 45 °C and the secondary oven was set to an initial temperature of 48 °C. Both

were held so that all three of these heated zones would be at about the same temperature from 48 °C until the end of the run. Modulation periods, P_M of 1.5 s were used for combinations A, B and E with a hot pulse time of 0.3 s; for combinations C and D, P_M of 2.0 s was used with a hot pulse time of 0.4 s (this larger P_M was used to avoid wrap around on secondary stationary phases expected to have stronger retention). By using these modulation periods, conditions are closer to those under which GC×GC experiments are usually performed. Wrap around was avoided by using shorter secondary columns this time (0.34-0.35 m instead of 0.6 m).

4.2.3 Mapping more typical GC×GC conditions – a first step towards accurate prediction

4.2.3.1 Standards

The standards used for these experiments were the same as described in section 4.2.2.1. However, only 26 molecules were run (this was because the instrument needed to be shut down, uninstalled and the laboratory moved to a new location, before all runs could be completed). The 26 molecules include, 1-octanol, 2,6-dimethylaniline, 2-decanone, 2-heptanone, 2-nonanone, 2-octanone, 2-tridecanone, 3-octanone, 5-nonanol, biphenyl, decanal, decane, dodecane, eicosane, hexadecane, methyl decanoate, methyl dodecanoate, naphthalene, octadecane, octanal, tetradecane, tributylphosphate, trimethylphosphate, tripropylphosphate, undecanal and undecane.

4.2.3.2 Instrumentation

The same instrumentation described in section 4.2.2.2 was used for these experiments. The column combination used was Combination A in Table 4-1 and all experimental conditions were as described for that combination in section 4.2.2.2 with the exception of oven programs. The primary oven was programmed from 40 °C (held for 3.86 min) to 320 °C (no hold) at 8.94 °C

min^{-1} (corresponding approximately to optimal heating rate [119], 10 °C t$_M$$^{-1}$; t$_m$ measured at 150 °C at 2.0 mL min^{-1} – approximately speed optimized flow [120,121]). The secondary oven was ramped at the same rate, 8.94 °C min^{-1} but held at an initial temperature of 45 °C for 3.67 min. The modulator was similarly ramped at 8.94 °C min^{-1} but held at an initial temperature of 48 °C for 3.86 min. These three heated zones were kept at about the same temperature from 48 °C to 320 °C.

4.3 Results and Discussion

4.3.1 Preliminary investigations using Rtx-5 and Stabilwax

In order to assess the feasibility of using characteristic parameters to map compound distribution in GC×GC space, experiments were performed to cause molecules to elute from the primary column at approximately their characteristic temperatures. Rtx-5MS and Stabilwax columns were chosen as they represent two very distant column polarities that are commonly used in GC×GC analyses. They were installed in an apolar/polar configuration as this is the most common configuration used (i.e. placing the column that is expected to do the bulk of the separation in the first dimension). Typically, columns with a small β are used to separate highly volatile compounds, as they encourage retention in the (often thicker) stationary phase while columns with large β are ideal for separating high molecular mass compounds that are prone to late elution as a result of high retention. As these experiments served as a proof of concept, a phase ratio of 250 was chosen for each column. This is a common middle-of-the road phase ratio for separating compounds across a range of more moderate volatilities and retentions, and often serves as a starting point in method development, particularly with untargeted/exploratory analyses. Sixteen compounds covering a variety of boiling points and intermolecular interactions

were chosen to evaluate the behaviour of the parameters across a range of elution temperatures and analyte chemistries.

Table 4-2 contains the calculated characteristic parameters for each compound on each stationary phase as well as the actual temperatures at which they eluted from the primary column. Additionally, it contains an estimation of their retention factors on the secondary column which is useful for generating a map of their distribution on this system for comparison with experimental results. Each compound was assigned a number, so that its location on the map and in the experimental chromatogram can be easily labeled.

Table 4-2 shows that most of the compounds investigated eluted within less than 4 °C of their $T_{char5\%}$ (< 11.8 s of their expected retention time). Hexadecane, eicosane and methyl dodecanoate, however, eluted within 5.2, 9.1 and 4.1 °C of the respective $T_{char5\%}$. Elution temperatures, $T_{e5\%}$ were calculated using first dimension retention times, ^1t_R, as attained from the peak tables in LECO ChromaTOF (LECO Coperation) and the experimental oven temperature ramp rate. These deviations appear particularly large on the surface and might seem to suggest that this approach is unreliable. The magnitude of the deviations also vary quite a bit from molecule to molecule (-0.1 °C to 9.1 °C, -0.3 s to 26.8 s) with no clear trend between the deviations and the type of molecule or its experimentally determined retention parameters. However, several things should be kept in mind when interpreting these numbers. 1) In order to avoid wrap-around, an unusually large modulation period, P_M, of 15 s was used. As ^1t_R is quantized by retention time, it is expected that the true first dimension retention times for some molecules could be very different from the ^1t_R recorded in the peak tables after data processing (i.e. the ^1t_R used to calculate $T_{e5\%}$). 2) The experiment was designed using 30 °C as an average characteristic thermal constant, θ_{char5}, for most molecules, leading to a ramp rate of

approximately 18 °C/$t_{M(150°C)}$ being chosen as the condition that causes molecules to elute at approximately $T_{char5\%}$ (with k=1). Table 4-2 shows that $\theta_{char5\%}$ for these molecules range from 29.7 to 36.1. This means, that some molecules may in fact elute with $k \neq 1$. 3) The characteristic parameters were not calculated with the intention of accurately predicting retention times (at this stage) nor were the experiments designed to assess their ability to do so. Instead, they were calculated to serve as a means of mapping the distribution of molecules in a GC×GC space with the aim of

Table 4-2 Calculated characteristic parameters and experimental retention information for 16 compounds separated on an Rtx-5 1° column and a Stabilwax 2 ° column (both with $\beta = 250$) at 18 °C/$t_{M(150\,°C)}$. $T_{char5\%}$: characteristic temperature on Rtx-5, T_{charw}: characteristic temperature on Stabilwax, $T_{e5\%}$: experimental elution temperature on Rtx-5, $\theta_{char5\%}$: characteristic thermal constant on Rtx-5, θ_{charw}: characteristic thermal constant on Stabilwax, ^2k_w: estimated retention factor on Stabilwax 2° column.

Compound	Assigned number	^1t_R (s)	^2t_R (s)	$T_{char5\%}$ (°C)	$T_{e5\%}$ (°C)	$T_{e5\%}$ - $T_{char5\%}$ (°C)	T_{charw} (°C)	$\theta_{char5\%}$ (°C)	θ_{charw} (°C)	^2k_w
decane	1	352	0.71	107.8	105.6	-2.2	58.5	29.7	24.9	0.14
1-octanol	2	397	1.55	120.1	120.9	0.7	147.0	30.4	28.8	2.54
undecane	3	412	0.76	125.2	126.0	0.8	75.9	30.5	25.7	0.15
2,6-dimethylaniline	4	457	2.29	140.9	141.3	0.4	186.9	34.1	34.7	3.77
methyl decanoate	5	517	1.04	160.5	161.7	1.1	151.4	32.3	30.1	0.74
methyl dodecanoate	6	607	1.06	188.2	192.2	4.1	177.0	33.7	31.2	0.70
dodecane	7	457	0.81	141.3	141.3	-0.1	90.5	31.3	25.7	0.14
tetradecane	8	547	0.86	171.0	171.9	0.9	120.6	32.6	27.0	0.15
hexadecane	9	637	0.90	197.3	202.4	5.2	147.8	33.7	28.2	0.17
octadecane	10	697	0.96	220.0	222.8	2.8	172.5	33.3	29.3	0.20
eicosane	11	772	1.00	239.2	248.3	9.1	195.1	30.6	30.3	0.23
2,4-dichlorobenzyl alcohol	12	562	4.13	175.4	177.0	1.5	243.4	36.1	34.9	7.03
4-tert-butylphenol	13	517	4.61	158.0	161.7	3.7	229.0	33.8	33.3	8.47
2,3-dimethylaniline	14	472	2.73	146.6	146.4	-0.2	198.5	34.5	35.4	4.34
p-ethylaniline	15	457	2.79	140.1	141.3	1.1	192.9	33.6	34.3	4.66
N-ethylaniline	16	427	2.11	133.4	131.1	-2.3	170.5	32.9	32.6	3.13

guiding the choice of column chemistries, configuration and phase ratios. While, they would be better at doing this were they capable of accurately predicting retention times, at this stage in the project, this was not the goal.

With this in mind, a series of plots were generated to enable a visual assessment of how useful these parameters were for their intended purpose. Figure 4-1 plots the characteristic temperatures of each compound on both dimensions. A great deal of information is contained within this plot, although extracting said information at a glance is admittedly unintuitive. The figure gives a partial representation as to how these compounds would distribute in a chromatographic space, based on their characteristic temperatures only, using these column sets in this configuration. The solid and dashed black lines were added to relate their positions to their retention factors on the second dimension. The solid black line is the "k=1" line, along which the characteristic temperatures of compounds on both columns would be equal. As such, any compound that fell along this line would be expected to elute from the second dimension column with a retention factor of 1. The topmost dashed line is the "k=2.72" line and lies at a vertical distance of about θ_{charw} above the k=1 line. Recall that θ_{char} is the temperature change that would cause an e-fold change in k of a compound at its T_{char}. This means that compounds sitting along this line would elute from the secondary column with a k of 2.72 upon eluting from the primary with a k of 1. A secondary oven offset of $+\theta_{charw}$, ~ +25 to 30 °C (depending on the compound) would be expected to cause these compounds to elute from the secondary column at their characteristic temperatures. The inverse can be said for the "k=0.37" line; compounds sitting along this line elute with k of about 0.37 on the secondary column and secondary oven offset of $-\theta_{charw}$, ~ -25 to -30 °C (depending on the compound) would allow them to be better retained and elute with k=1. Keep in mind that there are practical limitations to doing this proposed separation, as no

commercially available systems allow the secondary oven to operate at a temperature below the primary oven. Also, polymer temperature stability limits restrict the range of temperatures at which analyses can be performed. More diagonal lines of this nature can be generated for a range of k values and the line upon which a compound falls tells us a great deal about its retention behavior on the secondary column. From this figure, we not only acquire insight into the distribution of these molecules but a guide for influencing oven conditions in a thermally modulated GC×GC experiment to target analytes based on their calculated T_{char}. It is important to note that these lines are not parallel as θ_{char} tends to increase with T_{char}, so the vertical spacing between the lines becomes wider at higher T_{char}. As mentioned, figures like this may prove unintuitive to read, even for the experienced GC×GC chemist. Fortunately, with a 45 ° clockwise rotation of the plane, Figure 4-1 can be transformed into something that closer resembles the way chromatographers normally represent separations. This is done mathematically by subtracting $T_{char5\%}$ from T_{charw} then plotting the resulting values against $T_{char5\%}$. The result is Figure 4-2 in which the $k = 1$ line is now the x-axis. However, because the k lines were not parallel to begin with and θ_{char} (the vertical distance between them) increases with T_{char}, this figure on its own neither gives a true picture of distribution nor an easily interpretable visualization thereof. In order to acquire a parameter that gives a more meaningful interpretation of this data, and to visually account for this variation in characteristic thermal constant, the y-axis values of Figure 4-2 for each compound is normalized by the compounds θ_{charw} (equation 4-15). This number then serves as the exponent for e, yielding ^2k_w, the second dimension retention factor
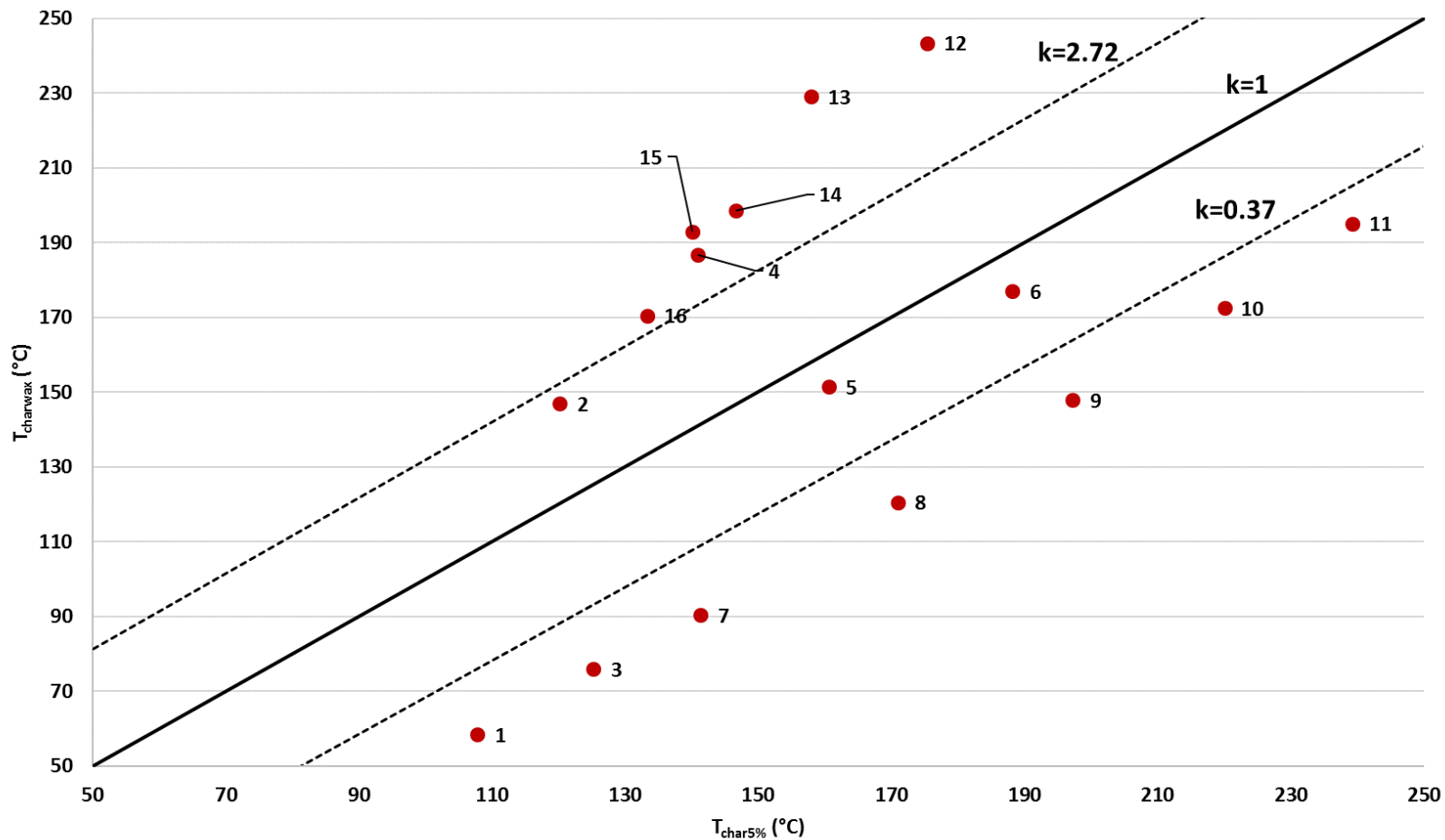
Figure 4-1 Characteristic temperatures of the sixteen compounds. Were a compound to elute from the second dimension having $k = 1$, it would fall on the solid black line. The dashed lines correspond to e-fold changes in k and their vertical distances from the $k = 1$ line indicate the temperature change required for a compound to elute from the second dimension column with $k = 1$.
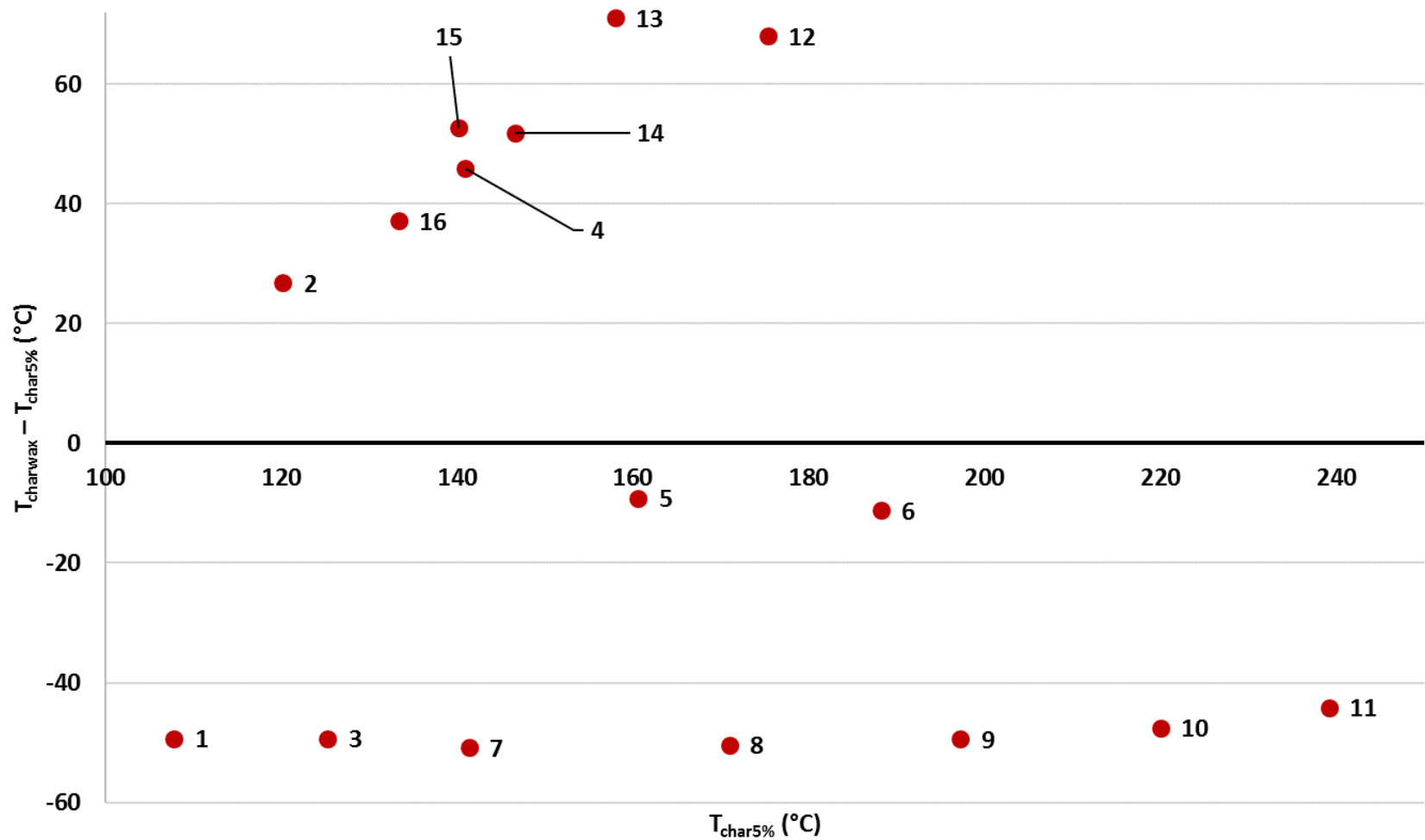
Figure 4-2 Characteristic temperatures transformed so that the *k*=1 line is horizontal. Image begins to resemble chromatogram.

with which the compound would elute. Plotting ^2k_w against $T_{char5\%}$ generated a Theoretical

Transformed GC×GC Distribution Map, Figure 4-3 - a more intuitive and realistic representation

of the distribution of these compounds in the separation space created by this column set. The

shape and spread of this map was then visually compared to a plot generated from the

experimental retention times of the compounds, Figure 4-4. Note that Figure 4-4 was created

using retention times directly from the peak table. It is shown in the place of an actual

chromatogram because many of the sixteen compounds were not run as one mixture but as

several smaller mixtures (or as individual compounds). This was done to ensure that the identity

of each compound was ascertained since an FID was used. Figure 4-3 and 4-4 show a similar

distribution of compounds. Figure 4-3 also illustrates that these two stationary phases (Rtx-5 and

Stabilwax), configured in an apolar/polar manner, with these phase ratios (250 each) are a good

choice for separating this mixture of compounds. This configuration effectively utilizes much of

the available second-dimension space and efficiently separates the polar molecules. Furthermore,

the map very quickly reveals that were Rtx-5 used on its own (in a 1D GC experiment),

compounds 7, 4 and 15 (dodecane, 2,6-dimethylaniline and p-ethylaniline) would have coeluted,

as well as compounds 5 and 13 (methyl decanoate and 4-tert-butylphenol).

Characteristic parameters were also calculated for these compounds on columns of different

phase ratios, and used to create maps that illustrate the effect of changing phase ratios on the

distribution of the molecules. Figures 4-5 to 4-7 show (in this order) the expected effects of

halving the phase ratio of the Stabilwax column, halving the phase ratio of the Rtx-5 column and

halving the phase ratio of both columns. At this stage, none of these maps were experimentally

confirmed; however, in each case the distribution of the molecules on the map changed, relative

to Figure 4-3, in an expected and explicable manner. The red circles on Figures 4-5 to 4-7

represent the distribution of the molecules when Rtx-5 (1°) and Stabilwax (2°) both have phase

ratios of 250. In Figure 4-5, the phase ratio of the hypothetical 2° column is reduced to 125

(indicated by black triangles with red boarders) and no change in $T_{char5\%}$ is observed while the ^2k

of each compound increases in accordance with its affinity for the Stabilwax column. This

behavior is expected as the separation on the primary (Rtx-5) column would proceed

uninfluenced by the properties of the secondary (Stabilwax) while the increased ratio of

stationary phase to mobile phase (decreased β) on the secondary column would cause molecules

eluting from the primary column to be more strongly retained than before (when $^2\beta = 250$).

Meanwhile, the magnitude of the change in ^2k between $^2\beta = 250$ and $^2\beta = 125$ is greater for

molecules that show stronger affinity for the 2° column than for those that show weaker affinity.

This is expected because regardless of the phase ratio, retention is still largely governed by

molecular interactions between the analytes and the stationary phase (of course, volatility/boiling

point also plays a role). Figure 4-6 shows (as black triangles with red boarders) the distribution

of these compounds when $^1\beta$ is reduced to 125. Compounds shift to later $T_{char5\%}$ (corresponding

to a shift to later elution temperatures/retention times on that phase) with their relative retention

on Rtx-5 remaining virtually the same. This shift to the right can be explained by the larger

stationary phase to mobile phase ratio on the Rtx-5 causing increased retention of all compounds.

However, as this phase is very non-polar, retention on this phase is largely based on London

dispersion forces (which all molecules possess) but is also governed by relative volatility/boiling

point. As such, relative retentions in this dimension remain mostly unchanged. In this figure, the

^2k of every compound is decreased. This is because retention on the second dimension is

dependent on the elution temperature at which the compounds leave the first dimension. A

thicker primary dimension film results in compounds leaving the primary column at a higher

temperature and being subsequently introduced to the secondary column at a higher temperature as well. This higher temperature causes the compounds to spend less time partitioned in the stationary phase of the secondary column resulting in a decreased ^2k compared to when $^1\beta = 125$. Figure 4-7 shows the effect of reducing the phase ratios of both columns to 125. Relative to the case where both columns have a phase ratio of 250, the peaks shift right (as they do in Figure 4-6) and downward. However, the vertical shift is not as intense as it is in Figure 4-6. Like the other maps, Figure 4-7 behaves as expected. The decrease in $^1\beta$ increases retention on the primary column which results in compounds encountering the secondary column at a higher temperature than they do in Figure 4-3. This higher temperature reduces their ^2k, however the extent of this reduction is less than seen in Figure 4-6 as the decrease in $^2\beta$ helps ensure greater retention. Overall, these preliminary maps suggested that, with some refinement, characteristic parameters could be used to map compound distribution in a GC×GC space and guide column selection.

Similar maps were also generated for the same columns but in a polar/apolar configuration (Stabilwax in the first dimension and Rtx-5 in the second). Figure 4-8 shows the expected distribution for such a set up. With this configuration, the polar compounds show a poorer (narrower) distribution in the second dimension. Decreasing the phase ratio of the second dimension column can widen this distribution but overall this is an inferior configuration compared to Figures 4-3 and 4-7 as is to be expected.
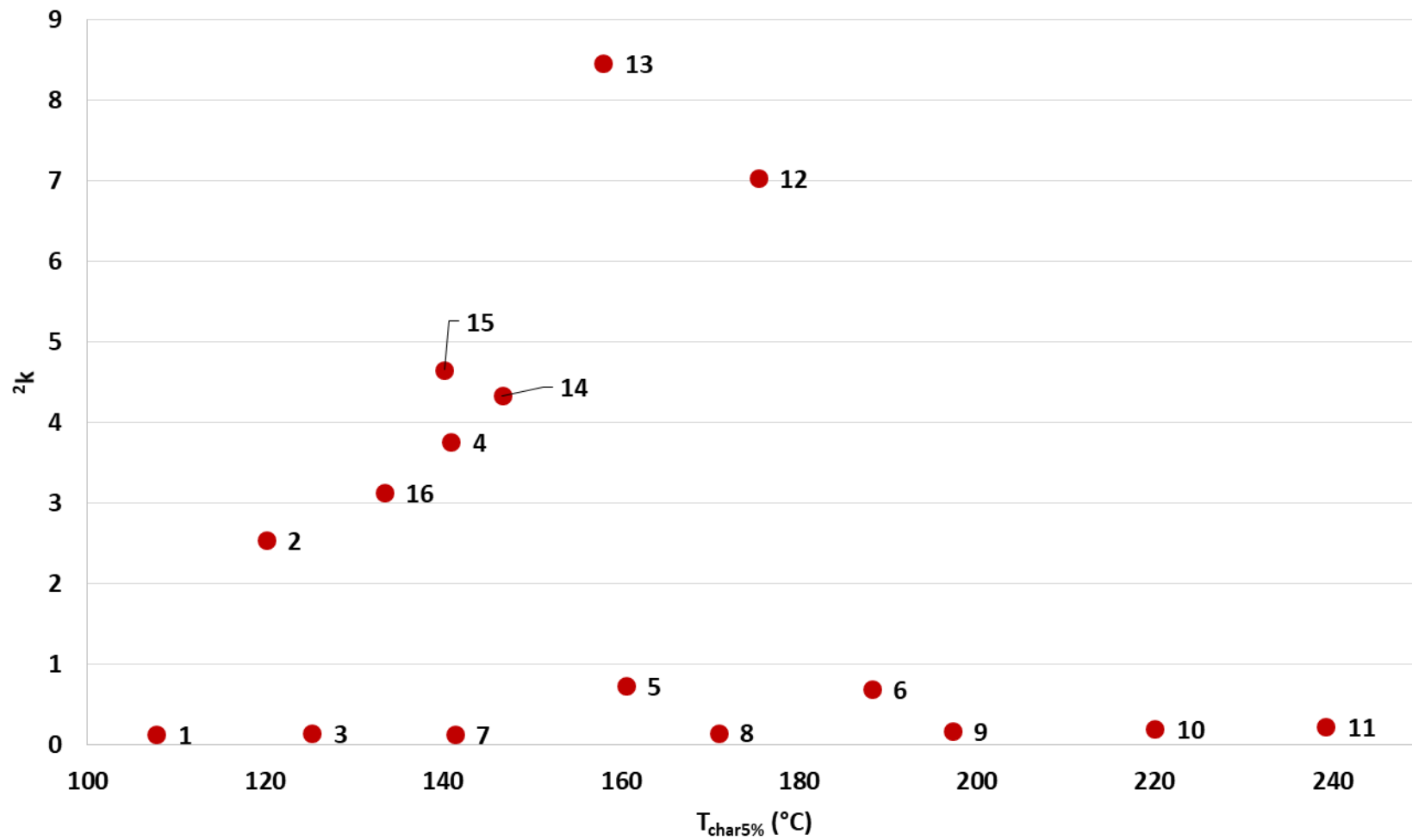
Figure 4-3 Theoretical Transformed Distribution Map of the sixteen compounds on the Rtx-5×Stabilwax GC×GC separation space ($^1\beta$ and $^2\beta = 250$).
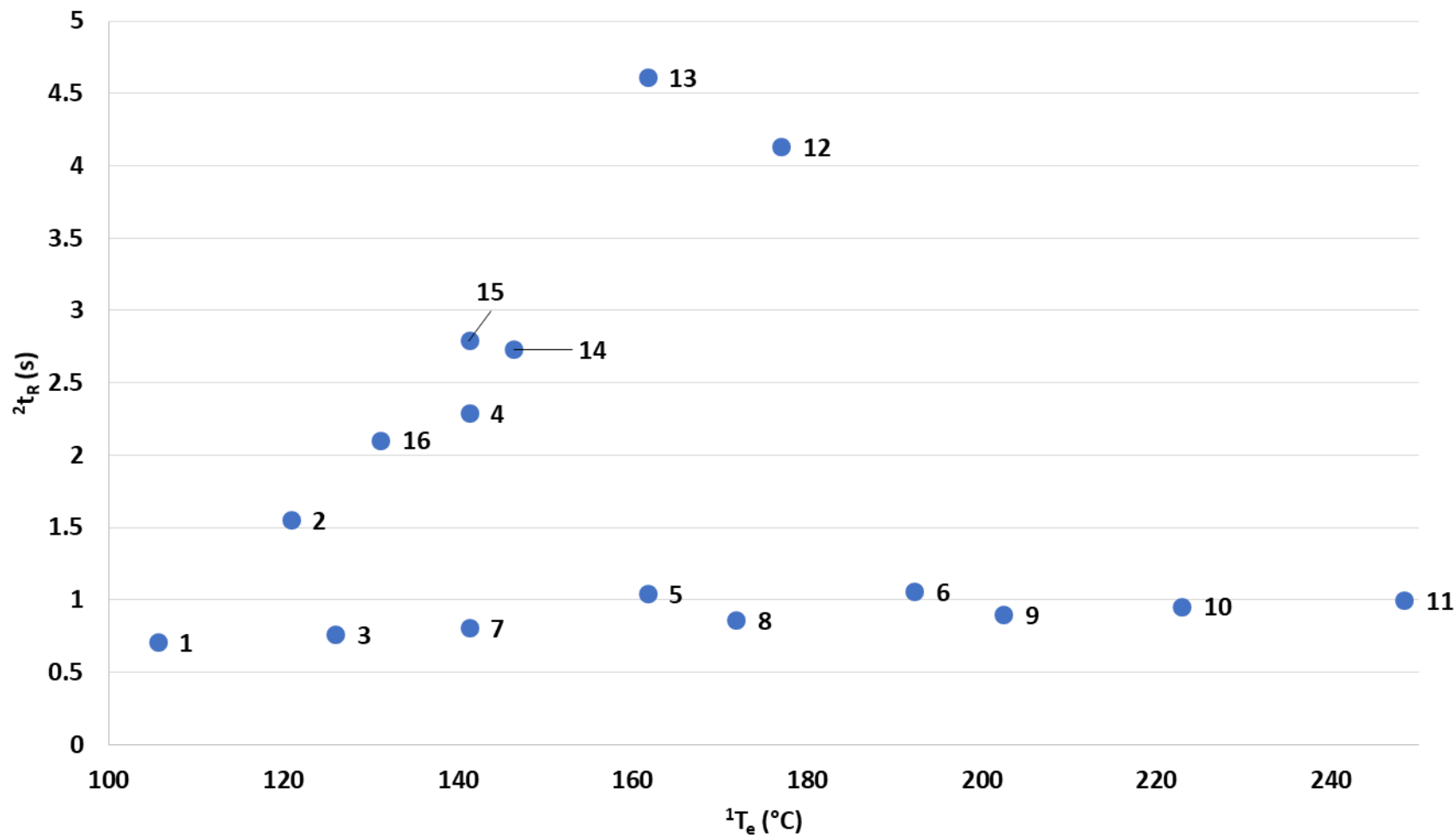
Figure 4-4 Experimental secondary retention times of the sixteen compounds and their primary elution temperatures as determined on the Rtx-5×Stabilwax GC×GC separation space ($^{1}\beta$ and $^{2}\beta = 250$)
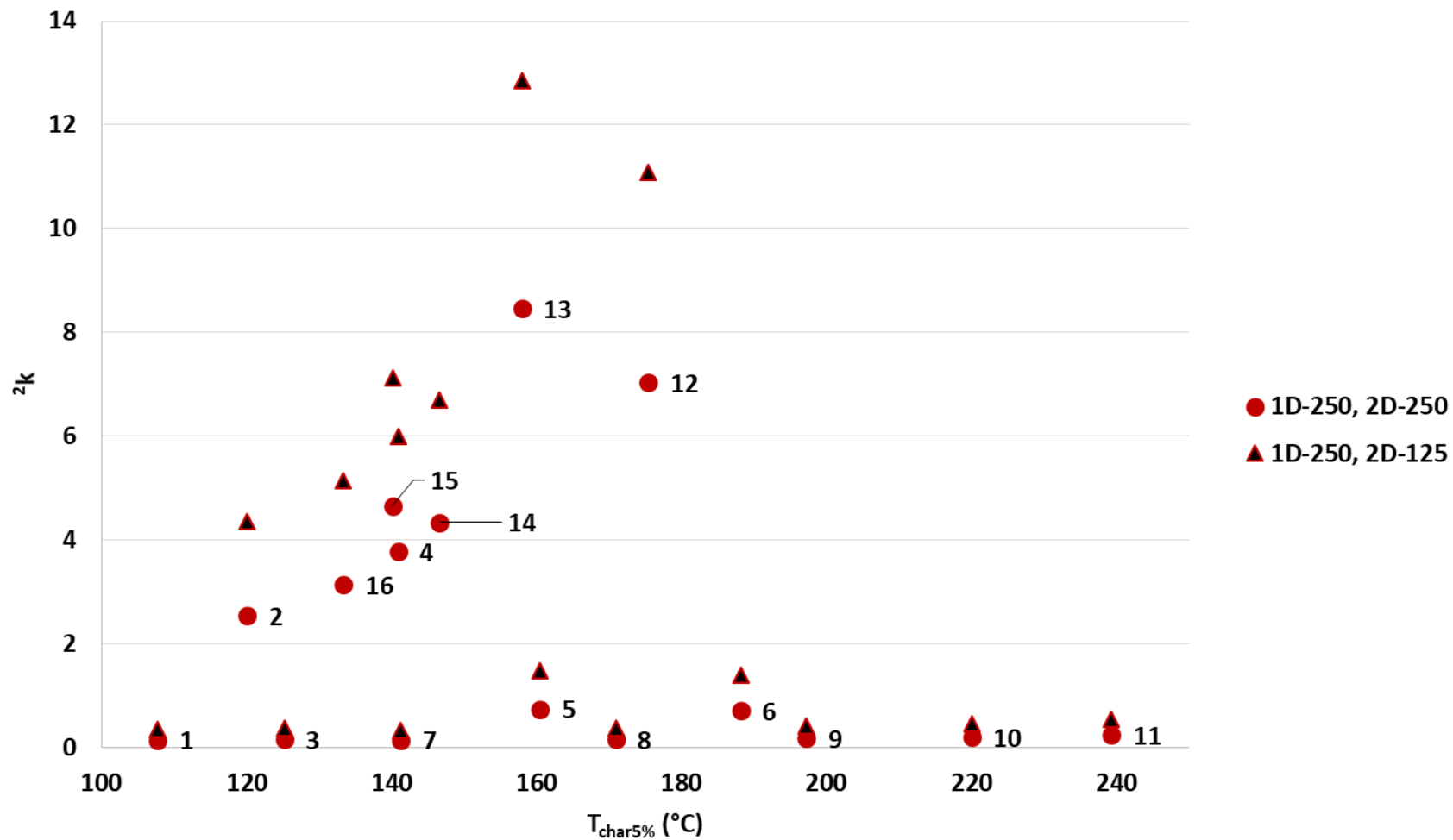
Figure 4-5 Map showing the theoretical shift in retention of sixteen compounds on the Rtx-5×Stabilwax GC×GC separation space when $^2\beta$ is reduced from 250 to 125 while $^1\beta$ remains unchanged
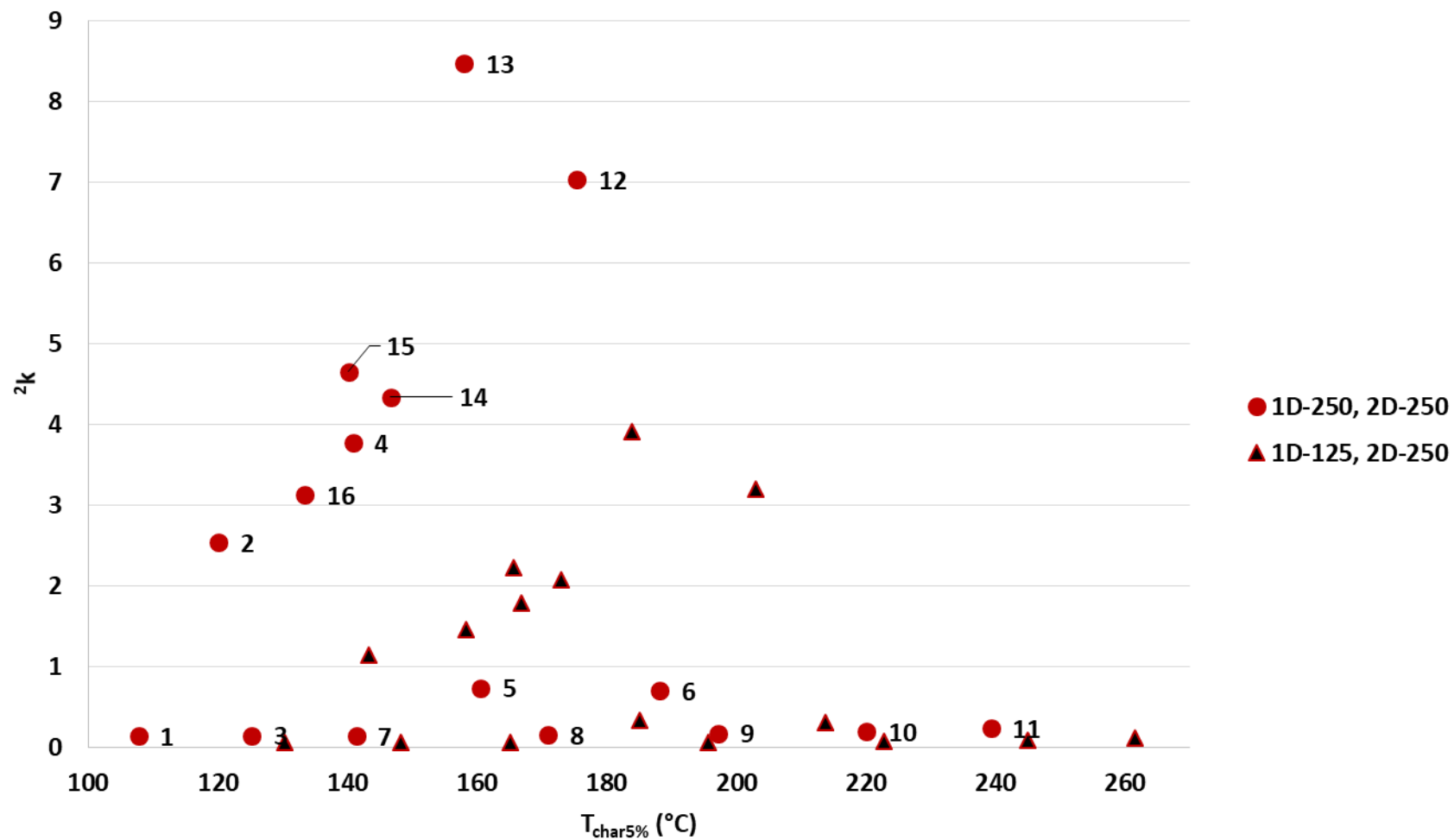
Figure 4-6 Map showing the theoretical shift in retention of sixteen compounds on the Rtx-5×Stabilwax GC×GC separation space when $^1\beta$ is reduced from 250 to 125 while $^2\beta$ remains unchanged
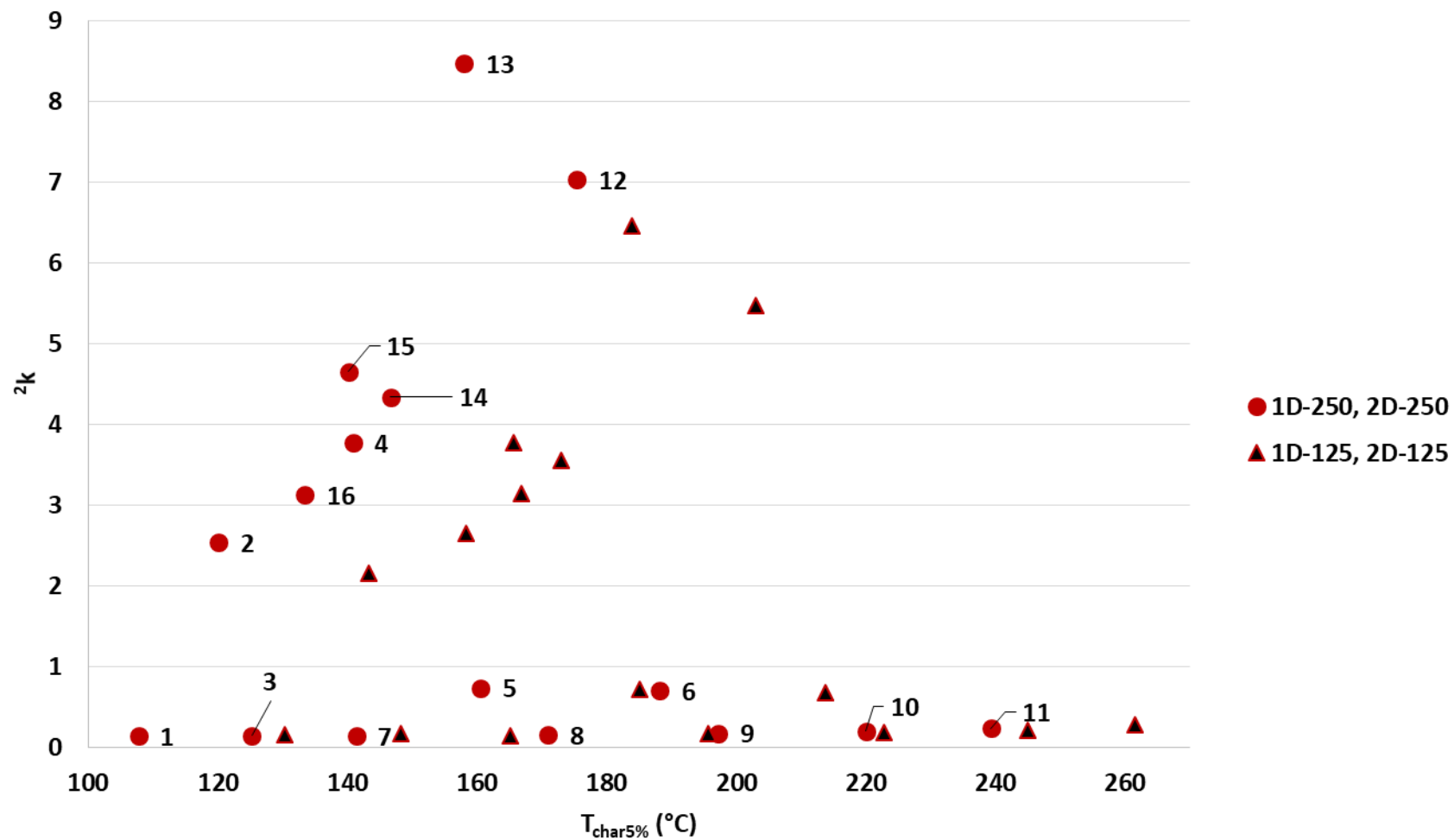
Figure 4-7 Map showing the theoretical shift in retention of sixteen compounds on the Rtx-5×Stabilwax GC×GC separation space when $^1\beta$ and $^2\beta$ are both reduced from 250 to 125
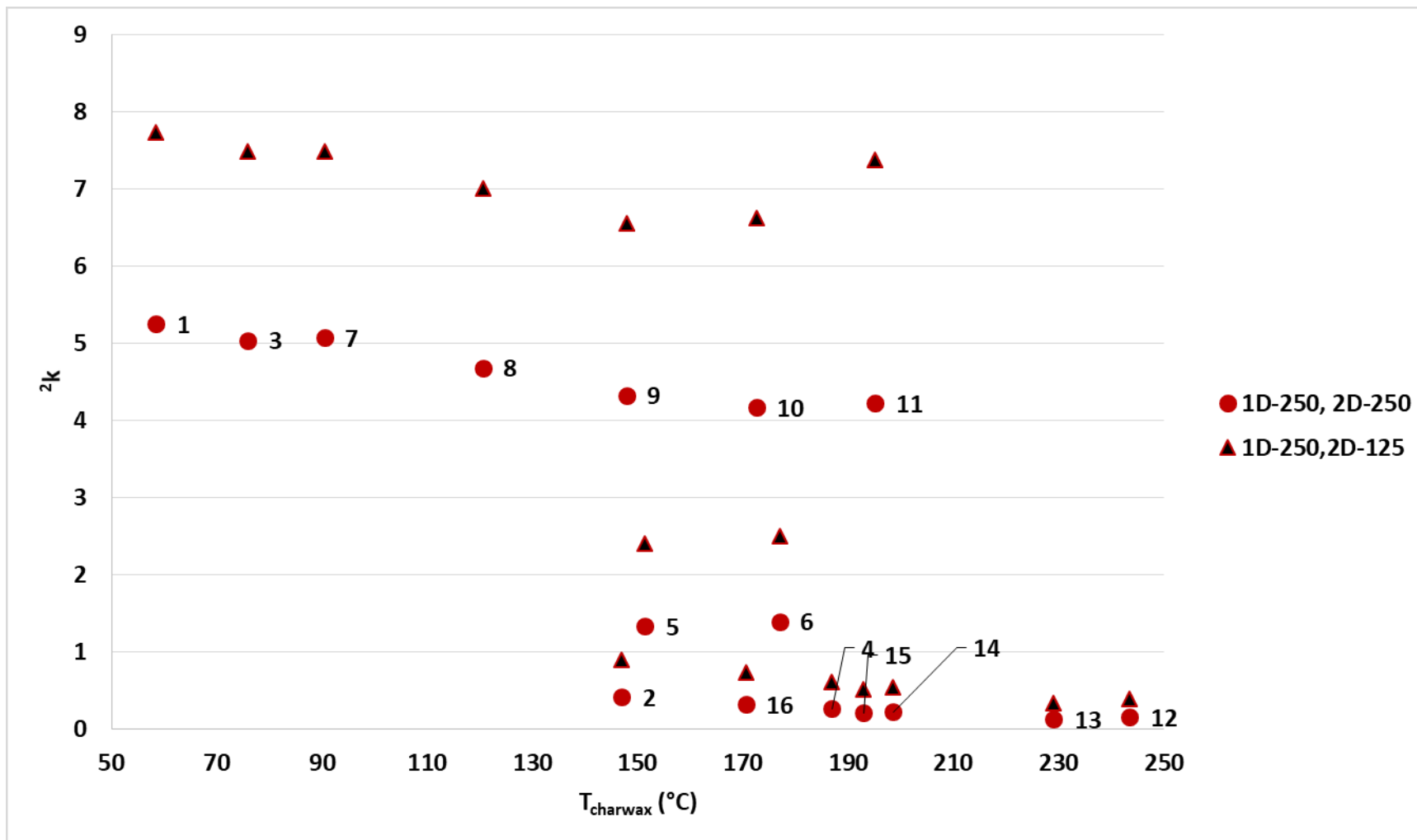
Figure 4-8 Map showing the theoretical shift in retention of sixteen compounds on the Stabilwax×Rtx-5 GC×GC separation space when $^2\beta$ is reduced from 250 to 125 and $^1\beta$ remains unchanged

4.3.2 Experimental confirmation with other phases, configurations, geometries and analyte chemistries

Despite the success of the preliminary investigation, several questions remained unanswered and further refinement of the experiments were required to answer them. The potential for mapping spaces built with different phase ratios needed to be experimentally confirmed. Stationary phase chemistries across a range of polarities, covering a variety of molecular interactions needed to be assessed. With this consideration in mind, it was also prudent to include a wider range of analyte chemistries and so biphenyl, PAHs, aldehydes, ketones and trialkylphosphates were added to the compound classes represented.

The figures and tables below illustrate the performance of these models for mapping GC×GC separation spaces and by extension, the capabilities of these maps to guide the selection of stationary phase chemistries, configurations and phase ratios.

Characteristic parameters for 39 compounds from the thermodynamic library (Appendix A) were calculated using an in-house MATLAB script. For each molecule, parameters were calculated on three stationary phase chemistries and two phase ratios of each stationary phase chemistry. Table 4-3 and Table 4-4 below show these parameters. Note that once again each molecule was assigned a number, however, the assigned number for a given compound for these studies does not necessarily match the number assigned during the preliminary investigations using Stabilwax.

Table 4-3 Characteristic parameters for 39 compounds on Rtx- 5MS, Rtx-200(MS) and Rxi-17Sil MS phases. $\beta = 250$

Assigned Number	Compound	T_{char} (°C)			θ_{char} (°C)		
		Rtx-5MS	Rtx-200	Rxi-17Sil-MS	Rtx-5MS	Rtx-200	Rxi-17Sil-MS
1	1,4-dimethylnaphthalene	184.3	162.3	194.5	37.6	32.3	36.2
2	1-octanol	120.3	103.9	113.1	30.4	27.0	27.7
3	1-tetradecanol	208.0	173.7	197.3	34.6	29.9	31.0
4	2,3-dimethylaniline	146.8	133.8	159.2	34.5	30.0	33.2
5	2,5-dichlorophenol	140.9	121.9	147.3	34.4	30.9	33.4
6	2,6-dichlorophenol	147.2	131.1	156.0	34.9	31.1	33.7
7	2,6-dimethylaniline	141.0	128.7	152.4	34.1	30.2	32.7
8	2-decanone	141.5	137.1	134.4	31.6	29.2	28.3
9	2-heptanone	87.8	92.1	84.9	28.9	27.4	26.4
10	2-nonanol	125.8	104.1	115.6	30.6	27.8	27.4
11	2-nonanone	124.8	123.1	118.9	30.7	28.6	27.8
12	2-octanone	106.9	108.2	102.4	29.9	28.1	27.0
13	2-tridecanone	185.5	181.1	176.1	33.7	30.3	30.1
14	3-octanone	106.2	108.5	101.0	29.9	27.4	27.1
15	3-tert-butylphenol	157.9	139.3	163.0	33.5	29.9	31.8
16	4-sec-butylphenol	160.3	139.6	165.6	33.6	29.9	32.2
17	4-tert-butylphenol	158.1	138.9	163.0	33.8	30.0	32.1
18	5-nonanol	123.9	105.8	113.1	30.6	26.9	27.5
19	anthracene	233.2	213.5	251.3	42.2	37.0	40.6
20	bipheyl	175.6	152.5	185.1	36.8	31.2	34.9
21	decanal	143.8	136.1	136.4	32.0	29.4	28.5
22	decane	107.9	76.3	83.3	29.7	25.7	26.3
23	dodecane	141.5	107.0	117.0	31.3	26.6	27.3
24	eicosane	239.4	200.1	218.4	30.6	30.3	29.4
25	hexadecane	197.4	157.8	173.2	33.7	28.4	29.2

Assigned Number	Compound	T_{char} (°C)			θ_{char} (°C)		
		Rtx-5MS	Rtx-200	Rxi-17Sil-MS	Rtx-5MS	Rtx-200	Rxi-17Sil-MS
26	methyl decanoate	160.7	144.1	151.5	32.3	28.4	28.9
27	methyl dodecanoate	188.3	168.1	178.0	33.7	29.5	29.8
28	naphthalene	145.8	129.5	155.7	35.7	31.0	34.4
29	N-ethylaniline	133.5	121.3	141.5	32.9	28.8	31.1
30	octadecane	220.2	180.3	197.6	33.3	29.4	30.2
31	octanal	109.4	106.7	104.4	30.2	28.2	27.2
32	p-ethylaniline	140.3	126.3	150.9	33.6	29.2	32.0
33	phenanthrene	232.0	212.3	250.5	42.0	36.8	40.7
34	tetradecane	171.1	134.2	146.9	32.6	27.6	28.5
35	tributylphosphate	203.4	201.7	203.6	33.9	31.3	30.5
36	trimethylphosphate	94.4	116.2	110.1	28.8	28.4	27.6
37	tripropylphosphate	168.4	173.2	172.2	32.3	30.1	29.6
38	undecanal	159.4	149.4	151.0	32.7	29.9	29.2
39	undecane	125.4	92.3	100.7	30.5	26.3	26.9

Table 4-4 Characteristic parameters for 39 compounds on Rtx- 5MS, Rtx-200 and Rxi-17Sil MS phases. $\beta = 125$

Assigned Number	Compound	T_{char} (°C)			θ_{char} (°C)		
		Rtx-5MS	Rtx-200	Rxi-17Sil-MS	Rtx-5MS	Rtx-200	Rxi-17Sil-MS
1	1,4-dimethylnaphthalene	212.8	186.4	221.5	44.8	37.2	41.9
2	1-octanol	143.3	124.0	133.7	36.2	31.1	31.9
3	1-tetradecanol	234.2	203.6	220.2	41.0	34.9	35.4
4	2,3-dimethylaniline	172.9	156.1	184.0	41.3	34.5	38.6
5	2,5-dichlorophenol	167.0	145.0	172.2	41.4	36.0	38.7
6	2,6-dichlorophenol	173.7	154.4	181.2	42.1	36.2	39.2
7	2,6-dimethylaniline	166.9	151.2	176.8	40.8	35.0	37.9

Assigned Number	Compound	T_{char} (°C)			θ_{char} (°C)		
		Rtx-5MS	Rtx-200	Rxi-17Sil-MS	Rtx-5MS	Rtx-200	Rxi-17Sil-MS
8	2-decanone	165.2	158.9	155.3	37.3	33.7	32.3
9	2-heptanone	109.7	112.5	104.7	34.5	31.8	30.7
10	2-nonanol	148.8	129.0	135.9	36.2	31.9	31.5
11	2-nonanone	147.9	144.4	139.5	36.2	33.0	31.9
12	2-octanone	129.4	129.1	122.4	35.3	32.5	31.0
13	2-tridecanone	210.9	195.8	198.4	39.8	34.1	34.4
14	3-octanone	128.7	124.8	121.1	35.4	32.2	31.2
15	3-*tert*-butylphenol	183.4	161.5	186.6	40.6	34.6	36.7
16	4-*sec*-butylphenol	185.9	161.9	189.7	40.5	34.7	37.4
17	4-*tert*-butylphenol	183.8	161.3	187.0	40.9	34.8	37.2
18	5-nonanol	147.0	125.8	133.6	36.3	30.9	31.7
19	anthracene	265.2	241.2	281.6	50.7	43.2	47.0
20	bipheyl	203.5	175.7	211.1	44.1	35.9	40.5
21	decanal	167.9	158.0	157.5	37.8	34.0	32.6
22	decane	130.3	95.6	102.9	35.0	30.1	30.5
23	dodecane	165.1	126.7	137.2	37.0	30.5	31.1
24	eicosane	261.5	222.6	239.8	33.1	35.0	32.5
25	hexadecane	222.8	178.8	194.8	39.8	32.5	33.1
26	methyl decanoate	185.0	165.2	172.8	38.3	32.6	33.0
27	methyl dodecanoate	213.7	190.1	200.1	40.0	34.1	34.1
28	naphthalene	172.8	152.6	181.5	42.7	35.8	40.1
29	N-ethylaniline	158.4	142.6	164.6	39.2	33.0	35.9
30	octadecane	244.9	202.1	219.9	38.2	33.7	34.4
31	octanal	132.2	127.7	124.6	35.8	32.6	31.3
32	p-ethylaniline	165.7	147.9	174.7	40.1	33.5	37.0
33	phenanthrene	263.8	239.8	280.9	50.3	42.9	47.2
34	tetradecane	195.6	154.6	168.0	38.5	31.5	32.5
35	tributylphosphate	229.0	225.0	226.1	40.2	36.1	34.7

Assigned Number	Compound	T_{char} (°C)			θ_{char} (°C)		
		Rtx-5MS	Rtx-200	Rxi-17Sil-MS	Rtx-5MS	Rtx-200	Rxi-17Sil-MS
36	trimethylphosphate	116.2	137.3	130.6	34.4	32.6	31.7
37	tripropylphosphate	192.8	195.5	194.1	38.3	34.6	33.9
38	undecanal	184.0	171.7	172.7	38.6	34.5	33.4
39	undecane	148.3	111.9	120.7	35.9	30.5	31.0

Experiments were performed as described in section 4.2.2 using five different combinations of these stationary phases, shown in Table 4-5.

Table 4-5 Column combinations experimentally investigated

Combination	Ramp rate (°C min^{-1})	1° column	2° column	$^{1}\beta$	$^{2}\beta$	Effect
A	16.05	Rtx-5MS	Rtx-200MS	250	250	"Default"
B	16.05	Rtx-5MS	Rtx-200	250	125	Lower 2° β
C	23.26	Rtx-5MS	Rtx-200MS	125	250	Lower 1° β
D	19.30	Rtx-200MS	Rtx-5MS	250	250	"Reverse" polarity
E	16.05	Rtx-5MS	Rxi-17Sil MS	250	250	Change selectivity

Table 4-6 contains the differences between the characteristic temperature of each compound on the primary column, $^{1}T_{char}$, and their elution temperatures, $^{1}T_{e}$, on that column using combination A. It also contains the differences between their theoretical secondary retention times, $^{2}t_{Rtheo}$, and their experimental secondary retention times, $^{2}t_{R}$. For this combination, absolute values of $^{1}T_{char}$ $-$ $^{1}T_{e}$ ranged from 0.0_{2} °C to 13.49_{5} °C (0.0_{7} s to 50.4_{5} s). It is not yet clear what caused the wide range of differences across compounds or the magnitude of these differences for each compound but three possible contributors have been hypothesized. 1) $^{1}T_{e}$ is calculated using the oven ramp rate and primary retention time, $^{1}t_{R}$, as obtained from the peak table. These values for $^{1}t_{R}$ are quantized to the modulation period, P_{M}, which means that their actual value could lie between $^{1}t_{R}$ $-$ 1.5 s and $^{1}t_{R}$ + 1.5 s. In the worst case, however, this only adds/subtracts about 0.40 ° C to/from $^{1}T_{e}$ so cannot on its own account for the observed differences. 2) These experiments were designed on the basis that an oven ramp rate of about 18 °C t_{M}^{-1} would cause most compounds to elute with a $^{1}k \approx 1$ (i.e. they would elute at $^{1}T_{char}$). However this approximation of oven ramp rate

assumes that the characteristic thermal constant for the compound on the primary column, $^1\theta_{char}$ is 30 °C and that the compound is neither poorly retained nor too strongly retained at the initial oven temperature. Looking at the data in Table 4-6 we see that the largest differences are associated with compounds whose $^1\theta_{char}$ are $\geq$ 6 °C above 30 °C. Anthracene for example has a $^1\theta_{char}$ of 42.2 °C and would require an oven ramp rate of $\sim$ 25.3 °C t_M^{-1} ($\sim$22.6 °C min^{-1}) in order to elute with $^1k \approx 1$. As such it is likely that anthracene and other compounds like it (with characteristic thermal constants high above 30 °C) would elute at lower than expected temperatures. 3) There might be a connection between compound chemistry and the magnitude of this difference. For this column combination, the largest differences between $^1T_{char}$ and ^1T_e were noted for biphenyl and the PAHs (1,4-dimethylnaphthalene, anthracene and phenanthrene). Naphthalene also had a relatively large difference (although smaller than the other PAHs). This might be tied to the requirement that the compounds should not be too strongly retained on the column at the initial oven temperature [115].

Table 4-6 Differences between $^1T_{char}$ and ^1T_e, and between $^2t_{Rtheo}$ and ^2t_R for Combination A

Assigned number	Compound	$^1T_{char} - ^2T_e$ (°C)	$^2t_{Rtheo} - ^2t_R$ (s)
1	1,4-dimethylnaphthalene	5.9	-0.008
2	1-octanol	-1.5	-0.013
3	1-tetradecanol	4.4	0.009
4	2,3-dimethylaniline	2.5	-0.013
5	2,5-dichlorophenol	1.4	-0.010
6	2,6-dichlorophenol	2.9	-0.008
7	2,6-dimethylaniline	2.4	-0.003
8	2-decanone	0.0	0.028
9	2-heptanone	2.1	-0.041
10	2-nonanol	-1.7	-0.045
11	2-nonanone	-0.6	0.023
12	2-octanone	-0.4	0.012

Assigned number	Compound	$^1T_{char} - {}^2T_e$ (°C)	$^2t_{Rtheo} - {}^2t_R$ (s)
13	2-tridecanone	3.1	0.022
14	3-octanone	-0.4	-0.023
15	3-tert-butylphenol	1.2	-0.001
16	4-sec-butylphenol	0.8	-0.005
17	4-tertbutylphenol	1.4	-0.015
18	5-nonanol	-1.1	-0.011
19	anthracene	13.5	-0.002
20	bipheyl	5.6	-0.014
21	decanal	0.3	0.017
22	decane	-0.7	-0.039
23	dodecane	-0.8	-0.016
24	eicosane	3.2	0.019
25	hexadecane	2.9	-0.001
26	methyl decanoate	0.3	0.012
27	methyl dodecanoate	2.7	0.012
28	naphthalene	3.5	-0.010
29	N-ethylaniline	0.8	-0.011
30	octadecane	4.1	0.008
31	octanal	-0.4	0.006
32	p-ethylaniline	1.6	-0.015
33	phenanthrene	13.4	0.002
34	tetradecane	1.1	-0.005
35	tributylphosphate	2.9	0.045
36	trimethylphosphate	-0.9	0.023
37	tripropylphosphate	0.1	0.064
38	undecanal	1.1	0.022
39	undecane	-1.3	-0.027

Using equations 4-16 and 4-17 a theoretical secondary retention time, $^2t_{Rtheo}$, was calculated for each compound. This was done in an effort to further present the map in a manner that is visually more meaningful, familiar and intuitive for chromatographers. It also allows for a fairer visual comparison between the maps and the experimental chromatograms. The absolute differences between the values of $^2t_{Rtheo}$ and the experimental secondary retention times, ^2t_R, (shown in Table 4-6) ranged from 0.00_0 s to 0.06_4 s (0.15_9 % to 7.32_2 %) with no clear relationship between these values and the differences between $^1T_{char}$ and ^1T_e. When assessing these values ($^2t_{Rtheo} - {}^2t_R$) it is

important to consider two factors. 1) The values of ^2t_M and ^1t_M used in the calculations of $^2t_{Rtheo}$ are merely calculated estimates of the dead times of the second dimension column and the transfer line at 150 °C (the same temperature used to determine the ramp rate that would theoretically cause compounds to elute with $^1T_e = {}^1T_{char}$). However, in reality, over the course of a constant-flow programmed-temperature separation on this column set, ^2t_M would range from about 0.45 s at 90 °C to 0.29 s at 320 °C while ^1t_M would range from about 0.14 s at 90 °C to 0.09 s at 320 °C. 2) The maps, as they were at this stage, were not built with the aim of accurately predicting of first- and second-dimension times but to serve as a rapid, easy-to-generate visual aid for guiding column choice selection prior to optimizing instrumental conditions in GC×GC experiments. Further mathematical refinement would be required to use these characteristic parameters and any values derived from them as accurate predictors of retention times (and by extension to use their predictions for optimizing instrument conditions). In many ways, the values of $^2t_{Rtheo}$ calculated here do not carry much meaning beyond their usefulness towards generating maps that serve the purpose outlined above. At this stage, the significance of the magnitude of any numerical differences between these values and the actual ^2t_R values cannot be fairly assessed. These values, however, (as the coming figures will show) have been demonstrated to be extremely useful in generating maps that answer the question "Would these two columns, with these stationary phases and phase ratios, arranged in this order be a good choice for my GC×GC separation?"

Figures 4-9 and 4-10 demonstrate this for Combination A. Figure 4-9 shows the theoretical map of these compounds in this separation space while Figure 4-10 is a plot of the experimental chromatogram of the same compounds. The distribution and relative retention times of compounds in the experimental space closely matches that of the map. The two figures most

noticeably deviate in the following cases. 1) The map suggests that compounds 12 and 14 (2-octanone and 3-octanone) would have greater separation in the second dimension than they actually did. The same goes for compounds 7 and 32 (2,6-dimethylaniline and p-ethylaniline) as well as 16 and 26 (4-sec-butylphenol and methyl decanoate). 2) The map suggests that compounds 15 and 17 (3-tert-butylphenol and 4-tert-butylphenol) would be more poorly separated in the second dimension than they actually were. 3) Compounds 19 and 33 (anthracene and phenanthrene) eluted from the primary column much early than the map suggested they should (as a reminder, these 2 compounds had values of $^1\theta_{char}$ that showed the greatest deviation from 30 °C). These deviations demonstrate that while these maps provide a good starting point for column selection (the beginning of the method development process) they do not yet eliminate the need to optimize oven and pneumatic conditions once a column set is selected.
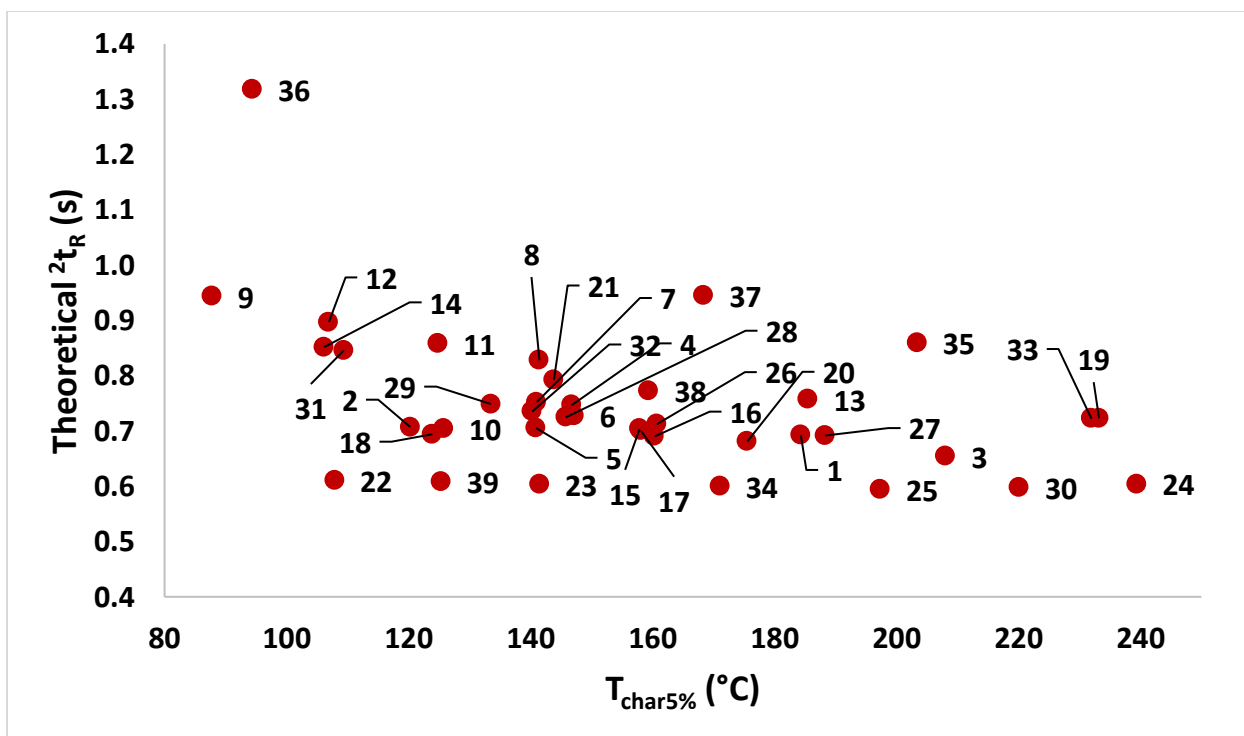
Figure 4-9 Map of the thirty-nine compounds on the Rtx-5MS×Rtx-200MS GC×GC separation space ($^1\beta$ and $^2\beta = 250$)
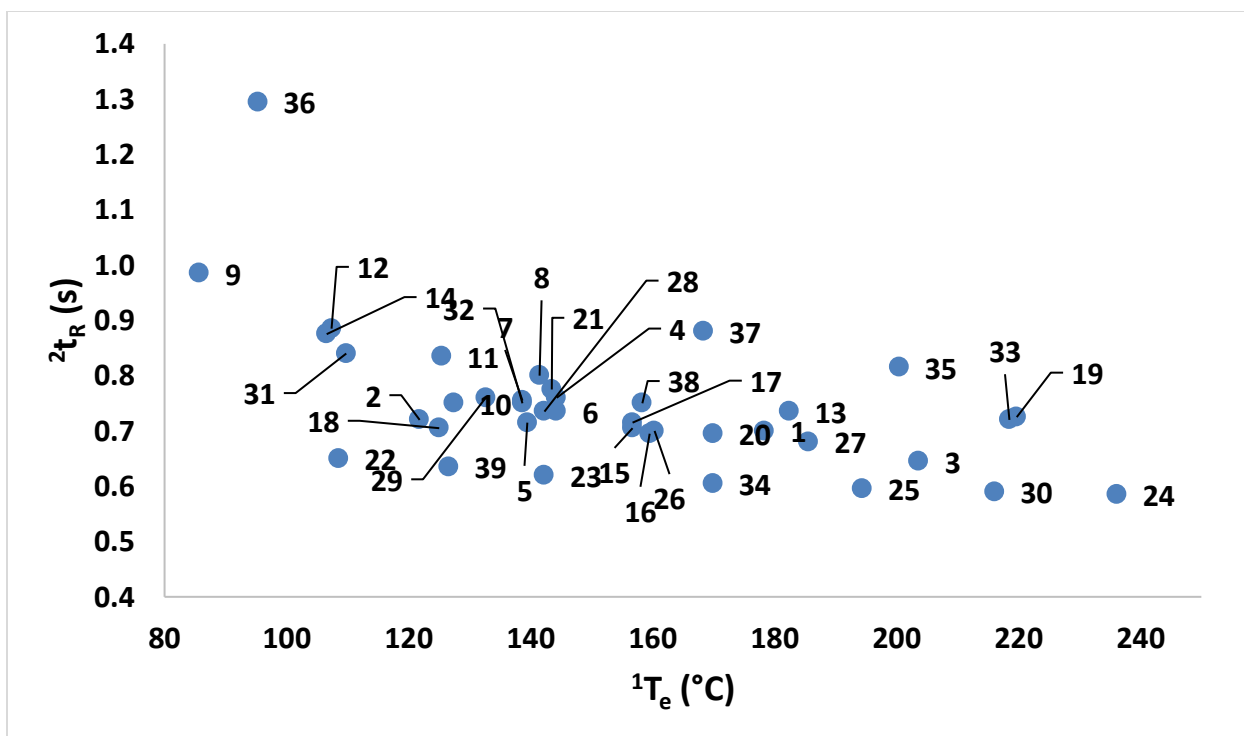
Figure 4-10 Experimental secondary retention times of the thirty-nine compounds and their primary elution temperatures as determined on the Rtx-5MS×Rtx-200MS GC×GC separation space ($^1\beta$ and + $^2\beta$ = 250)

Similar maps were generated for the other column combinations in Table 4-5. They are shown below with the experimental chromatograms.

Table 4-7 shows the differences between the characteristic temperature of each compound on the primary column, $^1T_{char}$, and their elution temperatures, ^1T_e, on that column using combination B. It also contains the differences between their theoretical secondary retention times, $^2t_{Rtheo}$, and their experimental secondary retention times, ^2t_R.

Table 4-7 Differences between $^1T_{char}$ and ^1T_e, and between $^2t_{Rtheo}$ and ^2t_R for Combination B

Assigned number	Compound	$^1T_{char} - {^2}T_e$ (°C)	$^2t_{Rtheo} - {^2}t_R$ (s)
1	1,4-dimethylnaphthalene	6.2	0.06
2	1-octanol	-1.7	0.09
3	1-tetradecanol	4.8	0.06
4	2,3-dimethylaniline	2.3	0.08
5	2,5-dichlorophenol	1.3	0.08
6	2,6-dichlorophenol	2.7	0.08
7	2,6-dimethylaniline	2.0	0.10
8	2-decanone	-0.3	0.16
9	2-heptanone	1.7	0.05
10	2-nonanol	-1.6	0.04
11	2-nonanone	-0.9	0.15
12	2-octanone	-0.6	0.13
13	2-tridecanone	3.1	0.10
14	3-octanone	-0.8	0.11
15	3-tert-butylphenol	1.2	0.09
16	4-sec-butylphenol	0.9	0.09
17	4-tertbutylphenol	1.4	0.08
18	5-nonanol	-1.3	0.06
19	anthracene	13.4	0.08
20	bipheyl	5.5	0.07
21	decanal	-0.1	0.14
22	decane	-0.7	0.03
23	dodecane	-0.8	0.04
24	eicosane	3.5	0.09
25	hexadecane	3.2	0.05
26	methyl decanoate	0.2	0.12
27	methyl dodecanoate	2.7	0.11
28	naphthalene	3.5	0.08
29	N-ethylaniline	0.8	0.08
30	octadecane	4.1	0.07
31	octanal	-0.3	0.12
32	p-ethylaniline	1.2	0.08
33	phenanthrene	13.7	0.06
34	tetradecane	1.0	0.05
35	tributylphosphate	2.8	0.18
36	trimethylphosphate	-0.8	0.11
37	tripropylphosphate	-0.1	0.21

Assigned number	Compound	$^1T_{char} - {}^2T_e$ (°C)	$^2t_{Rtheo} - {}^2t_R$ (s)
38	undecanal	1.1	0.13
39	undecane	-1.4	0.04

Figure 4-11 shows the map of Combination B represented by black triangles with red borders while the map of Combination A is represented with red circles. The experimental data for Combination B is plotted in Figure 4-12 using black triangles with blue borders while the experimental data for Combination A is represented with blue circles. The upward expected shift in going from Combination A to Combination B (i.e. decreasing the phase ratio of the secondary column) is demonstrated on the map and supported by the experimental data. The upward shift on the map is slightly greater than that observed in the experiment. The likely reason for this is that θ_{char} is larger on columns with smaller phase ratios and so the experimental condition of 18 °C t_M^{-1} is not a sufficiently fast enough ramp rate to cause the compounds to elute with the expected retention factor. Hence, all compounds eluted from the second column a bit earlier than the map would show.
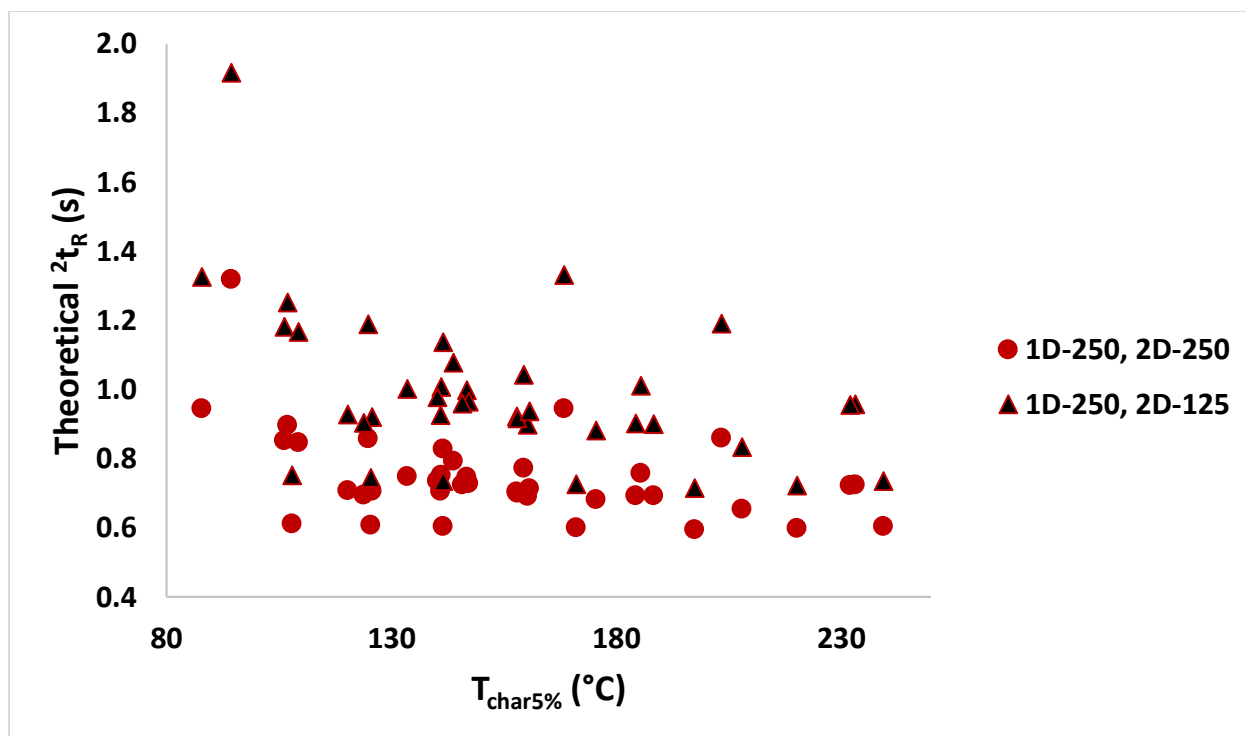
Figure 4-11 Map showing the theoretical shift in retention of thirty-nine on the Rtx-5MS×Rtx-200MS GC×GC separation space when $^2\beta$ is reduced from 250 to 125 while $^1\beta$ remains unchanged
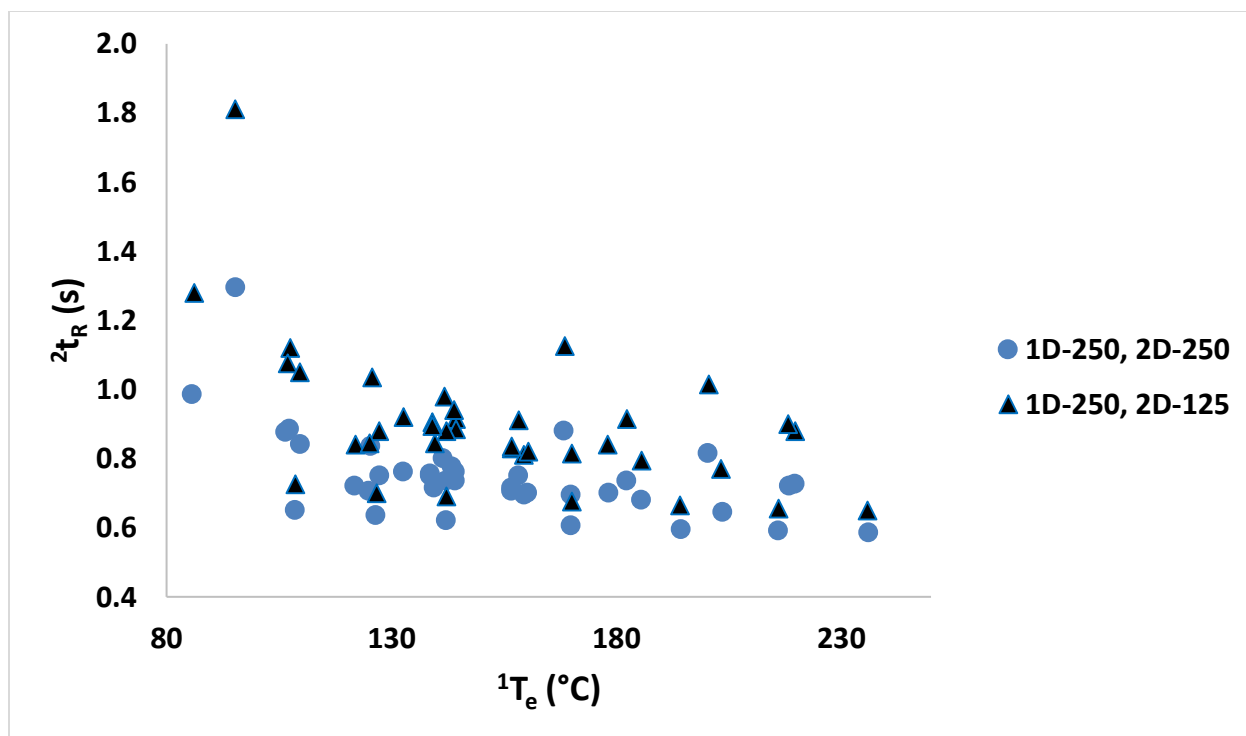
Figure 4-12 Experimental retention of thirty-nine compounds on the Rtx-5MS×Rtx-200MS GC×GC separation space when $^2\beta$ is reduced from 250 to 125 while $^1\beta$ remains unchanged

Table 4-8 shows the differences between the characteristic temperature of each compound on the primary column, $^1T_{char}$, and their elution temperatures, ^1T_e, on that column using Combination C. It also contains the differences between their theoretical secondary retention times, $^2t_{Rtheo}$, and their experimental secondary retention times, ^2t_R.

Table 4-8 Differences between $^1T_{char}$ and ^1T_e, and between $^2t_{Rtheo}$ and ^2t_R for Combination C

Assigned number	Compound	$^1T_{char} - ^2T_e$ (°C)	$^2t_{Rtheo} - ^2t_R$ (s)
1	1,4-dimethylnaphthalene	12.9	-0.02
2	1-octanol	2.7	-0.02
3	1-tetradecanol	10.2	0.01
4	2,3-dimethylaniline	8.3	-0.04
5	2,5-dichlorophenol	7.2	-0.02

Assigned number	Compound	$^1T_{char} - {}^2T_e$ (°C)	$^2t_{Rtheo} - {}^2t_R$ (s)
6	2,6-dichlorophenol	8.6	-0.02
7	2,6-dimethylaniline	7.5	-0.02
8	2-decanone	4.5	-0.01
9	2-heptanone	3.4	-0.05
10	2-nonanol	2.5	-0.05
11	2-nonanone	3.1	-0.02
12	2-octanone	2.9	-0.03
13	2-tridecanone	8.1	0.00
14	3-octanone	2.7	-0.05
15	3-tert-butylphenol	6.7	-0.02
16	4-sec-butylphenol	6.7	-0.01
17	4-tertbutylphenol	7.1	-0.03
18	5-nonanol	3.1	-0.02
19	anthracene	22.4	-0.01
20	bipheyl	12.3	-0.02
21	decanal	4.7	-0.01
22	decane	2.3	-0.01
23	dodecane	3.8	0.00
24	eicosane	4.7	0.04
25	hexadecane	8.4	0.01
26	methyl decanoate	5.4	0.00
27	methyl dodecanoate	8.1	0.00
28	naphthalene	9.6	-0.03
29	N-ethylaniline	5.8	-0.04
30	octadecane	8.3	0.02
31	octanal	3.2	-0.03
32	p-ethylaniline	6.8	-0.03
33	phenanthrene	21.9	0.00
34	tetradecane	5.9	0.01
35	tributylphosphate	8.3	-0.01
36	trimethylphosphate	1.3	-0.05
37	tripropylphosphate	5.0	-0.01
38	undecanal	6.3	-0.01
39	undecane	2.4	0.00

The map and experimental data for Combination C is shown in Figure 4-13 and Figure 4-14. The right and downward shift that is expected for this combination is generated using the map and supported experimentally. The shift to higher primary elution temperature shown on map is larger than observed experimentally. This is likely caused by the impact of phase ratio on θ_{char} (discussed above).
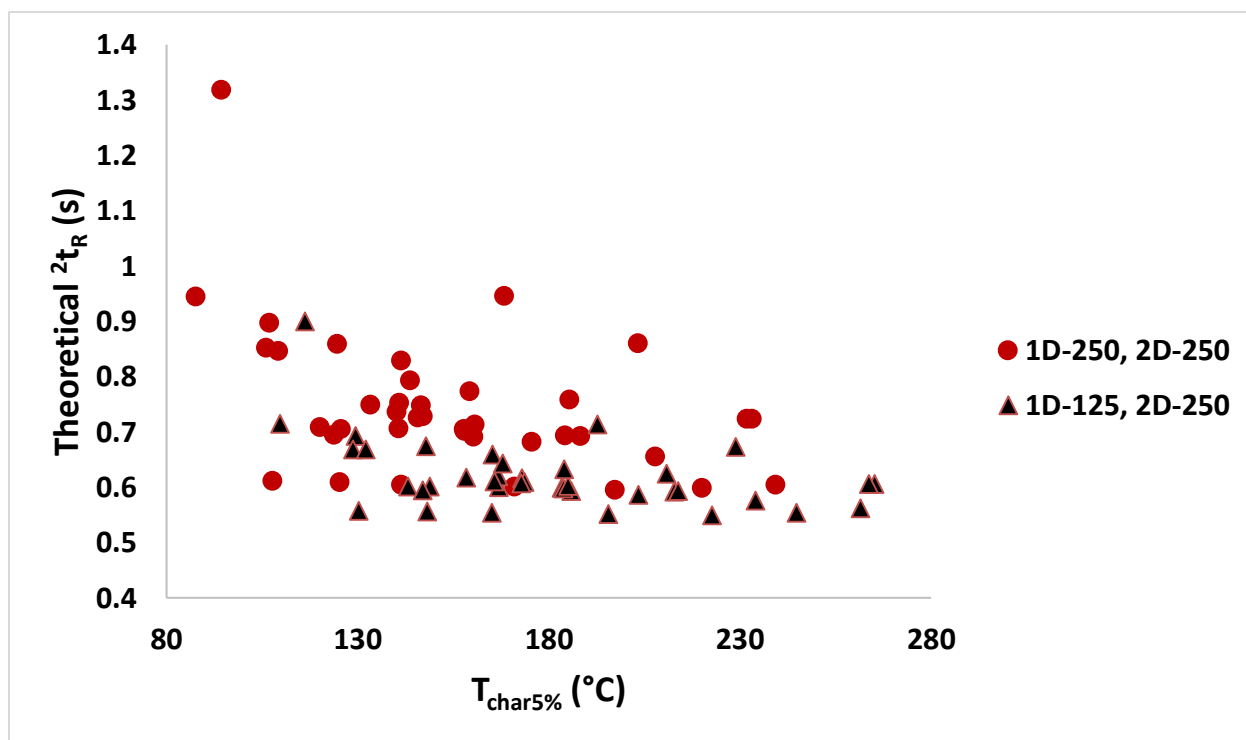
Figure 4-13 Map showing the theoretical shift in retention of thirty-nine on the Rtx-5MS×Rtx-200MS GC×GC separation space when $^1\beta$ is reduced from 250 to 125 while $^2\beta$ remains unchanged
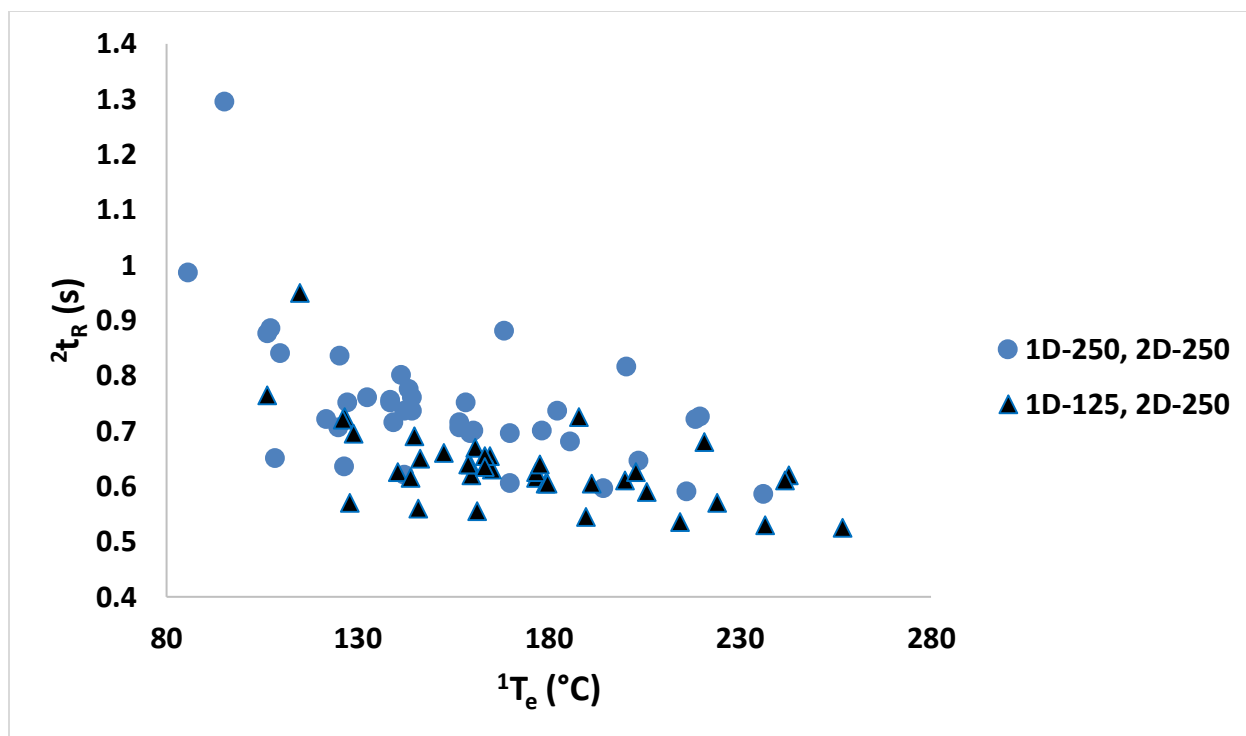
Figure 4-14 Experimental retention of thirty-nine compounds on the Rtx-5MS×Rtx-200MS

GC×GC separation space when $^1\beta$ is reduced from 250 to 125 while $^2\beta$ remains unchanged

Table 4-9 shows the differences between the characteristic temperature of each compound on the

primary column, $^1T_{char}$, and their elution temperatures, ^1T_e, on that column using Combination D.

It also contains the differences between their theoretical secondary retention times, $^2t_{Rtheo}$, and

their experimental secondary retention times, ^2t_R.

Table 4-9 Differences between $^1T_{char}$ and ^1T_e, and between $^2t_{Rtheo}$ and ^2t_R for Combination D

Assigned number	Compound	$^1T_{char} - {}^2T_e$ (°C)	$^2t_{Rtheo} - {}^2t_R$ (s)
1	1,4-dimethylnaphthalene	-0.5	0.13
2	1-octanol	-4.6	0.14
3	1-tetradecanol	-1.1	0.21
4	2,3-dimethylaniline	-2.7	0.12
5	2,5-dichlorophenol	-2.1	0.10

Assigned number	Compound	$^1T_{char} - {}^2T_e$ (°C)	$^2t_{Rtheo} - {}^2t_R$ (s)
6	2,6-dichlorophenol	-2.2	0.09
7	2,6-dimethylaniline	-2.4	0.12
8	2-decanone	-3.2	0.11
9	2-heptanone	-1.7	0.02
10	2-nonanol	-5.4	0.05
11	2-nonanone	-4.0	0.09
12	2-octanone	-3.5	0.06
13	2-tridecanone	-1.5	0.15
14	3-octanone	-3.7	0.03
15	3-tert-butylphenol	-3.4	0.14
16	4-sec-butylphenol	-3.1	0.15
17	4-tertbutylphenol	-3.0	0.13
18	5-nonanol	-5.1	0.16
19	anthracene	6.5	0.11
20	bipheyl	-1.0	0.14
21	decanal	-3.4	0.13
22	decane	-0.4	-0.02
23	dodecane	-5.4	0.25
24	eicosane	-0.7	0.39
25	hexadecane	-4.2	0.31
26	methyl decanoate	-4.0	0.18
27	methyl dodecanoate	-2.4	0.19
28	naphthalene	-1.6	0.11
29	N-ethylaniline	-4.3	0.14
30	octadecane	-1.9	0.30
31	octanal	-3.4	0.08
32	p-ethylaniline	-4.0	0.14
33	phenanthrene	6.8	0.11
34	tetradecane	-5.4	0.30
35	tributylphosphate	-0.7	0.12
36	trimethylphosphate	-4.7	0.01
37	tripropylphosphate	-2.1	0.08
38	undecanal	-2.6	0.13
39	undecane	-3.9	0.16

Combination D, which places the more polar column in the first dimension and the more apolar column in the second dimension, is shown in Figures 4-15 and 4-16. This combination was the most poorly mapped with $^1T_{char}$ being smaller than ^1T_e for most compounds (i.e. compounds eluted from the primary column at higher temperature than expected). On this phase, most compounds had θ_{char} values at about or well below 30 °C. It is also worth noting that the compounds that eluted at a lower temperature than expected have θ_{char} values above 36 °C. The alkanes are particularly poorly mapped and this might be associated with poorer retention near the start of the run on this more polar phase. Compounds 10 and 14 (2-nonanol and 3-octanone) are also mapped quite a ways out of position. The possible reason for this is not quite clear. Lastly, the experiment for this combination was carried out at 23.26 °C min^{-1} whereas 18 °C $t_M$$^{-1}$ would mean that it should have been performed at 23.38 °C min^{-1}. It is therefore hard to pinpoint which factor(s) might be responsible for the relatively poor performance of this map. Despite this, all other compounds ran on Combination D were mapped in a manner that agrees fairly well with the experimental results – the relative positions of compounds still sufficiently matches the experimental data to inform decisions about the use of this combination.
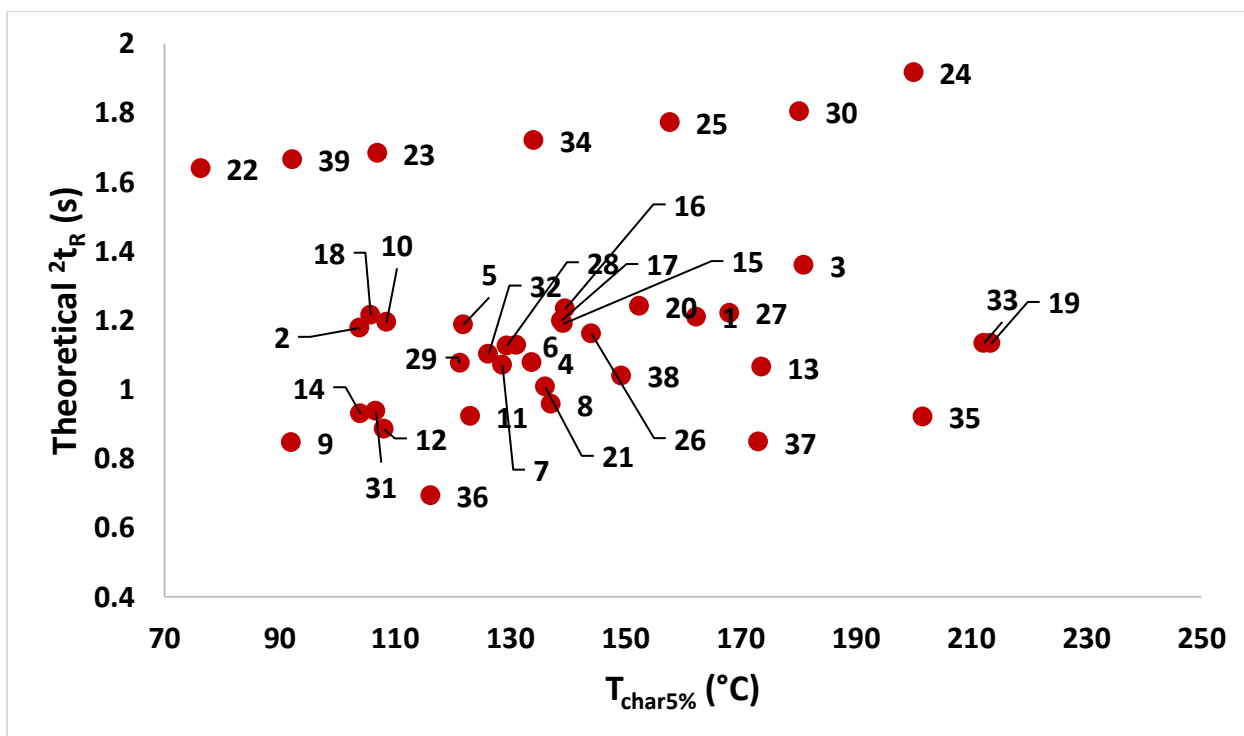
Figure 4-15 Map of the thirty-nine compounds on the Rtx-200×Rtx-5MS GC×GC separation space ($^1\beta$ and $^2\beta = 250$)
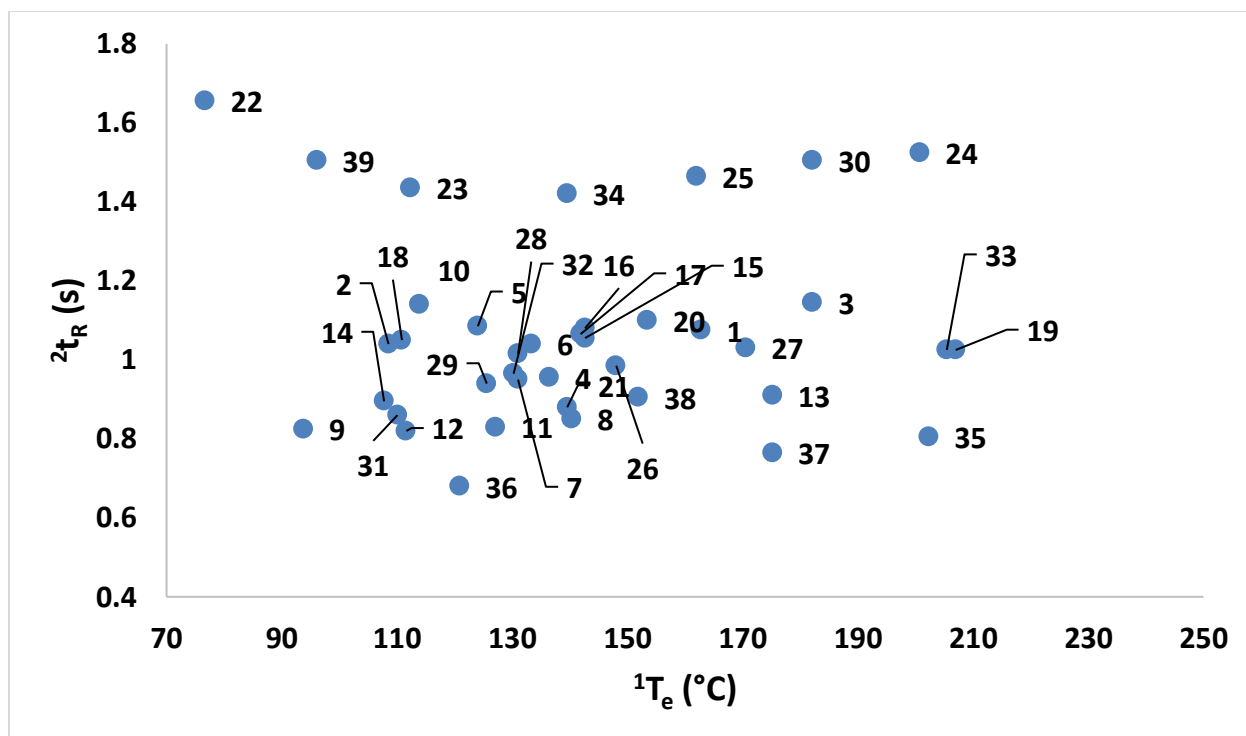
Figure 4-16 Experimental secondary retention times of the thirty-nine compounds and their primary elution temperatures as determined on the Rtx-200×Rtx-5MS GC×GC separation space ($^1\beta$ and $^2\beta$ = 250)

Table 4-10 Differences between $^1T_{char}$ and ^1T_e, and between $^2t_{Rtheo}$ and ^2t_R for Combination E

Assigned number	Compound	$^1T_{char} - {}^2T_e$ (°C)	$^2t_{Rtheo} - {}^2t_R$ (s)
1	1,4-dimethylnaphthalene	5.9	0.05
2	1-octanol	-1.5	0.03
3	1-tetradecanol	4.4	0.04
4	2,3-dimethylaniline	2.5	0.06
5	2,5-dichlorophenol	1.4	0.06
6	2,6-dichlorophenol	2.5	0.06
7	2,6-dimethylaniline	2.0	0.07
8	2-decanone	0.0	0.03
9	2-heptanone	2.1	0.02
10	2-nonanol	-1.7	-0.03
11	2-nonanone	-0.6	0.03
12	2-octanone	-0.4	0.04

Assigned number	Compound	$^1T_{char} - {}^2T_e$ (°C)	$^2t_{Rtheo} - {}^2t_R$ (s)
13	2-tridecanone	2.7	0.04
14	3-octanone	-0.4	-0.01
15	3-tert-butylphenol	0.8	0.07
16	4-sec-butylphenol	0.8	0.07
17	4-tertbutylphenol	1.4	0.06
18	5-nonanol	-1.1	0.02
19	anthracene	13.5	0.02
20	bipheyl	5.6	0.05
21	decanal	0.3	0.04
22	decane	-0.7	0.04
23	dodecane	-0.8	0.01
24	eicosane	3.2	0.04
25	hexadecane	2.9	0.02
26	methyl decanoate	0.3	0.04
27	methyl dodecanoate	2.7	0.04
28	naphthalene	3.5	0.06
29	N-ethylaniline	0.8	0.05
30	octadecane	4.1	0.03
31	octanal	-0.4	0.04
32	p-ethylaniline	1.6	0.06
33	phenanthrene	13.4	0.02
34	tetradecane	1.1	0.02
35	tributylphosphate	2.9	0.06
36	trimethylphosphate	-0.9	0.05
37	tripropylphosphate	0.1	0.08
38	undecanal	1.1	0.04
39	undecane	-1.3	0.02

The last combination, Combination E, is mapped in Figure 4-17 with experimental data shown in figure 4-18. This combination is well mapped with the exception of compound 10 and 14, both of which elute out of position from their mapped distribution. Again, it is not quite clear why these two compounds display this anomalous behaviour.
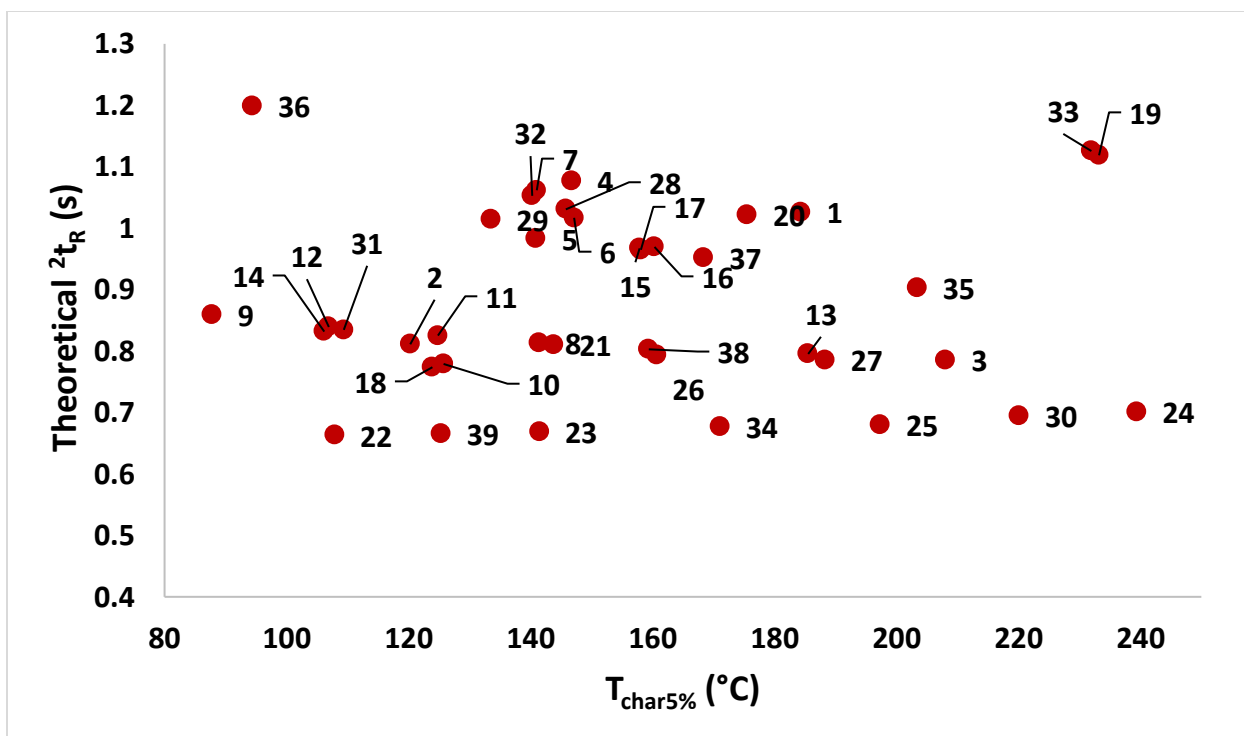
Figure 4-17 Map of the thirty-nine compounds on the Rtx-5MS×Rxi-17Sil MS GC×GC

separation space ($^1\beta$ and $^2\beta = 250$)

Figure 4-18 Experimental secondary retention times of the thirty-nine compounds and their primary elution temperatures as determined on the Rtx-5MS×Rxi-17Sil MS GC×GC separation space ($^{1}\beta$ and $^{2}\beta = 250$)

Across all of these combinations, the maps continue to serve as good indicators of distribution and provide helpful insight that a chromatographer can use in selecting stationary phases for their separation. They are fast to generate, as long as the thermodynamic parameters A, B and C for the compounds of interest are known. With further mathematical rigor, they could prove very useful for predicting retention times for the sake of optimizing experimental conditions.

4.3.3 Mapping more typical GC×GC conditions – a first step towards accurate prediction

In assessing the quality of the maps generated from characteristic parameters, experiments were performed to give conditions that would permit elution of compounds from the primary column

with k ≈ 1. This made sense because the characteristic parameters are defined at this value of retention factor, primarily for mathematical simplicity/elegance. In practice, however, it is not common to perform GC×GC separations at ramp rates as fast as 18 °C t_M^{-1}. Oven ramp rates tend to be slower than this and an advisable starting point for many separations is to estimate optimal heating rate, OHR [119] at about 10 °C t_M^{-1}. With this in mind, attempts were made at generating a map that would closer reflect an experiment performed at a more typical ramp rate as well as performing initial investigations into using these parameters for GC×GC retention time prediction. The steps involved in this attempt are outlined in section 4.2.3 above.

Table 4-11 shows the differences between predicted elution temperature and actual elution temperature as well as between predicted secondary retention times and actual retention times. Briefly, absolute errors in primary elution temperatures, ^1T_e, ranged from 0.4 °C to 1.8 °C. All were less than 1 °C except the trialkylphosphates, which might further suggest the influence of compound chemistry on the accuracy of predictions. To put this into context that is more common in chromatography, errors in ^1t_R ranged from 2.7 s to 12.1 s (5.8 s max without the trialkylphosphates) and a median of 4.8 s. These values are unusually large and fall within ranges we typically consider unacceptable for good simulation (although still arguably useful for method optimization). The magnitude of these errors could be attributed to two possible factors. 1) Currently, we do not have a convenient means of calibrating GC×GC target systems to allow accurate transfer of thermodynamic parameters. As such, the thermodynamic parameters used here were calculated using nominal geometries for both reference and target systems. Geometric calibration is especially important in GC×GC given the short length of the second dimension column (which could make deviations in its geometry from nominal more pronounced) and the dead volumes within the press-fits (the connectors between columns). Additionally, in this

system, modulation takes place after about 4-5 cm of secondary column which likely needs to be accounted for in any calibration method developed. 2) These calculations were performed using a method that assumes the outlet of the column is at atmospheric pressure (or vacuum if attached to a mass spectrometer). The outlet of the primary column, however, would be at some other pressure (about 2-3 psi higher for this set-up) than atmospheric in a GC×GC configuration. Calculating this pressure would not be too difficult in theory, however updating the existing MATLAB code to calculate and update this pressure with each iteration (as temperature and inlet pressure increased) was not feasible in the available time. A similar calculation and iterative update would also have to be done for the outlet of the secondary column while the outlet of the transfer line would have to remain at constant pressure throughout the run. It is expected that addressing these factors in the future will reduce the magnitude of these errors. However, it should be noted that these errors in first dimension retention time correspond to relative errors from 0.27 % to 2.61 % with a median of 0.65 %, which is quite impressive given the more rudimentary nature of this initial trial.

Table 4-11 Differences between $^1T_{e,theo}$ and ^1T_e, and between $^2t_{Rtheo}$ and ^2t_R

Assigned number	Compound	$^1T_{e,theo} - {}^1T_e$ (°C)	$^2t_{Rtheo} - {}^2t_R$ (s)
1	1-octanol	-0.8	0.007
3	2,6-dimethylaniline	-0.8	0.061
4	2-decanone	-0.5	0.075
5	2-heptanone	-0.7	-0.003
7	2-nonanone	-0.6	0.055
8	2-octanone	-0.8	0.035
9	2-tridecanone	-0.4	0.104
10	3-octanone	-0.9	-0.002
11	5-nonanol	-0.5	0.004
13	bipheyl	-0.4	0.059
14	decanal	-0.4	0.065

Assigned number	Compound	$^1T_{e,theo} - {}^1T_e$ (°C)	$^2t_{Rtheo} - {}^2t_R$ (s)
15	decane	-0.7	-0.035
16	dodecane	-0.8	-0.010
17	eicosane	-0.6	0.063
18	hexadecane	-0.8	0.023
19	methyl decanoate	-0.7	0.056
20	methyl dodecanoate	-0.5	0.077
21	naphthalene	-1.0	0.059
22	octadecane	-0.6	0.043
23	octanal	-0.6	0.028
25	tetradecane	-0.8	0.013
26	tributylphosphate	-1.1	0.156
27	trimethylphosphate (unwrapped)	-1.8	0.029
28	tripropylphosphate	-1.3	0.132
29	undecanal	-0.4	0.078
30	undecane	-0.7	-0.019

Absolute prediction errors in ^2t_R ranged from 0.00_2 s to 0.15_6 s with a median of 0.04_9 s (relative errors from 0.17_7 % to 14.3_2 %, median 6.39_0 %). Note that the trimethylphosphate peak was wrapped around once so the calculation was carried out for the unwrapped peak. This is not a bad thing as the map showed that that compound would wrap around, which is something the chromatographer would want to consider when developing the GC×GC method. Also, note that the two largest errors were associated with tributylphosphate and tripropylphosphate, both above 10 %. Given the small numerical values of second dimension retention times and the speed of the separation on that phase, it is reasonable to expect their relative errors to be larger than those of ^1t_R. Ideally, I would prefer they be below 5 %. However, the errors observed here are quite decent for an initial trial. They are likely influenced by the same thermodynamic calibration factors as the first dimension errors, perhaps to a greater extent. Also, these predicted second dimension retention times were calculated using ^2t_M and ^1t_M at 150 °C. Again, the calculation of the dead times of these columns is not difficult in and of itself but time did not permit me to

rewrite the MATLAB scripts to calculate and update these values with each iteration. Doing this would likely reduce these errors and will definitely add more meaning to their interpretation.

The plot of the map for this work is show in in Figure 4-17 while the experimental data is plotted in Figure 4-18. This set-up is well mapped overall. Note that on the map two points are shown for compound 27, trimethylphosphate (the wrapped and unwrapped prediction).
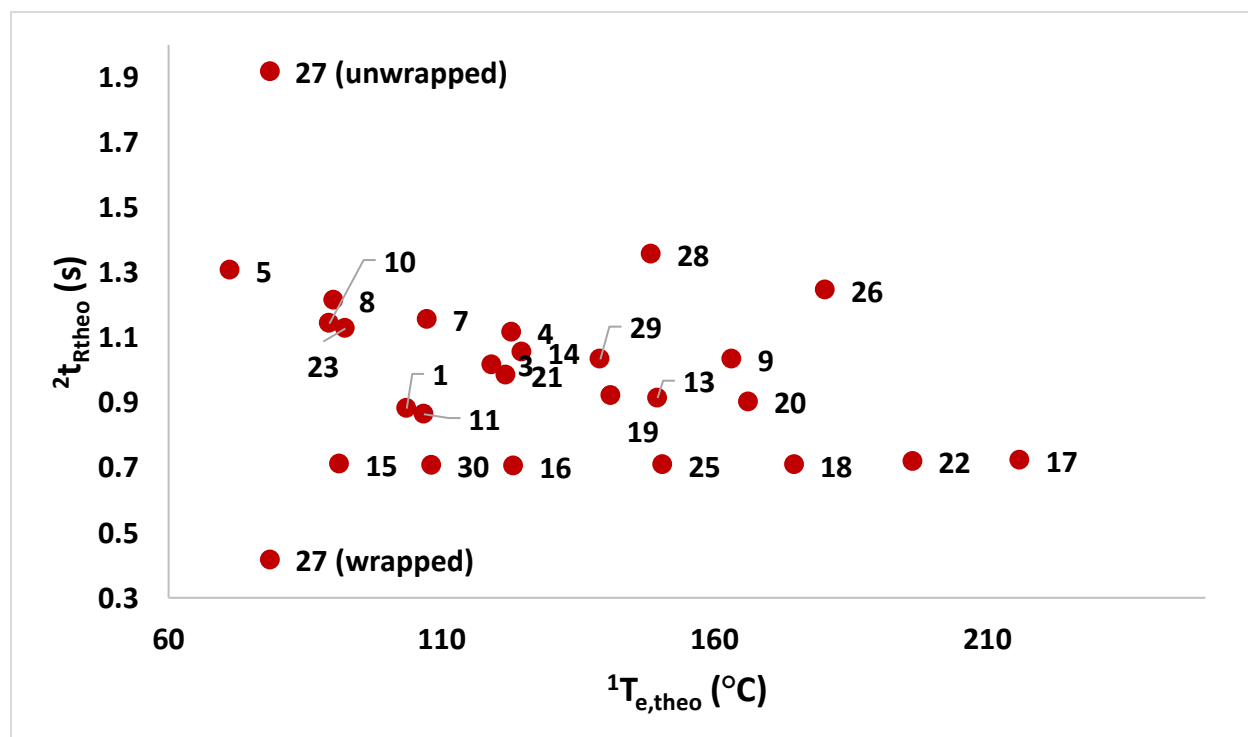
Figure 4-19 Map of the thirty-nine compounds on the Rtx-5MS×Rtx-200MS GC×GC separation space ($^{1}\beta$ and $^{2}\beta = 250$) under normal conditions
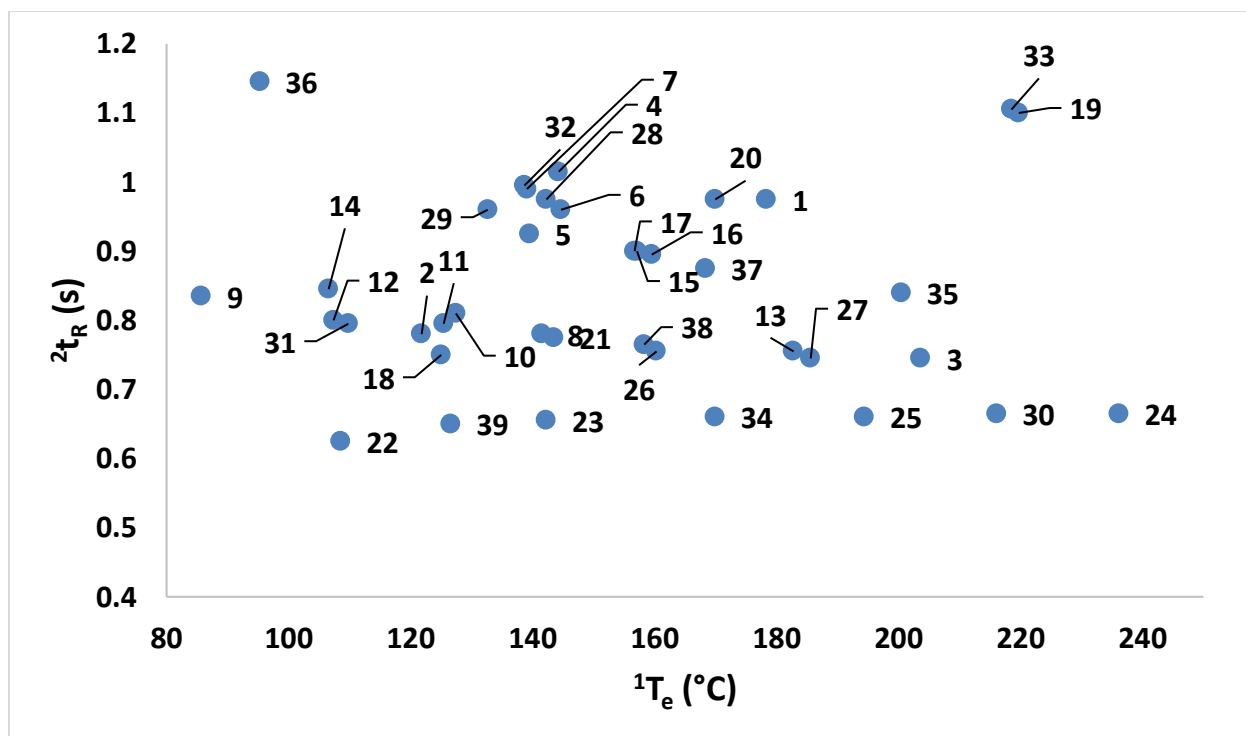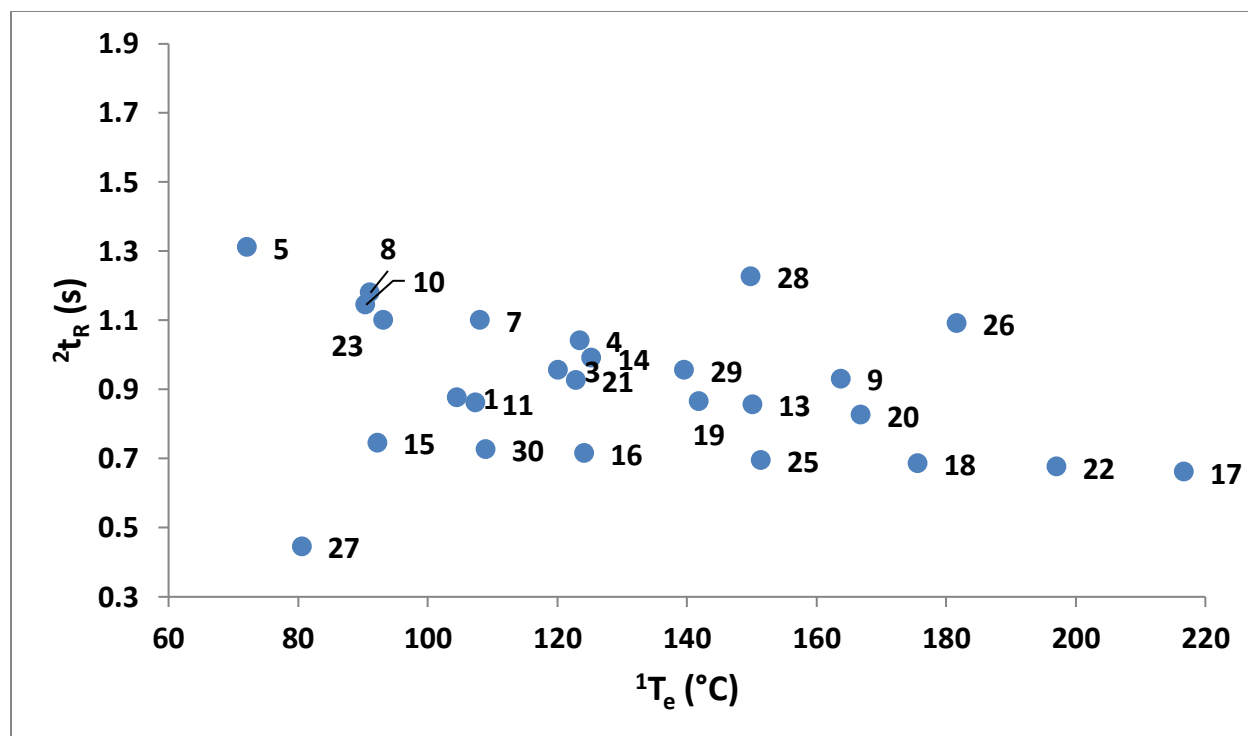
Figure 4-20 Experimental secondary retention times of the 39 compounds and their primary elution temperatures as determined on the Rtx-5×Rtx-200MS GC×GC separation space ($^1\beta$ and $^2\beta = 250$)

Lastly, it is worth mentioning that thermally modulated GC×GC separations are generally performed with the modulator and secondary oven temperatures at some positive offset to the primary oven and each to other. In future, this would have to be factored into these models to improve their usefulness in predicting and optimizing these separations. That said, plots such as Figure 4-1 along with the characteristic thermal constants of each analyte already provide insight into how secondary oven temperature offsets might impact the maps and predictions.

4.4 Conclusions

Characteristic thermodynamic parameters acquired through distribution-centric thermodynamic models provide useful and chromatographically meaningful parameters. They can be used to generate maps that guide stationary phase chemistry, stationary phase configuration and stationary phase ratio selection in GC×GC. With careful mathematical refinement, it would be possible to quickly and accurately predict and simulate GC×GC separations under normal conditions, thereby allowing the optimization of pneumatic and temperature conditions.

Chapter 5: Conclusions and Future Work

5.1 Conclusions

One of the major obstacles that prevents the widespread usage of thermodynamics-based predictive retention models is the absence of a readily available database/library of thermodynamics-based parameters. The creation and growth of such a database was hindered by the tedious and often manually intensive work that was once required to acquire estimates of thermodynamic parameters from isothermal data. Were the establishment of such a database more feasible, it would be fair to say that thermodynamic models would become more commonplace as tools for predicting retention parameters with the ultimate aim of GC(×GC) method development and optimization.

Our research group, over the years has contributed greatly to the creation of experimental, data analysis, and numerical optimization/curve-fitting methods that have significantly reduced the amount of time and effort once required to obtain accurate and reliable estimates. Bryan Karolat, during his time as a Masters student investigated the performance of 2-parameter, 3-paramater and 4-parameter retention models for the determination of GC thermodynamic parameters from isothermal retention data. His work demonstrated the superior performance of the linearized 3-parameter model over the others, a model which played a fundamental role in all the work carried out in my thesis. Dr. Teague McGinitie, often in collaboration with Dr. Heshmatollah Ebrahimi-Najafabadi, built on the work laid out by Bryan Karolat in several areas. These include (but are not limited to) the creation of a rapid method for acquiring thermodynamic parameters from temperature-programmed experiments, the development of a method for calibrating thermodynamic data to be useful across column geometries and the application of the rapidly

obtained parameters to predicting GC(×GC) separations in flow- and thermal-modulated systems. His work resulted in an interlaboratory round-robin study aimed at evaluating his models and methods across instruments and laboratories. It was at this point that I entered into the story as a Masters student (initially aiding in the experiments, data analysis and calculations towards the end of the round-robin study).

With so many great accomplishments in the areas of thermodynamic predictive modeling of GC and GC×GC, my goals upon arrival to the group as a then Masters student were few, and on the surface, simple. One major task involved performing the required calculations on all the data from the round-robin study in order to assess the prediction accuracy of the models across instruments and labs. It was expected the models would have performed exceptionally well in this regard, leaving me one last but extensive remaining goal – the creation of (using existing tools) an accessible library/database of thermodynamic parameters for hundreds/thousands of compounds on several stationary phase chemistries using H_2 (g) and He (g) mobile phases. Fortunately (or unfortunately), these models did not perform as well as expected when predicting across labs and instruments. This created an opportunity for my research (*and grey hairs*) to grow beyond its (*their*) initial scope (*numbers*).

Before a thermodynamic database could be built, it was important to ensure that the parameters contained within could provide accurate and reliable retention time prediction across columns of the same stationary phase, not just with different geometries but installed in different instruments. Developing a way to do that, while maintaining/improving upon the speed and efficiency our group had already built into previous approaches, became the new "initial" focus of my work. This led to the work presented in Chapter 2 of this thesis. Through experimental redesign, I was able to reduce the number of experiments (as well as the time for

experimentation) required to obtain calibrated, transferable estimates of column geometry and thermodynamics-based parameters by eliminating the need for counting the rings of a wound up column or uncoiling the column to attain its length. The need to perform replicated injections of methane to calculate the calibrated inner diameter of the reference column was also eliminated through experimental and computational redesign. The number of experiments required from the user of the target column was also reduced, representing an overall improvement in ease of use and implementation. Chapter 2 also demonstrated an improvement in the predictive accuracy of retention times across columns of the same stationary phase but of different diameters and installed in different instruments. Upon evaluation of the data from the round-robin study (as well the results of each step of the calculation involved), I noticed that the Nelder-Mead simplex converged on different values of $\Delta H(T_0)$, $\Delta S(T_0)$ and ΔC_p when the optimization was started from a different initial guess. This suggested that a more reliable numerical optimization method might have to be attempted. It become clearer to me that other numerical optimization methods would have to be explored. Unfortunately, despite knowing of various optimization methods, the relevant equations that would have to be solved/derived to implement them, and understanding the steps involved in obtaining the minimum of a given objective function, I lacked the mathematical and programming prowess required to solve/derive many of the equations and create a program to implement the method(s). Apart from my lack of ability to perform higher order vector calculus and matrix calculus, and to write code that would operate on such equations, I also lacked the time to required to become sufficiently competent at these skills. However, Dr. Siyuan Hou brought a high level of mathematical and computational competence to the project that complemented my insight into chromatographic theory, thermodynamic modelling, fluid dynamics, and GC experimental design and execution. Together we created a

quasi-Newton based approach to thermodynamic parameter estimation and retention time prediction that was demonstrated to give accurate predictions across column geometries and GC systems. The approach did not compromise on the computational speed available from the Nelder-Mead simplex but instead performed faster. This speed, accuracy and consistency permitted its use in the creation of a small database of thermodynamic parameters for ~115-180 compounds on four stationary phase chemistries.

Once a reliable means of obtaining transferable thermodynamic parameters was obtained, a greater range of projects than initially envisioned became possible. One very important step towards simulating GC separations for method development purposes involved the creation of a method for predicting peak widths. The existing academic literature did not lack any materials on this matter and although it was not as widely covered as retention time predictions, several other researchers had published good work on the area of peak width prediction. There remained, however, a set of specifications that were required in a peak width predictive model that appeared to be unmet in the literature. It had to integrate well into our existing fast, accurate and reliable models and prediction methods. That meant that it had to 1) use thermodynamic parameters obtainable through our existing methods, 2) require little or no additional experimentation for the user (and preferably its implementation) and 3) quickly and accurately predict peak widths on a column of a given stationary phase regardless of its geometry or the system in which it is installed. Moreover, it also became apparent to me that most attempts at peak width modelling in literature produced typical prediction errors of up to 10%. This appeared to the be result of modelling only ideal on-column contributions to band broadening and ignoring coating-efficiency or extra-column contributions all together. In cases in which these contributions were not ignored, no useful way was presented for approximating their value.

In one case, a value for coating efficiency of 90 % was assumed, without explanation, then tossed into the equations [79]. The work presented in Chapter 3 of this document demonstrated a fast, accurate and well-integrated thermodynamics-based method for predicting peak with in GC separations. The method met the three requirements listed above and illustrated a way to estimate quickly the contributions of coating efficiency and extra-column band broadening specifically on the system and column of the user. This resulted in prediction errors typically well below 5%, making this approach useful for predicting the resolution between peaks with close retention times as well as guiding a choice of modulation period for a GC×GC separation. This work resulted in another useful thermodynamic tool for GC method development and optimization.

Following the extensive work that went into the results presented in Chapters 2 and 3, the next step involved using the newly developed tools for thermodynamic parameter estimation to model retention in GC×GC systems. Work carried out by Dr. McGinitie has successfully resulted in retention time predictions in flow modulated and thermally modulated GC×GC systems. The former gave prediction errors in ^1t_R ranging 0.1 s to 18.5 s and in ^2t_R ranging from 0.0 s to 0.3 s while the latter showed errors spanning 0.1 s to 56.0 s in ^1t_R and 0.0 s to 0.4 s in ^2t_R. In both cases, the accuracy in prediction ranged from excellent to very poor with errors from the thermally modulated system being generally worse in both dimensions than the flow modulated system. This was understandable as flow modulated systems tend to be easier to model given that they typically consist of a single oven (as opposed to three independently heated zones in thermally modulated systems). Also, pressures at the beginning of each column can be easily calculated and set (the second-dimension column has its own electronic pneumatics control instead of relying on inlet pressure). Therefore, despite having a new way to acquire reliable (with consistent convergence) thermodynamics-based parameters, the fundamental oven

temperature and column pneumatics challenges associated with modelling thermally modulated GC×GC experiments still remained. However, a conversation with Dr. Leonid Blumberg about his paper on distribution-centric thermodynamic modelling, at the ISCC and GC×GC conference in 2017, generated new ideas about modelling GC×GC. By using characteristic thermodynamic parameters and oven ramp rates normalized by dead times (a base unit of time in GC that would contain information about pressures throughout the system) a new approach to looking at GC×GC predictions was envisioned. Given the more involved mathematical, experimental and computational requirements involved in making accurate GC×GC retention time predictions, the work (presented in Chapter 4) initially focused instead on mapping distribution (or relative retention) of compounds on different GC×GC stationary phase chemistries, configurations and phase ratios. The aim was to use this distribution as a fast, easy means of informing decisions surrounding the choice of columns for separating a variety of molecules. The maps, corroborated by experimental data, proved very useful towards this end. Initial attempts into performing accurate GC×GC retention prediction under typical (albeit simplified with regards to heated zones) conditions proved promising – prediction errors in ^1t_R ranging from 2.7 s to 12.1 s and in ^2t_R ranging from 0.00 s to 0.16 s. It is not fair to say this represents an improvement in prediction accuracy as the model used for prediction still requires more mathematical rigour in order to more truly represent the conditions of a GC×GC separation. However, one can rapidly (in seconds) generate dozens of these retention maps for different stationary phase combinations, providing an incredibly fast route to answering the question of column phase combinations and phase ratios which should be used in a GC×GC separation.

The work described in this thesis represents several major contributions towards the areas of gas chromatography, comprehensive multidimensional gas chromatography and thermodynamic

modelling of their processes. As a result of this work, thermodynamic parameters can be accurately transferred across column geometries and GC systems enabling very fast and accurate simulation of GC separations, including retention times and peak widths. The building of a library of thermodynamic parameters has been initiated and can continue with the use of the tools presented herein. Also, characteristic parameters and a distribution centric approach to thermodynamic modelling has been presented as a meaningful and viable tool for mapping distribution, and ultimately predicting retention in GC×GC.

5.2 Future Work

Despite the progress and contributions made through this work, there remains unfinished tasks as well as areas in which improvements can still be made. As is the case with graduate studies, limitations related to time restricted the ability to perform most of the following suggestions.

The code that is used to perform the quasi-Newton optimization needs to be improved so that it can estimate thermodynamic and geometric parameters using retention data from molecules that elute outside of the oven ramp duration (e.g. molecules that elute from the reference column during the hold time at the final temperature). While it is a simple task to predict retention times and peak widths of molecules eluting from the target column during hold times, obtaining thermodynamic parameters from such molecules on the reference column is a slightly more challenging but necessary coding task.

It would be wise to carry out several more studies to assess further just how much of an improvement the quasi-Newton approach coupled with a reduction in experimental time made on the predictions. These studies could include an interlaboratory round-robin study similar to the one carried out prior to this work. Another study would be an evaluation of how well the model

predicts across columns of nominally identical chemistries but from different manufactures (e.g. Restek Rtx-5 and Agilent HP-5) as well as within the same brand, columns with similar selectivities but structurally different polymers that reduce column bleed/increase stability (e.g. Rtx-5 and Rxi-5Sil MS). It is also important and advisable to assess the stability of the calibrated thermodynamic and geometric parameters of a reference column after many injections and cycles of heating and cooling have been carried out on it. Although I am confident the model will work just fine, it is important to experimentally verify its ability to be used with non-atmospheric pressure detectors such as mass spectrometers.

The library of thermodynamic parameters needs to grow. It needs to include near as many compounds as there are retention indices readily available for and more interesting stationary phases. In the 2018 Fall Term, an undergraduate student, Caleb Sinn, carried out preliminary experiments using three different ionic liquid columns. The library should also contain thermodynamic parameters for compounds on systems in which $H_2(g)$ is the carrier gas as these are not uncommon. Alternatively, a means of translating predictions across carrier gases should be developed and a good basis for this would be the work on method translation published by L.M. Blumberg [118] discussing the use of dead times as a base time unit in GC. Of course, such tasks require a great deal of time and effort but could be pursued as grand collaborative efforts (much like retention index libraries). Ideally however, I would like to see a stronger shift towards using Quantitative-Structure Retention Relationship (QSRR) models that can accurately and reliably correlate *A*, *B* and *C* terms with molecular descriptors. This will eliminate the need for experiments in building the library and add a layer of compound identification capabilities to the models. Work has been done in this area but has generally suffered from unacceptable prediction errors.

The code that is used to predict peak widths is currently just a well-commented MATLAB script into which input data can be pasted and from which output data can be copied. I would like for it to be incorporated into the graphic user interface developed from the retention time prediction software with its inputs and outputs being read and written in a more seamless manner. Any further assessment of the retention time prediction model (such as the ones suggested above) should be accompanied by an assessment of the peak width prediction model on the same data.

A fair bit of work remains to be done on the K-centric models used to acquire characteristic parameters for predicting GC×GC retention times. The codes used to predict the first dimension retention time need to be modified. They should include the option to add outlet pressures that ramp for the first dimension and the second dimension while maintaining constant pressure at the outlet of the transfer line (in keeping with the physics of constant flow separations). The pressures at these points should update iteratively. Additionally, the codes should calculate the void time of each column (including the transfer line) as a compound elutes from the primary column. These two changes would permit more representative modelling of the second dimension retention time from retention factors calculated using characteristic parameters. Experimental verification of the effect of secondary and modulator oven offsets on the secondary retention factors of analytes should be carried out as well to allow the model to be useful under conditions in which the analytes experience three heated zones during a separation.

Although the calculation of characteristic parameters from A, B and C can be performed in under 10 seconds for 39 molecules, as the libraries grow it would be prudent to add these parameters to the libraries themselves instead of requiring their calculation everytime they are needed. Lastly, the code for generating the maps should also be elegantly incorporated into the existing GUI with more seamless data entry and result output.

Bibliography

1. Tsvet, M. Physikalisch-chemische Studien über das chlorophyll. Die Adsorptionen. *Berichte der Deutschen botanischen Gesellschaft* **1906**, *24*, 20.

2. *https://www.businesswire.com/news/home/20180427006031/en/Global-Chromatography-Instruments-Market-8.02-Billion-2017* (accessed Dec 6, 2018).

3. Valcárcel, M.; Ríos, A. The analytical problem. *Trends in Analytical Chemistry* **1997**, *16*, 385-393.

4. James, A. T.; Martin, A. J. P. Gas-liquid partition chromatography; the separation and micro-estimation of volatile fatty acids from formic acid to dodecanoic acid. *Biochemical Journal* **1952**, *50*, 679-690.

5. Heines, V. Chromatography-history of a parallel development. *Chemical Technology* **1971**, *1*, 280-285.

6. Ettre, L. S. Development of chromatography. *Analytical Chemistry* **1971**, *43*, 20-31.

7. Ettre, L. S. *Milestones in the Evolution of Chromatography;* ChromSource Inc: United States of America, 2002; .

8. Pollo, B. J.; Alexandrino, G. L.; Augusto, F.; Hantao, L. W. The impact of comprehensive two-dimensional gas chromatography on oil & gas analysis: Recent advances and applications in petroleum industry. *Trends in Analytical Chemistry* **2018**, *105*, 202-217.

9. Elder, D. GC-MS applications in pharmaceutical analysis. *European Pharmaceutical Review* **2017**, *22*, 48-52.

10. Cordero, C.; Kiefl, J.; Schieberle, P.; Reichenbach, S. E.; Bicchi, C. Comprehensive two-dimensional gas chromatography and food sensory properties: potential and challenges. *Analytical and Bioanalytical Chemistry* **2015**, *407*, 169-191.

11. Souza-Silva, É A.; Gionfriddo, E.; Pawliszyn, J. A critical review of the state of the art of solid-phase microextraction of complex matrices II. Food analysis. *Trends in Analytical Chemistry* **2015**, *71*, 236-248.

12. Song, H.; Liu, J. GC-O-MS technique and its applications in food flavor analysis. *Food Research International* **2018**, *187-198*.

13. Al-Rubaye, A. F.; Hameed, I. H.; Kadhim, M. J. A Review: Uses of Gas Chromatography-Mass Spectrometry (GC-MS) Technique for Analysis of Bioactive Natural Compounds of

Some Plants. *International Journal of Toxicological and Pharmacological Research* **2017**, *9*, 81-85.

14. Souza-Silva, É A.; Jiang, R.; Rodríguez-Lafuente, A.; Gionfriddo, E.; Pawliszyn, J. A critical review of the state of the art of solid-phase microextraction of complex matrices I. Environmental analysis. *Trends in Analytical Chemistry* **2015**, *71*, 224-235.

15. Sampat, A.; Lopatka, M.; Sjerps, M.; Vivo-Truyols, G.; Schoenmakers, P.; van Asten, A. Forensic potential of comprehensive two-dimensional gas chromatography. *Trends in Analytical Chemistry* **2016**, *80*, 345-363.

16. Grob, R. L.; Barry, E. F. *Modern Practice of Gas Chromatography;* John Wiley & Sons: 2004; .

17. Martin, A. J. P.; Synge, R. L. M. A new form of chromatogram employing two liquid phases. *Biochemical Journal* **1941**, *35*, 1358.

18. Skoog, D. A.; Crouch, S. R.; Holler, F. J. *Principles of instrumental analysis;* Thomson: Belmont, Calif, 2007; .

19. Harris, D. C. *Quantitative Chemical Analysis;* W. H. Freeman: 2010; .

20. van Deemter, J. J.; Zuiderweg, F. J.; Klinkenberg, A. Longitudinal diffusion and resistance to mass transfer as causes of nonideality in chromatography. *Chemical Engineering Science* **1956**, *5*, 271-289.

21. Seeley, J. V. Recent advances in flow-controlled multidimensional gas chromatography. *Journal of Chromatography A* **2012**, *1255*, 24-37.

22. *http://www.chromatographyonline.com/nomenclature-and-conventions-comprehensive-multidimensional-chromatography-update* (accessed Dec 6, 2018).

23. Watson, N. E.; Bahaghighat, H. D.; Cui, K.; Synovec, R. E. Comprehensive Three-Dimensional Gas Chromatography with Time-of-Flight Mass Spectrometry. *Analytical Chemistry* **2017**, *89*, 1793-1800.

24. Watson, N. E.; Siegler, W. C.; Hoggard, J. C.; Synovec, R. E. Comprehensive Three-Dimensional Gas Chromatography with Parallel Factor Analysis. *Analytical Chemistry* **2007**, *79*, 8270-8280.

25. Liu, Z.; Phillips, J. B. Comprehensive Two-Dimensional Gas Chromatography using an On-Column Thermal Modulator Interface. *Journal of Chromatographic Science* **1991**, *29*, 227 231.

26. Giddings, J. C. Two-dimensional separations: concept and promise. *Analytical Chemistry* **1984**, *56*, 1270A.

27. Giddings, J. C. Concepts and comparisons in multidimensional separation. *Journal of High Resolution Chromatography* **1987**, *10*, 319-323.

28. Giddings, J. C. Sample dimensionality: A predictor of order-disorder in component peak distribution in multidimensional separation. *Journal of Chromatography A* **1995**, *703*, 3-15.

29. von Mühlen, C.; Khummueng, W.; Zini, C. A.; Caramão, E. B.; Marriott, P. J. Detector technologies for comprehensive two-dimensional gas chromatography. *Journal of Separation Science* **2006**, *29*, 1909-1921.

30. Khummueng, W.; Harynuk, J.; Marriott, P. J. Modulation ratio in comprehensive two-dimensional gas chromatography. *Analytical Chemistry* **2006**, *78*, 4578-4587.

31. Murphy, R. E.; Schure, M. R.; Foley, J. P. Effect of Sampling Rate on Resolution in Comprehensive Two-Dimensional Liquid Chromatography. *Analytical Chemistry* **1998**, *70*, 1585-1594.

32. Seeley, J. V.; Micyus, N. J.; Bandurski, S. V.; Seeley, S. K.; McCurry, J. D. Microfluidic deans switch for comprehensive two-dimensional gas chromatography. *Analytical Chemistry* **2007**, *79*, 1840-1847.

33. Bahaghighat, H. D.; Freye, C. E.; Synovec, R. E. Recent advances in modulator technology for comprehensive two dimensional gas chromatography. *Trends in Analytical Chemistry* **2018**.

34. Deans, D. R. An improved technique for back-flushing gas chromatographic columns. *Journal of Chromatography A* **1965**, *18*, 477-481.

35. Deans, D. R. Use of heart cutting in gas chromatography: A review. *Journal of Chromatography A* **1981**, *203*, 19-28.

36. Tranchida, P. Q.; Purcaro, G.; Dugo, P.; Mondello, L.; Purcaro, G. Modulators for comprehensive two-dimensional gas chromatography. *Trends in Analytical Chemistry* **2011**, *30*, 1437-1461.

37. Silva, A. C. A.; Ebrahimi-Najafadabi, H.; McGinitie, T. M.; Casilli, A.; Pereira, H. M. G.; Aquino Neto, F. R.; Harynuk, J. J. Thermodynamic-based retention time predictions of endogenous steroids in comprehensive two-dimensional gas chromatography. *Analytical and Bioanalytical Chemistry* **2015**, *407*, 4091-4099.

38. Reichenbach, S. E. Chapter 4 Data Acquisition, Visualization, and Analysis. *Comprehensive Analytical Chemistry* **2009**, *55*, 77-106.

39. Harynuk, J.; Górecki, T. Experimental variables in GC×GC: A complex interplay. *American Laboratory* **2007**, *39*, 36-39.

40. Gerbino, T. C.; Castello, G.; D'Amato, G. Gas chromatographic identification of halogenated hydrocarbons by using the correlation between their retention and boiling points. *Journal of Chromatography A* **1992**, *609*, 289-296.

41. Gerbino, T. C.; Castello, G. The use of predicted boiling points for the identification of halobenzenes and substituted phenols in capillary gas chromatography. *Journal of High Resolution Chromatography* **1996**, *19*, 377-382.

42. Héberger, K.; Kowalska, T. Thermodynamic properties of alkylbenzenes from retention-boiling point correlations in gas chromatography. *Chromatographia* **1997**, *44*, 179-186.

43. Héberger, K.; Kowalska, T. Thermodynamic significance of boiling point correlations for alkylbenzenes in gas chromatography: Extension of Trouton's rule. *Journal of Chromatography A* **1999**, *845*, 13-20.

44. Pérez-Parajón, J. M.; Santiuste, J. M.; Takács, J. M. Prediction of the Retention Indices of Benzene and Methylbenzenes Based on their Retention Data-Physico Chemical Properties Relationship. *Chromatographia* **2004**, *60*, 199-206.

45. Kováts, E. Gas-chromatographische Charakterisierung organischer Verbindungen. Teil 1: Retentionsindices aliphatischer Halogenide, Alkohole, Aldehyde und Ketone. *Helvetica* **1958**, *41*, 1915-1932.

46. van Den Dool, H.; Dec. Kratz, P. A generalization of the retention index system including linear temperature programmed gas—liquid partition chromatography. *Journal of Chromatography A* **1963**, *11*, 463-471.

47. Zellner, B. d.; Bicchi, C.; Dugo, P.; Rubiolo, P.; Dugo, G.; Mondello, L. Linear retention indices in gas chromatographic analysis: a review. *Flavour and Fragrance Journal* **2008**, *23*, 297-314.

48. von Mühlen, C.; Marriott, P. J. Retention indices in comprehensive two-dimensional gas chromatography. *Analytical and Bioanalytical Chemistry* **2011**, *401*, 2351-2360.

49. Zhang, J.; Koo, I.; Wang, B.; Gao, Q.; Zheng, C.; Zhang, X. A large scale test dataset to determine optimal retention index threshold based on three mass spectral similarity measures. *Journal of Chromatography A* **2012**, *1251*, 188-193.

50. Castells, R. C.; Arancibia, E. L.; Miguel Nardillo, A. Regression against temperature of gas chromatographic retention data. *Journal of Chromatography A* **1990**, *504*, 45-53.

51. Lomsugarit, S.; Jeyashoke, N.; Krisnangkura, K. Relationship between carbon number and peak width in gas chromatography. *Journal of Chromatography A* **2001**, *926*, 337-340.

52. Lomsugarit, S.; Krisnangkura, K. An alternative approach for predicting peak width in gas chromatography. *Chromatographia* **2002**, *56*, 99-103.

53. Krisnangkura, K.; Pongtonkulpanich, V. Prediction of gas chromatographic peak width in capillary columns at different temperatures, carrier gas flows, column lengths, inside diameters and carbon numbers. *Journal of Separation Science* **2006**, *29*, 81-89.

54. Castello, G.; Moretti, P.; Vezzani, S. Retention models for programmed gas chromatography. *Journal of Chromatography A* **2009**, *1216*, 1607-1623.

55. Aldaeus, F.; Thewalim, Y.; Colmsjö, A. Prediction of retention times and peak widths in temperature-programmed gas chromatography using the finite element method. *Journal of Chromatography A* **2009**, *1216*, 134-139.

56. Karolat, B.; Harynuk, J. Prediction of gas chromatographic retention time via an additive thermodynamic model. *Journal of Chromatography A* **2010**, *1217*, 4862-4867.

57. Zhu, S.; He, S.; Worton, D. R.; Goldstein, A. H. Predictions of comprehensive two-dimensional gas chromatography separations from isothermal data. *Journal of Chromatography A* **2012**, *1233*, 147-151.

58. McGinitie, T. M.; Harynuk, J. J. Prediction of retention times in comprehensive two-dimensional gas chromatography using thermodynamic models. *Journal of Chromatography A* **2012**, *1255*, 184-189.

59. McGinitie, T. M.; Ebrahimi-Najafabadi, H.; Harynuk, J. J. Rapid determination of thermodynamic parameters from one-dimensional programmed-temperature gas chromatography for use in retention time prediction in comprehensive multidimensional chromatography. *Journal of Chromatography A* **2014**, *1325*, 204-212.

60. Barcaru, A.; Anroedh-Sampat, A.; Janssen, H.; Vivó-Truyols, G. Retention time prediction in temperature-programmed, comprehensive two-dimensional gas chromatography: Modeling and error assessment. *Journal of Chromatography A* **2014**, *1368*, 190-198.

61. Blumberg, L. M. Distribution-centric 3-parameter thermodynamic models of partition gas chromatography. *Journal of Chromatography A* **2017**, *1491*, 159-170.

62. Hou, S.; Stevenson, Keisean A. J. M.; Harynuk, J. J. A simple, fast, and accurate thermodynamic-based approach for transfer and prediction of gas chromatography retention times between columns and instruments Part I: Estimation of reference column geometry and thermodynamic parameters. *Journal of Separation Science* **2018**, *41*, 2544-2552.

63. Hou, S.; Stevenson, Keisean A. J. M.; Harynuk, J. J. A simple, fast, and accurate thermodynamic-based approach for transfer and prediction of GC retention times between columns and instruments Part II: Estimation of target column geometry. *Journal of Separation Science* **2018**, *41*, 2553-2558.

64. Hou, S.; Stevenson, Keisean A. J. M.; Harynuk, J. J. A simple, fast, and accurate thermodynamic-based approach for transfer and prediction of gas chromatography retention

times between columns and instruments Part III: Retention time prediction on target column. *Journal of Separation Science* **2018**, *41*, 2559-2564.

65. Ebrahimi-Najafabadi, H.; McGinitie, T. M.; Harynuk, J. J. Quantitative structure-retention relationship modeling of gas chromatographic retention times based on thermodynamic data. *Journal of Chromatography A* **2014**, *1358*, 225-231.

66. Asadpour, S.; CHamsaz, M.; Haron, M. J. Application of MLR, PLS and Artificial Neural Networks for Prediction of GC/ECD Retention Times of Chlorinated Pesticides, Herbicides, and Organohalides. *Research Journal of Pharmaceutical, Biological and Chemical Sciences* **2012**, *3*.

67. Drosos, J. C.; Viola-Rhenals, M.; Vivas-Reyes, R. Quantitative structure–retention relationships of polycyclic aromatic hydrocarbons gas-chromatographic retention indices. *Journal of Chromatography A* **2010**, *1217*, 4411-4421.

68. Cheng, L. P.; Zhang, X. L. QSRR Study on GC Retention Time of Aromatic Components in Red Raspberry Wine*; Advanced Materials Research*; Trans Tech Publ: 2013; Vol. 781, pp 1434-1438.

69. D'Archivio, A. A.; Incani, A.; Ruggieri, F. Cross-column prediction of gas-chromatographic retention of polychlorinated biphenyls by artificial neural networks. *Journal of Chromatography A* **2011**, *1218*, 8679-8690.

70. *https://webbook.nist.gov/chemistry/gc-ri/* (accessed Dec 6, 2018).

71. Bieri, S.; Marriott, P. J. Dual-Injection System with Multiple Injections for Determining Bidimensional Retention Indexes in Comprehensive Two-Dimensional Gas Chromatography. *Analytical Chemistry* **2008**, *80*, 760-768.

72. Amos, R. I. J.; Haddad, P. R.; Szucs, R.; Dolan, J. W.; Pohl, C. A. Molecular modeling and prediction accuracy in Quantitative Structure-Retention Relationship calculations for chromatography. *Trends in Analytical Chemistry* **2018**, *105*, 352-359.

73. Görgényi, M.; Héberger, K. Solvation enthalpies and heat capacities of n-alkanes in four polymer phases by capillary gas chromatography. *Journal of Separation Science* **2005**, *28*, 506-512.

74. Clarke, E. C. W.; Glew, D. N. Evaluation of thermodynamic functions from equilibrium constants. *Transations of the Faraday Society* **1966**, *62*, 539-547.

75. Claumann, C. A.; Wüst Zibetti, A.; Bolzan, A.; Machado, R. A. F.; Pinto, L. T. Fast and accurate numerical method for predicting gas chromatography retention time. *Journal of Chromatography A* **2015**, *1406*, 258-265.

76. McGinitie, T. M.; Ebrahimi-Najafabadi, H.; Harynuk, J. J. A standardized method for the calibration of thermodynamic data for the prediction of gas chromatographic retention times. *Journal of Chromatography A* **2014**, *1330*, 69-73.

77. Claumann, C. A.; Wüst Zibetti, A.; Bolzan, A.; Machado, R. A. F.; Pinto, L. T. Robust estimation of thermodynamic parameters (ΔH, ΔS and ΔCp) for prediction of retention time in gas chromatography – Part I (Theoretical). *Journal of Chromatography A* **2015**, *1425*, 249-257.

78. Vezzani, S.; Moretti, P.; Castello, G. Fast and accurate method for the automatic prediction of programmed-temperature retention times. *Journal of Chromatography A* **1994**, *677*, 331-343.

79. Snijders, H.; Janssen, H.; Cramers, C. Optimization of temperature-programmed gas chromatographic separations I. Prediction of retention times and peak widths from retention indices. *Journal of Chromatography A* **1995**, *718*, 339-355.

80. Snijders, H.; Janssen, H.; Cramers, C. Optimization of temperature-programmed gas chromatographic separations II. Off-line Simplex optimization and column selection. *Journal of Chromatography A* **1996**, *756*, 175-183.

81. Beens, J.; Boelens, H.; Tijssen, R.; Blomberg, J. Quantitative aspects of comprehensive two-dimensional gas chromatography (GC x GC). *Journal of High Resolution Chromatography* **1998**, *21*, 47-54.

82. Zhu, S.; Lu, X.; Qiu, Y.; Pang, T.; Kong, H.; Wu, C.; Xu, G. Determination of retention indices in constant inlet pressure mode and conversion among different column temperature conditions in comprehensive two-dimensional gas chromatography. *Journal of Chromatography A* **2007**, *1150*, 28-36.

83. Wang, Y.; Liu, J.; Li, N.; Shi, G.; Jiang, G.; Ma, W. Preliminary study of the retention behavior for different compounds using cryogenic chromatography at different initial temperatures. *Microchemical Journal* **2005**, *81*, 184-190.

84. Riahi, S.; Ganjali, M. R.; Pourbasheer, E.; Norouzi, P. QSRR study of GC retention indices of essential-oil compounds by multiple linear regression with a genetic algorithm. *Chromatographia* **2008**, *67*, 917-922.

85. Beteringhe, A.; Radutiu, A. C.; Culita, D. C.; Mischie, A.; Spafiu, F. Quantitative structure - Retention relationship (QSRR) study for predicting gas chromatographic retention times for some stationary phases. *QSAR and Combinatorial Science* **2008**, *27*, 996-1005.

86. Morsali, A.; Beyramabadi, S. A.; Bozorgmehr, M. R.; Raanaee, M.; Keyvani, B.; Jafari, G. R. Prediction of gas chromatography retention of BTEX and other substituted benzenes based on quantum chemical parameters. *Scientific Research and Essays* **2010**, *5*, 349-351.

87. Gupta, V. K.; Khani, H.; Ahmadi-Roudi, B.; Mirakhorli, S.; Fereyduni, E.; Agarwal, S. Prediction of capillary gas chromatographic retention times of fatty acid methyl esters in human blood using MLR, PLS and back-propagation artificial neural networks. *Talanta* **2011**, *83*, 1014-1022.

88. Alizadeh, M.; Chamsaz, M.; Asadpour, S. Quantitative structure-retention relationships study of phenols using neural network and classic multivariate analysis. *Asian Journal of Chemistry* **2011**, *23*, 2571-2576.

89. D'Archivio, A. A.; Incani, A.; Ruggieri, F. Retention modelling of polychlorinated biphenyls in comprehensive two-dimensional gas chromatography. *Analytical and Bioanalytical Chemistry* **2011**, *399*, 903-913.

90. Karimi, H.; Farmany, A.; Noorizadeh, H. Prediction of Linear Retention Index of Teucrium chamaedrys Volatiles in GC×GC-TOF/MS by Linear Model. *World Applied Sciences Journal* **2011**, *15*, 1086-1088.

91. Noorizadeh, H.; Noorizadeh, M. QSRR-based estimation of the retention time of opiate and sedative drugs by comprehensive two-dimensional gas chromatography. *Medicinal Chemistry Research* **2012**, *21*, 1997-2005.

92. Ghavami, R.; Sepehri, B. Investigation of retention behavior of polychlorinated biphenyl congeners on 18 different HRGC columns using molecular surface average local ionization energy descriptors. *Journal of Chromatography A* **2012**, *1233*, 116-125.

93. D'Archivio, A. A.; Giannitto, A.; Maggi, M. A. Cross-column prediction of gas-chromatographic retention of polybrominated diphenyl ethers. *Journal of Chromatography A* **2013**, *1298*, 118-131.

94. Konoz, E.; Sarrafi, A. H. M.; Feizbakhsh, A.; Dashtbozorgi, Z. Prediction of gas chromatography-mass spectrometry retention times of pesticide residues by chemometrics methods. *Journal of Chemistry* **2013**.

95. Noorizadeh, H.; Farmany, A. Prediction of Retention Behavior of Pesticides in Fruits and Vegetables in Low-Pressure Gas Chromatography-Time-of-Flight Mass Spectrometry. *Food Analytical Methods* **2014**, *7*, 580-590.

96. D'Archivio, A. A.; Maggi, M. A.; Ruggieri, F. Cross-column prediction of gas-chromatographic retention indices of saturated esters. *Journal of Chromatography A* **2014**, *1355*, 269-277.

97. Zhang, X. T.; Zhang, X.; Li, Q.; Sun, Z. L.; Song, L. J.; Sun, T. Prediction of GC retention times of PBDE congeners based on QSRR. *Advanced Materials Research*; Trans Tech Publ: 2014; Vol. 955, pp 1307-1310.

98. Gieleciak, R.; Hager, D.; Heshka, N. E. Application of a quantitative structure retention relationship approach for the prediction of the two-dimensional gas chromatography retention times of polycyclic aromatic sulfur heterocycle compounds. *Journal of Chromatography A* **2016**, *1437*, 191-202.

99. Roth, M.; Novak, J. Thermodynamics of poly (dimethylsiloxane)-alkane systems by gas-liquid chromatography. *Macromolecules* **1986**, *19*, 364-369.

100. Dorman, F. L.; Schettler, P. D.; Vogt, L. A.; Cochran, J. W. Using computer modeling to predict and optimize separations for comprehensive two-dimensional gas chromatography. *Journal of Chromatography A* **2008**, *1186*, 196-201.

101. McGinitie, T. M.; Karolat, B. R.; Whale, C.; Harynuk, J. J. Influence of carrier gas on the prediction of gas chromatographic retention times based on thermodynamic parameters. *Journal of Chromatography A* **2011**, *1218*, 3241-3246.

102. McGinitie, T. M.; Harynuk, J. J. Considerations for the automated collection of thermodynamic data in gas chromatography. *Journal of Separation Science* **2012**, *35*, 2228-2232.

103. Burel, A.; Vaccaro, M.; Cartigny, Y.; Tisse, S.; Coquerel, G.; Cardinael, P. Retention modeling and retention time prediction in gas chromatography and flow-modulation comprehensive two-dimensional gas chromatography: The contribution of pressure on solute partition. *Journal of Chromatography A* **2017**, *1485*, 101-119.

104. Gleiberman, R.; Stevenson, K.; Cochran, J.; Marriott, P. J.; Hou, S.; Harynuk, J. J. In *Interlaboratory validation of gas chromatographic retention time predictions;* Poster session presented at: The 8th Annual Multidimensional Chromatography Workshop; 2017; .

105. Tomick, J. J. On convergence of the nelder-mead simplex algorithm for unconstrained stochastic optimization, The Pennsylvania State University, 1995.

106. McKinnon, K. Convergence of the Nelder--Mead Simplex Method to a Nonstationary Point. *SIAM Journal on Optimization* **1998**, *9*, 148-158.

107. Weast, R. C. *CRC handbook of chemistry and physics;* CRC Press: Boca Raton, Fla, 1988; .

108. Stewart, J. *Calculus: Early Transcendentals;* Brooks/Cole Publishing Company: New York, 1999; .

109. Montgomery, D. C.; Peck, E. A. *Introduction to linear regression analysis;* Wiley: New York, 1992; .

110. Burel, A.; Vaccaro, M.; Cartigny, Y.; Tisse, S.; Coquerel, G.; Cardinael, P. Retention modeling and retention time prediction in gas chromatography and flow-modulation

comprehensive two-dimensional gas chromatography: The contribution of pressure on solute partition. *Journal of Chromatography A* **2017**, *1485*, 101-119.

111. Zhu, S.; Zhang, W.; Dai, W.; Tong, T.; Guo, P.; He, S.; Chang, Z.; Gao, X. A simple model for separation prediction of comprehensive two-dimensional gas chromatography and its applications in petroleum analysis. *Analytical Methods* **2014**, *6*, 2608-2620.

112. Fuller, E. N.; Schettler, P. D.; Giddings, J. C. New method for prediction of binary gas-phase diffusion coefficients. *Industrial and Engineering Chemistry Research* **1966**, *58*, 18-27.

113. Aldaeus, F.; Thewalim, Y.; Colmsjö, A. Prediction of retention times of polycyclic aromatic hydrocarbons and n-alkanes in temperature-programmed gas chromatography. *Analytical and Bioanalytical Chemistry* **2007**, *389*, 941-950.

114. Aldaeus, F.; Thewalim, Y.; Colmsjö, A. Prediction of retention times of polycyclic aromatic hydrocarbons and n-alkanes in temperature-programmed gas chromatography. *Analytical and Bioanalytical Chemistry* **2007**, *389*, 941-950.

115. Blumberg, L. M.; Klee, M. S. Characteristic Thermal Constant and Dimensionless Heating Rate. The Links to Optimum Heating Rate in GC. *Analytical Chemistry* **2000**, *72*, 4080-4089.

116. Blumberg, L. M. *Temperature-Programmed Gas Chromatography;* Wiley-VCH: DE, 2011; .

117. Brenner, N.; Callen, J. E.; Weis, M. D., Eds.; In *Gas Chromatography;* Academic Press: New York, 1962; .

118. Blumberg, L. M.; Klee, M. S. Method Translation and Retention Time Locking in Partition GC. *Analytical Chemistry* **1998**, *70*, 3828-3839.

119. Blumberg, L. M.; Klee, M. S. Optimal heating rate in gas chromatography. *Journal of Microcolumn Separations.* **2000**, *12*, 508-514.

120. Blumberg, L. M. Theory of Fast Capillary Gas Chromatography – Part 3: Column Performance vs. Gas Flow Rate. *Journal of High Resolution Chromatography* **1999**, *22*, 403-413.

121. Klee, M. S.; Blumberg, L. M. Theoretical and practical aspects of fast gas chromatography and method translation. *Journal of Chromatographic Science* **2002**, *40*, 234-247.

Appendix A

Table A2-1 Thermodynamics-based parameter library data on Rtx-5MS column (RESTEK)

(30.9 m x 0.25 mm; 0.25 µm; 5% diphenyl 95% polydimethylsiloxane)

COMPOUND NAME	CAS NUMBER	TERM A	TERM B	TERM C
1,2,3-trichlorobenzene	87-61-6	-76.8847	9252.3453	10.0081
1,3-dibromobenzene	108-36-1	-74.4699	8987.2980	9.6941
1,3-diphenoxy-2-propanol	622-04-8	-17.8248	8492.1477	1.1369
1,3-diphenyl-1,3-propanedione	120-46-7	-17.9140	8388.4549	1.2118
1,3-diphenyl-2-propanone	781-35-1	-103.6322	13011.7889	13.3761
1,4-dimethylnaphthalene	571-58-4	-78.8520	10191.6692	10.1362
1,9-nonanediol	3937-56-2	-115.3729	12879.5362	15.1129
1-bromotetradecane	112-71-0	-110.5867	13797.1051	14.2121
1-chlorooctane	111-85-3	-82.5868	9224.4838	10.8219
1-methoxynaphthalene	2216-69-5	-83.3264	10566.5522	10.7364
1-methylphenanthrene	832-69-9	-81.2811	11794.6834	10.2534
1-octadecanol	112-92-5	33.9162	5665.6984	-6.2776
1-octanol	111-87-5	-95.5190	10073.5894	12.6262
1-octene	111-66-0	-101.2206	8853.0815	13.8434
1-tetradecanol	112-72-1	-121.2032	14242.8523	15.7249
2,2,4-trimethylhexane	16747-26-5	-76.8270	7550.0327	10.3156
2,2-dimethylpentane	590-35-2	-116.5778	8567.5702	16.4043
2,3-dichloroaniline	608-27-5	-88.5654	10505.2527	11.5536
2,3-dimethylaniline	87-59-2	-84.2907	9734.3563	11.0306
2,3-dimethylbutane	79-29-8	-195.8811	12020.4745	28.1938
2,3-dimethylheptane	3074-71-3	-77.2606	7972.4727	10.2648
2,3-dimethylnaphthalene	581-40-8	-78.6569	10193.8820	10.1047
2,3-dimethylphenol	526-75-0	-107.7688	11131.9372	14.3303
2,4,5-trichlorophenol	88-06-2	-94.8866	10919.1790	12.4408
2,4,6-tribromoaniline	147-82-0	-89.0346	11617.0900	11.4542
2,4,6-trichloroaniline	634-93-5	-84.8488	10466.5985	10.9972
2,4,6-trichlorophenol	88-06-2	-96.1191	10993.1385	12.6108
2,4,6-trimethylphenol	527-60-6	-92.7280	10318.1619	12.1914
2,4-dichloroaniline	95-82-9	-90.7250	10578.6359	11.8668
2,4-dichlorobenzyl alcohol	1777-82-8	-102.7384	11618.6026	13.4879
2,4-dichlorophenol	120-83-2	-109.5354	11120.9298	14.6005
2,4-dimethyl-6-nitroaniline	1635-84-3	-99.0462	12095.3975	12.8489
2,4-dimethylaniline	95-68-1	-83.0494	9566.1196	10.8583

170

COMPOUND NAME	CAS NUMBER	TERM A	TERM B	TERM C
2,4-dimethylphenol	105-67-9	-110.5536	11174.8123	14.7480
2,5-dichloroaniline	95-82-9	-90.0306	10568.4030	11.7528
2,5-dichlorophenol	583-78-8	-91.6415	9993.6994	12.1180
2,5-diethoxyaniline	94-85-9	-109.6471	12858.6144	14.2618
2,6-dichloroaniline	608-31-1	-79.0468	9497.1306	10.2898
2,6-dichlorophenol	87-65-0	-88.9664	9973.8519	11.7122
2,6-dimethylnaphthalene	581-42-0	-83.7163	10391.2869	10.8345
2-chloro-4-nitroaniline	121-87-9	-113.2043	13308.7624	14.7886
2-decanone	693-54-9	-92.1178	10421.8723	12.0282
2-ethylaniline	578-54-1	-84.6545	9618.3073	11.0949
2-ethylphenol	90-00-6	-113.9601	11355.3269	15.2301
2-heptanone	110-43-0	-86.7070	8678.1998	11.5783
2-isopropylaniline	643-28-7	-89.9892	10195.2540	11.8003
2-methoxy-5-nitroaniline	99-59-2	-113.6443	13525.5918	14.8026
2-methoxynaphthalene	93-04-09	-88.3345	10861.0189	11.4542
2-methyl-2-heptanol	625-25-2	-92.9721	9214.4551	12.4337
2-methyl-3-nonanol	26533-33-5	-96.4225	10510.3078	12.6826
2-methyl-5-nitroaniline	99-55-8	-102.6362	12313.4263	13.3567
2-methyl-5-nonanol	29843-62-7	-97.8654	10560.0489	12.8876
2-methyl-6-nitroaniline	570-24-1	-96.2680	11491.2849	12.5506
2-methylanthracene	0613-12-7	-85.4162	12031.8712	10.8344
2-methylnaphthalene	91-57-6	-79.3332	9698.5533	10.3028
2-nitrophenol	88-75-5	-79.6849	9140.4120	10.4489
2-nonanol	628-99-9	-93.3340	10091.6147	12.2818
2-nonanone	821-55-6	-85.6330	9602.9863	11.1954
2-octanol	123-96-6	-98.2090	9852.0907	13.1043
2-octanone	111-13-7	-83.2899	9000.3509	10.9634
2-propylaniline	1821-39-2	-90.4422	10295.7725	11.8561
2-tert-butylphenol	88-18-6	-119.7124	12317.9487	15.9109
2-tridecanone	593-08-08	-108.2103	12679.9328	14.0467
3,4,5-trichlorophenol	609-19-8	-135.7738	14742.1240	17.8986
3,4-dichloraniline	95-76-1	-94.1101	11179.8167	12.2640
3,4-dimethylaniline	95-64-7	-88.2339	9974.4756	11.5813
3,4-dimethylphenol	95-65-8	-116.5710	11712.1233	15.5696
3,5,5-trimethyhexanal	5435-64-3	-80.4186	8636.9460	10.6288
3,5-dimethoxyphenol	154.1632	-124.9738	13508.9094	16.4717
3,5-dimethylaniline	108-69-0	-85.1641	9752.2978	11.1401
3,5-dimethylphenol	108-68-9	-113.6599	11481.1774	15.1586
3-bromophenol	591-20-8	-123.3586	12552.1982	16.4354

COMPOUND NAME	CAS NUMBER	TERM A	TERM B	TERM C
3-chlorophenol	108-43-0	-121.4827	12115.0831	16.2198
3-decyne-1-ol	51721-39-2	-101.4157	11323.8921	13.2787
3-dodecanone	1534-27-6	-103.1147	11912.9289	13.4203
3-ethyl-5-methylphenol	698-71-5	-112.5211	11842.7618	14.8981
3-nonanol	624-51-1	-92.0436	9977.4556	12.1085
3-octanone	106-68-3	-84.7930	9054.6893	11.1881
3-tert-butylphenol	585-34-2	-119.6808	12392.8562	15.8991
4,4-dimethyl-2-pentene	26232-98-4	-3254.0501	160927.0524	477.7833
4-bromo-2-chloroaniline	38762-41-3	-89.2351	10815.1289	11.5996
4-bromo-2-chlorophenol	3964-56-5	-86.1302	9998.9193	11.2755
4-bromo-2-methylaniline	583-75-5	-90.7948	10807.0131	11.8351
4-chloro-2,6-dinitoaniline	5388-62-5	-107.2899	13194.2326	13.8965
4-chloro-2-nitroaniline	89-63-4	-102.9533	12372.2009	13.3878
4-chloro-3-nitroaniline	635-22-3	-113.0992	13332.3335	14.7588
4-chloroaniline	106-47-8	-91.1818	10138.5649	12.0137
4-chlorophenol	106-48-9	-121.6385	12097.3935	16.2557
4-ethylphenol	123-07-9	-114.7727	11536.5817	15.3155
4-isopropylaniline	99-88-7	-86.2845	10043.9568	11.2572
4-methoxy-2-nitroanline	96-96-8	-113.8784	13212.0352	14.8934
4-methyl-4-nonanol	23418-38-4	-91.3518	10039.2999	11.9963
4-nitroaniline	100-01-6	-105.8422	12544.8286	13.8029
4-nonanol	5932-79-6	-93.6160	10032.4754	12.3444
4-pentenoic acid	591-80-0	-279.6221	18796.3869	39.5473
4-propylaniline	2696-84-6	-92.0668	10489.9518	12.0641
4-sec-butylphenol	99-71-8	-115.5187	12217.1762	15.2922
4-tert-butylphenol	98-54-4	-117.9306	12257.8174	15.6631
5H-dibenzo[a,d]cyclohepten-5-one	222-33-5	-35.1700	9248.1260	3.7248
5-nonanol	623-93-8	-92.4118	9972.9820	12.1675
7,12-dimethylbenz[a]anthracene	57-97-6	108.2576	322.8735	-16.1794
9-methylanthracene	779-02-02	-75.3410	11496.3145	9.4131
acenaphthylene	208-96-58	-76.7804	10029.2856	9.8671
aniline	62-53-3	-83.3754	8765.9757	11.0799
anthracene	120-12-7	-88.0995	11793.4735	11.2935
benzo[a]pyrene	50-32-8	106.5266	322.6874	-15.8733
benzyl alcohol	100-51-6	-95.6952	9728.7309	12.7782
biphenyl	92-52-4	-87.9693	10601.2830	11.4407
caffeine	58-08-2	-99.1951	13014.3784	12.6941
chrysene	218-01-9	53.9114	3782.8091	-8.6742

COMPOUND NAME	CAS NUMBER	TERM A	TERM B	TERM C
cis-2-octene	7642-04-8	-87.7640	8309.7160	11.8438
cyclohexanone	3350-30-9	-75.6475	7312.7680	10.2156
decanal	112-31-2	-93.3613	10525.6004	12.2054
decane	124-18-5	-80.4146	8908.4352	10.5271
dibenz[a,h]anthracene	53-70-3	141.9700	-1985.0859	-20.7209
docosane	629-97-0	78.6445	2985.2260	-12.5529
dodecane	112-40-3	-90.1262	10374.8623	11.7192
eicosane	112-95-8	6.5734	7327.1668	-2.4581
fluorene	86-73-7	-82.9525	10885.9304	10.6503
heptadecane	629-78-7	-119.9158	14312.5717	15.5019
heptanoic acid	111-14-8	-161.0331	13891.1831	21.9622
hexacosane	630-01-3	167.8186	-2702.4101	-24.8683
hexadecane	544-76-3	-117.2230	13708.3262	15.2111
m-bromoaniline	591-19-5	-92.5632	10542.1628	12.1528
m-cresol	108-39-4	-115.8605	11183.8698	15.5615
m-ethoxyphenol	621-34-1	-123.6607	12713.2865	16.4259
methyl decanoate	110-42-9	-99.6813	11496.2739	12.9603
methyl dodecanoate	111-82-0	-110.0875	12979.2339	14.2608
methyl nonanoate	1731-84-6	-93.9860	10723.1293	12.2406
m-ethylaniline	587-02-0	-89.2502	9967.1744	11.7298
m-nitrophenol	554-84-7	-157.0711	15450.5733	21.0251
m-phenylphenol	580-51-8	-119.1744	13883.0379	15.5511
N,N-diethyl-2,4-dimethylaniline	6287-43-0	-87.8231	10328.9598	11.4223
N,N-dimethyl-4-nitrosoaniline	138-89-6	-96.3353	11889.2558	12.4759
N,N-dimethyl-m-nitrosoaniline	1282489-71-7	-94.4467	11646.9844	12.2321
N,N-dipropylaniline	2217-07-4	-98.3485	11494.9138	12.7980
naphthalene	91-20-3	-73.5333	8921.7831	9.5656
N-butylaniline	1126-78-9	-96.4913	11076.1963	12.6119
n-butylbenzene	104-51-8	-75.3849	8706.1312	9.8356
N-ethylaniline	103-69-5	-84.9143	9554.8598	11.1410
N-isopentylaniline	103-69-5	-97.0132	11374.5197	12.6300
nitrobenzene	2051-84-5	-74.9052	8697.8422	9.7983
nonadecane	629-92-5	-40.3663	10066.3245	4.1619
nonane	111-84-2	-79.4623	8364.1189	10.5048
N-propylaniline	622-80-00	-86.7313	10077.3753	11.3091
n-propylbenzene	103-65-1	-74.7760	8190.9961	9.8589
o-bromophenol	95-56-7	-81.6514	8945.9174	10.8025
octacosane	630-02-4	196.9199	-4655.0190	-28.8320
octadecane	593-45-3	-90.2719	12873.9914	11.2409

COMPOUND NAME	CAS NUMBER	TERM A	TERM B	TERM C
octanal	124-13-0	-85.6281	9158.7238	11.3006
octane	111-65-9	-83.8904	8065.8937	11.2817
o-fluorophenol	367-12-4	-107.4370	9667.9669	14.6097
p-bromoaniline	106-40-1	-92.2626	10528.5616	12.1117
pentachlorophenol	87-86-5	-104.2700	12858.8397	13.5243
pentadecane	629-62-9	-109.0141	12796.1564	14.1345
p-ethylaniline	589-16-2	-87.1970	9817.9754	11.4477
phenanthrene	85-01-8	-86.2754	11652.9551	11.0403
phenol	108-95-2	-122.8701	11117.0958	16.6676
p-terphenyl	92-94-4	14.6099	6428.1472	-3.3382
p-tert-pentylphenol	80-46-6	-115.7625	12536.1059	15.2761
p-xylene	106-42-3	-75.1859	7814.4020	10.0154
pyrene	129-00-0	-35.7188	9193.2856	3.8525
pyridine	110-86-1	-86.3245	7709.5104	11.8127
sebaic acid	111-20-6	-131.4796	15187.1045	17.0818
tetracosane	646-31-1	130.6248	-273.8962	-19.7633
tetradecane	629-59-4	-103.5027	12034.7681	13.4415
trans-5-decene	7433-56-9	-78.5652	8780.4359	10.2676
tributylphosphate	126-73-8	-123.7544	14347.3689	16.0810
tridecane	629-50-5	-97.3528	11235.3947	12.6576
trihexylphosphate	2528-39-7	81.9109	2790.5023	-13.0114
triisopropylphosphate	513-02-0	-108.6568	11434.2797	14.3578
trimethylphosphate	512-56-1	-95.8321	9396.9044	12.8297
trioctylphosphate	1806-54-8	149.9099	-1480.9146	-22.4403
tripentylphosphate	2528-38-3	-26.8107	9293.4732	2.2411
triphenylphosphate	115-86-6	85.3137	2195.8925	-13.2565
tripropylphosphate	513-08-6	-111.2719	12446.1940	14.5482
tris-2-ethylhexylphosphate	78-42-2	149.1850	-1444.9594	-22.3348
undecanal	112-44-7	-97.7706	11229.8287	12.7396
undecane	1120-21-4	-82.9174	9518.0519	10.7819
α-bromo-p-tolualdehyde	824-54-4	-94.3445	11103.0731	12.3237

Table A2-2 Thermodynamics-based parameter library data on Stabilwax column (RESTEK)

(30.3 m x 0.25 mm; 0.25 μm; polyethylene glycol)

COMPOUND NAME	CAS NUMBER	TERM A	TERM B	TERM C
1-bromotetradecane	112-71-0	-77.3623	11180.2936	9.6435
1-chlorooctane	111-85-3	-45.7379	6981.6880	5.5264
1-methoxynaphthalene	2216-69-5	-73.4999	10898.3312	9.2143
1-octanol	111-87-5	-70.3107	9667.1558	8.7460
1-tetradecanol	112-72-1	-84.7394	12552.2470	10.4422
2,3-dichloroaniline	608-27-5	-68.6164	11245.9774	8.3775
2,3-dimethylaniline	87-59-2	-79.8819	11039.8785	10.0706
2,3-dimethylheptane	3074-71-3	24.1511	2135.1319	-4.4635
2,3-dimethylnaphthalene	581-40-8	-63.3515	9842.8778	7.8723
2,3-dimethylphenol	526-75-0	-77.7796	11807.9656	9.5434
2,4,6-trichloroaniline	634-93-5	-82.1459	11665.3727	10.3580
2,4,6-trichlorophenol	88-06-2	-34.9566	9691.5040	3.4439
2,4,6-trimethylphenol	527-60-6	-83.6555	11661.9853	10.4811
2,4-dichloroaniline	95-82-9	-80.9487	11928.0375	10.1149
2,4-dichlorobenzyl alcohol	1777-82-8	-36.4457	9586.9060	3.7471
2,4-dimethylaniline	95-68-1	-74.9313	10577.6851	9.3846
2,4-dimethylphenol	105-67-9	-82.2153	11945.7256	10.1754
2,5-dichloroaniline	95-82-9	-75.9602	11699.0706	9.3928
2,5-dichlorophenol	583-78-8	-94.7523	12895.1121	11.9595
2,5-diethoxyaniline	94-85-9	-21.2020	8768.9837	1.5602
2,6-dichloroaniline	608-31-1	-85.0636	11228.8802	10.8694
2,6-dichlorophenol	87-65-0	-95.3867	12584.6945	12.1360
2,6-di-tert-4-methylphenol	128-37-0	-67.2729	10490.2484	8.1610
2-decanone	693-54-9	-59.7017	8603.7607	7.3798
2-ethylaniline	578-54-1	-78.8004	10797.3171	9.9296
2-ethylphenol	90-00-6	-81.1117	11887.1299	10.0142
2-heptanone	110-43-0	-44.4161	6684.0959	5.3759
2-isopropylaniline	643-28-7	-85.0801	11309.8630	10.7945
2-isopropylphenol	88-69-7	-80.9920	12080.5712	9.9507
2-methoxynaphthalene	93-04-09	-72.3768	10876.8094	9.0510
2-methyl-2-heptanol	625-25-2	-61.8154	8348.7447	7.6441
2-methyl-3-nonanol	26533-33-5	-73.7802	9839.9894	9.2286
2-methyl-5-nonanol	29843-62-7	-72.8712	9819.6735	9.0818
2-nitrophenol	88-75-5	-85.4051	10810.6264	10.9899
2-nonanol	628-99-9	-70.7294	9623.6325	8.7994
2-nonanone	821-55-6	-55.0006	7983.0571	6.7704
2-octanol	123-96-6	-66.1640	9012.3026	8.2056

COMPOUND NAME	CAS NUMBER	TERM A	TERM B	TERM C
2-octanone	111-13-7	-48.3904	7260.8307	5.8837
2-propylaniline	1821-39-2	-85.5326	11390.0826	10.8607
2-tert-butylphenol	88-18-6	-80.7547	12284.4482	9.8746
2-tridecanone	593-08-08	-75.0066	10546.3058	9.3698
3,4-dimethylphenol	95-65-8	-74.2598	11728.6534	9.0382
3,5,5-trimethylhexanal	5435-64-3	-51.8790	7093.1604	6.4826
3,5-dimethylaniline	108-69-0	-80.0208	11099.6836	10.0659
3,5-dimethylphenol	108-68-9	-67.1042	11178.2700	8.0504
3-chlorophenol	108-43-0	-20.0851	8697.1249	1.4005
3-decyne-1-ol	51721-39-2	-87.9606	11767.8539	11.0799
3-dodecanone	1534-27-6	-64.0824	9458.6804	7.8925
3-ethyl-5-methylphenol	698-71-5	-61.8962	11142.5241	7.2496
3-ethylphenol	620-17-7	-75.9556	11770.5497	9.2750
3-nonanol	624-51-1	-64.4307	9175.6008	7.9116
3-octanone	106-68-3	-46.2047	7041.0734	5.5846
3-tert-butylphenol	585-34-2	-58.4238	10999.5249	6.7612
4-bromo-2-chlorophenol	3964-56-5	-61.0445	11056.9280	7.1867
4-chloroaniline	106-47-8	-94.9264	12611.6733	12.0971
4-chlorophenol	106-48-9	-19.2633	8655.0390	1.2821
4-ethylphenol	123-07-9	-69.2640	11337.4067	8.3342
4-isopropylaniline	99-88-7	-91.1785	11861.6848	11.6318
4-methyl-4-nonanol	23418-38-4	-72.4749	9524.5639	9.0809
4-nonanol	5932-79-6	-73.8623	9656.6734	9.2733
4-propylaniline	2696-84-6	-84.3016	11553.1350	10.6424
4-sec-butylphenol	99-71-8	-52.2722	10636.6834	5.8856
4-tert-butylphenol	98-54-4	-58.0318	10948.7674	6.7136
5-nonanol	623-93-8	-68.0816	9344.1217	8.4390
aniline	62-53-3	-79.1616	10504.6809	10.0359
benzyl alcohol	100-51-6	-74.4043	10615.4556	9.2882
biphenyl	92-52-4	-68.6358	10193.4031	8.5798
cis-2-octene	7642-04-8	114.1863	-2162.6704	-17.7201
cyclohexanone	3350-30-9	-46.2858	7757.3414	5.6277
decanal	112-31-2	-60.3686	8648.3651	7.4774
decane	124-18-5	-57.1275	6796.7156	7.2756
docosane	629-97-0	-69.0325	11745.9421	8.1589
dodecane	112-40-3	-61.5328	7849.4500	7.7378
eicosane	112-95-8	-97.6429	12814.8009	12.3530
fluorene	86-73-7	-68.4553	10798.3652	8.5155
heptadecane	629-78-7	-79.9873	10732.3969	10.0330
hexadecane	544-76-3	-64.6966	9582.4240	7.8537

COMPOUND NAME	CAS NUMBER	TERM A	TERM B	TERM C
m-cresol	108-39-4	-74.0170	11333.7757	9.0880
m-ethoxyphenol	621-34-1	8.1862	7198.3064	-2.6682
methyl decanoate	110-42-9	-67.0782	9461.4601	8.3302
methyl dodecanoate	111-82-0	-73.0570	10505.5822	9.0563
methyl nonanoate	1731-84-6	-59.8201	8703.1786	7.3521
m-ethylaniline	587-02-0	-81.6404	11209.9532	10.2865
N,N-diethyl-2,4-dimethylaniline	6287-43-0	-53.4144	8241.9930	6.4959
N,N-dimethyl-m-nitrosoaniline	1282489-71-7	-59.7173	10599.2978	7.1955
N,N-dipropylaniline	2217-07-4	-63.5725	9604.7470	7.8038
naphthalene	91-20-3	-53.6215	8497.4409	6.6066
n-butylbenzene	104-51-8	-39.6831	6778.6327	4.6411
N-ethylaniline	103-69-5	-65.9505	9659.8475	8.1540
N-isopentylaniline	103-69-5	-79.2459	11158.4996	9.9256
nitrobenzene	2051-84-5	-60.1489	8916.7074	7.5202
nonadecane	629-92-5	-88.4685	11917.8241	11.1159
nonane	111-84-2	-73.1827	7098.9633	9.7608
N-propylaniline	622-80-00	-80.1864	10740.0683	10.1436
n-propylbenzene	103-65-1	-38.3288	6346.6535	4.5106
o-bromophenol	95-56-7	-98.1887	12410.1818	12.5670
octadecane	593-45-3	-89.8599	11652.0989	11.3782
octanal	124-13-0	-51.8950	7453.7290	6.3925
octane	111-65-9	-147.4522	10118.4150	20.8671
o-fluorophenol	367-12-4	-59.5112	9696.4017	7.0936
p-bromoaniline	106-40-1	-70.1320	11397.0467	8.5709
pentadecane	629-62-9	-71.9405	9556.3536	9.0153
p-ethylaniline	589-16-2	-84.9878	11350.2199	10.7669
phenol	108-95-2	-70.1194	10886.8544	8.5389
p-tert-pentylphenol	80-46-6	-21.4838	8850.7769	1.5583
p-xylene	106-42-3	-46.6188	6451.4863	5.8177
pyridine	110-86-1	-51.9582	6870.1095	6.5678
tetracosane	646-31-1	10.6773	7212.5693	-3.1159
tetradecane	629-59-4	-64.0875	8757.9465	7.9538
trans-5-decene	7433-56-9	-47.4913	6414.3266	5.8603
tridecane	629-50-5	-61.3247	8232.5177	7.6273
undecanal	112-44-7	-60.1639	8994.9165	7.3822
undecane	1120-21-4	-58.6342	7298.0231	7.3997
α-bromo-p-tolualdehyde	824-54-4	-53.4934	7380.3621	6.5588

Table A2-3 Thermodynamics-based parameter library data on Rtx-200 column (RESTEK) (23.8

m x 0.25 mm; 0.25 µm; trifluoropropylmethyl polysiloxane)

COMPOUND NAME	CAS NUMBER	TERM A	TERM B	TERM C
1,2,3-trichlorobenzene	87-61-6	-54.5614	7908.70865	6.743182
1,3-diphenoxy-2-propanol	622-04-8	-56.5769	11169.52728	6.41804
1,3-diphenyl-1,3-propanedione	120-46-7	-40.5774	10057.4097	4.262052
1,3-diphenyl-2-propanone	781-35-1	-131.053	14946.55532	17.11607
1,4-dimethylnaphthalene	571-58-4	-65.4211	9405.343772	8.12002
1,9-nonanediol	3937-56-2	-96.4624	11828.94309	12.3548
1-bromotetradecane	112-71-0	-99.1306	12631.69647	12.60125
1-chlorooctane	111-85-3	-62.0505	7993.660898	7.796812
1-methoxynaphthalene	2216-69-5	-71.9875	9973.141776	9.021187
1-methylphenanthrene	832-69-9	-80.6677	11783.43836	10.07383
1-octadecanol	112-92-5	-65.7281	11903.88692	7.589853
1-octanol	111-87-5	-83.7327	9302.282274	10.88671
1-tetradecanol	112-72-1	-104.524	12867.69618	13.35455
2,2,4-trimethylhexane	16747-26-5	-77.7812	7313.91818	10.44303
2,3-dichloroaniline	608-27-5	-65.9103	9192.850524	8.254846
2,3-dimethylaniline	87-59-2	-64.5111	8791.454181	8.058982
2,3-dimethylheptane	3074-71-3	-71.1855	7348.968476	9.359986
2,3-dimethylnaphthalene	581-40-8	-67.4168	9587.22561	8.398191
2,3-dimethylphenol	526-75-0	-70.7214	8914.312903	8.979924
2,4,5-trichlorophenol	88-06-2	-66.3127	9014.432385	8.351689
2,4,6-tribromoaniline	147-82-0	-72.4862	10367.89494	9.082017
2,4,6-trichloroaniline	634-93-5	-66.5529	9280.833961	8.339156
2,4,6-trichlorophenol	88-06-2	-65.7908	9083.196901	8.242765
2,4,6-trimethylphenol	527-60-6	-69.2948	8983.569382	8.732957
2,4-dichloroaniline	95-82-9	-65.0842	9076.070918	8.141211
2,4-dichlorobenzyl alcohol	1777-82-8	-71.7666	9650.866783	9.046777
2,4-dimethyl-6-nitroaniline	1635-84-3	-86.2837	11607.63656	10.95061
2,4-dimethylaniline	95-68-1	-66.0086	8762.857488	8.281251
2,4-dimethylphenol	105-67-9	-69.3359	8758.754871	8.782115
2,5-dichloroaniline	95-82-9	-68.931	9274.868508	8.692449
2,5-dichlorophenol	583-78-8	-67.9303	8484.225426	8.692259
2,5-diethoxyaniline	94-85-9	-98.1539	12328.25357	12.51265
2,6-dichloroaniline	608-31-1	-61.046	8454.274396	7.634634
2,6-dichlorophenol	87-65-0	-65.9848	8623.218217	8.359014
2,6-dimethylnaphthalene	581-42-0	-68.1001	9548.173079	8.494295
2,6-di-*tert*-butyl-4-methylphenol	128-37-0	-90.1048	11177.44117	11.49415
2-chloro-4-nitroaniline	121-87-9	-87.7539	11966.44906	11.13479

COMPOUND NAME	CAS NUMBER	TERM A	TERM B	TERM C
2-decanone	693-54-9	-80.417	9956.033629	10.24914
2-ethylaniline	578-54-1	-66.0019	8693.172514	8.297891
2-ethylphenol	90-00-6	-68.6427	8627.970771	8.70054
2-heptanone	110-43-0	-71.5835	8237.727455	9.244
2-isopropylaniline	643-28-7	-71.9152	9249.948981	9.094308
2-isopropylphenol	88-69-7	-77.1227	9327.640627	9.868252
2-methoxy-5-nitroaniline	99-59-2	-91.3135	12535.03022	11.55378
2-methyl-2-heptanol	625-25-2	-81.9833	8647.866326	10.7553
2-methyl-3-nonanol	26533-33-5	-75.7257	9238.895574	9.643803
2-methyl-5-nitroaniline	99-55-8	-77.9126	11098.01887	9.785498
2-methyl-5-nonanol	29843-62-7	-83.1673	9634.122592	10.71782
2-methyl-6-nitroaniline	570-24-1	-75.9096	10580.89029	9.563176
2-nitrophenol	88-75-5	-66.8861	8615.112112	8.521205
2-nonanol	628-99-9	-88.076	9685.647818	11.47537
2-nonanone	821-55-6	-72.7166	9137.214943	9.223358
2-octanol	123-96-6	-156.106	12672.12238	21.51723
2-octanone	111-13-7	-73.6532	8768.705774	9.450978
2-propylaniline	1821-39-2	-69.6775	9199.842131	8.765747
2-*tert*-butylphenol	88-18-6	-82.9331	9843.201456	10.67552
2-tridecanone	593-08-08	-78.6288	11021.54631	9.747314
3,4,5-trichlorophenol	609-19-8	-89.3447	11232.09873	11.45686
3,4-dichloraniline	95-76-1	-73.0947	9954.15859	9.218002
3,4-dimethylaniline	95-64-7	-63.2424	8767.876759	7.8551
3,4-dimethylphenol	95-65-8	-69.2402	8962.920705	8.736612
3,5,5-trimethyhexanal	5435-64-3	-58.8108	7764.114498	7.38199
3,5-dimethoxyphenol	500-99-2	-92.006	11525.11861	11.74179
3,5-dimethylaniline	108-69-0	-66.2178	8873.283927	8.282706
3,5-dimethylphenol	108-68-9	-71.3942	9002.217571	9.051777
3-bromophenol	591-20-8	-76.8775	9462.957866	9.856839
3-chlorophenol	108-43-0	-73.2627	8995.66624	9.374003
3-decyne-1-ol	51721-39-2	-80.6206	9978.216001	10.24745
3-dodecanone	1534-27-6	-87.5206	11058.42308	11.11379
3-ethyl-5-methylphenol	698-71-5	-74.2483	9508.569551	9.385407
3-nonanol	624-51-1	-72.2906	8809.243781	9.195445
3-octanone	106-68-3	-74.9046	8755.398298	9.642993
3-*tert*-butylphenol	585-34-2	-81.795	10005.03278	10.47023
4-bromo-2-chloroaniline	38762-41-3	-70.1288	9627.683635	8.825989
4-bromo-2-chlorophenol	3964-56-5	-60.6355	8377.723593	7.58971
4-bromo-2-methylaniline	583-75-5	-69.9177	9675.511205	8.769911
4-chloro-2,6-dinitoaniline	5388-62-5	-91.1866	12505.28304	11.53325

COMPOUND NAME	CAS NUMBER	TERM A	TERM B	TERM C
4-chloro-2-nitroaniline	89-63-4	-75.3232	10829.75251	9.42471
4-chloro-3-nitroaniline	635-22-3	-91.7392	12256.28389	11.68189
4-chloroaniline	106-47-8	-64.2144	8735.814343	8.054206
4-chlorophenol	106-48-9	-76.3997	9210.626427	9.819214
4-ethylphenol	123-07-9	-72.5706	8994.198448	9.239436
4-isopropylaniline	99-88-7	-73.2417	9375.639144	9.275271
4-methoxy-2-nitroanline	96-96-8	-85.9454	11747.36035	10.86437
4-methyl-4-nonanol	23418-38-4	-72.36	8946.574457	9.175566
4-nitroaniline	100-01-6	-87.9082	11817.70315	11.18741
4-nitrophenol	100-02-7	-87.0251	11280.75457	11.1147
4-nonanol	5932-79-6	-69.6796	8660.048903	8.815812
4-propylaniline	2696-84-6	-73.0303	9477.963362	9.225533
4-sec-butylphenol	99-71-8	-82.3442	10040.83202	10.54879
4-tert-butylphenol	98-54-4	-82.5456	10012.80471	10.58965
5H-dibenzo[a,d]cyclohepten-5-one	222-33-5	-48.891	10388.04085	5.518751
5-nonanol	623-93-8	-72.4043	8812.796929	9.206838
acenaphthylene	208-96-58	-66.5843	9530.313598	8.306101
aniline	62-53-3	-61.3284	7769.9762	7.767543
anthracene	120-12-7	-82.3677	11461.71042	10.39725
benzo[a]pyrene	50-32-8	114.1513	400.6527482	-17.1973
benzyl alcohol	100-51-6	-61.4573	7956.918387	7.741874
biphenyl	92-52-4	-68.3761	9434.381501	8.544777
caffeine	58-08-2	-85.7652	12650.82863	10.63351
chrysene	218-01-9	44.52643	4850.79884	-7.59474
cis-2-octene	7642-04-8	-120.25	9547.711399	16.61864
cyclohexanone	3350-30-9	-66.6517	8909.513502	8.4323
decanal	112-31-2	-79.6178	9841.352547	10.157
decane	124-18-5	-73.1037	8101.201623	9.464986
dibenz[a,h]anthracene	53-70-3	163.034	-2756.85165	-23.9252
docosane	629-97-0	-56.9077	11509.60995	6.278272
dodecane	112-40-3	-77.5849	9198.535402	9.915393
eicosane	112-95-8	-124.75	14962.48109	16.01556
fluorene	86-73-7	-75.104	10400.55602	9.450185
heptadecane	629-78-7	-106.612	12775.66369	13.6677
hexacosane	630-01-3	109.5005	1803.89965	-17.2037
hexadecane	544-76-3	-95.3425	11767.5282	12.12541
m-bromoaniline	591-19-5	-65.3431	9035.853849	8.181928
m-cresol	108-39-4	-73.8577	8708.989831	9.506525
m-ethoxyphenol	621-34-1	-85.134	10371.36006	10.89821
methyl decanoate	110-42-9	-88.9339	10841.13032	11.34786

COMPOUND NAME	CAS NUMBER	TERM A	TERM B	TERM C
methyl dodecanoate	111-82-0	-105.969	12578.74201	13.62621
methyl nonanoate	1731-84-6	-81.3121	10034.72732	10.33061
m-ethylaniline	587-02-0	-63.8389	8693.151121	7.953598
m-nitrophenol	554-84-7	-84.8709	10890.25872	10.85169
m-phenylphenol	580-51-8	-92.6763	12062.4703	11.78089
N,N-diethyl-2,4-dimethylaniline	6287-43-0	-81.1932	9633.021436	10.4294
N,N-dimethyl-4-nitrosoaniline	138-89-6	-83.0002	11646.28489	10.44921
N,N-dimethyl-m-nitrosoaniline	1282489-71-7	-80.9695	11134.24296	10.23177
N,N-dipropylaniline	2217-07-4	-83.2622	10627.26689	10.52917
naphthalene	91-20-3	-55.4035	7976.725698	6.853644
N-butylaniline	1126-78-9	-76.7934	10009.21991	9.689102
n-butylbenzene	104-51-8	-57.9583	7669.453129	7.228554
N-ethylaniline	103-69-5	-62.2911	8464.691942	7.753832
N-isopentylaniline	103-69-5	-77.8455	10320.81573	9.789534
nitrobenzene	2051-84-5	-325.439	21470.59855	46.37554
nonadecane	629-92-5	-119.208	14262.96104	15.3053
nonane	111-84-2	-42.802	6194.344517	5.110538
N-propylaniline	622-80-00	-74.0603	9458.109797	9.381107
n-propylbenzene	103-65-1	-67.1041	7694.225372	8.666674
o-bromophenol	95-56-7	-59.8539	7684.818637	7.597705
octacosane	630-02-4	157.4534	-1235.12178	-23.847
octadecane	593-45-3	-106.253	13130.22517	13.53833
octanal	124-13-0	-70.3815	8528.848142	8.997761
o-fluorophenol	367-12-4	-70.9999	7646.34204	9.299567
p-bromoaniline	106-40-1	-68.2126	9224.929987	8.591501
pentachlorophenol	87-86-5	-79.95	11040.66472	10.08795
pentadecane	629-62-9	-92.9562	11235.26294	11.87307
p-ethylaniline	589-16-2	-64.8253	8701.920103	8.106042
phenanthrene	85-01-8	-81.0563	11361.35585	10.21316
phenol	108-95-2	-71.3332	8143.742683	9.229121
p-terphenyl	92-94-4	-39.2121	10074.54893	4.015805
p-*tert*-pentylphenol	80-46-6	-80.3084	10206.14899	10.21463
p-xylene	106-42-3	-61.1932	7080.217002	7.873337
pyrene	129-00-0	-67.9761	11395.09285	8.255295
pyridine	110-86-1	-78.143	7562.6381	10.47963
tetracosane	646-31-1	36.44746	6123.674288	-6.92744
tetradecane	629-59-4	-83.5435	10329.56052	10.59973
trans-5-decene	7433-56-9	-106.069	9713.677123	14.30096
tributylphosphate	126-73-8	-111.524	13945.19169	14.22552
tridecane	629-50-5	-82.0189	9844.061587	10.46722

COMPOUND NAME	CAS NUMBER	TERM A	TERM B	TERM C
trihexylphosphate	2528-39-7	84.96446	3088.827422	-13.6596
triisopropylphosphate	513-02-0	-80.1198	10395.31095	10.0828
trimethylphosphate	512-56-1	-62.5822	8368.520467	7.813933
tripentylphosphate	2528-38-3	1124.976	-61181.4181	-160.569
triphenylphosphate	115-86-6	98.38004	1933.657156	-15.3341
tripropylphosphate	513-08-6	-91.1638	11750.25977	11.53132
undecanal	112-44-7	-83.433	10449.06117	10.62152
undecane	1120-21-4	-72.7368	8525.770694	9.305697
α-bromo-p-tolualdehyde	824-54-4	-77.7471	10335.79041	9.867257

Table A2-4 Thermodynamics-based parameter library data on Rxi-17Sil MS column (RESTEK)

(28.8 m x 0.25 mm; 0.25 µm; (50% phenyl)-methylpolysiloxane-like)

COMPOUND NAME	CAS NUMBER	TERM A	TERM B	TERM C
1,2,3-trichlorobenzene	87-61-6	-54.045	8248.22	6.65628
1,3-diphenoxy-2-propanol	622-04-8	54.1407	4296.32	-9.0026
1,3-diphenyl-1,3-propanedione	120-46-7	49.2673	4437.18	-8.2317
1,3-diphenyl-2-propanone	781-35-1	-54.413	10617.6	6.29436
1,4-dimethylnaphthalene	571-58-4	-60.567	9511.6	7.44092
1,9-nonanediol	3937-56-2	-93.244	12048.6	11.8242
1-bromotetradecane	112-71-0	-90.546	12592.7	11.3163
1-chlorooctane	111-85-3	-65.836	8365.71	8.31494
1-methoxynaphthalene	2216-69-5	-63.117	9890.58	7.74524
1-methylphenanthrene	832-69-9	-22.976	8589.67	1.99038
1-octadecanol	112-92-5	32.9699	5968.17	-6.2747
1-octanol	111-87-5	-72.78	8959.89	9.25021
1-tetradecanol	112-72-1	-91.906	12538.9	11.5002
2,2,4-trimethylhexane	16747-26-5	-110.53	8732.28	15.3438
2,3-dichloroaniline	608-27-5	-65.032	9608.57	8.10288
2,3-dimethylaniline	87-59-2	-67.163	9272.92	8.44121
2,3-dimethylheptane	3074-71-3	-88.442	8135.02	11.9456

COMPOUND NAME	CAS NUMBER	TERM A	TERM B	TERM C
2,3-dimethylnaphthalene	581-40-8	-62.575	9642.25	7.71729
2,3-dimethylphenol	526-75-0	-70.484	9319.1	8.91676
2,4,5-trichlorophenol	88-06-2	-60.387	9149.94	7.47217
2,4,6-tribromoaniline	147-82-0	-66.297	10735.6	8.15257
2,4,6-trichloroaniline	634-93-5	-58.334	9285.98	7.13483
2,4,6-trichlorophenol	88-06-2	-58.141	9104.63	7.11518
2,4,6-trimethylphenol	527-60-6	-67.235	9223.64	8.43345
2,4-dichloroaniline	95-82-9	-61.683	9340.5	7.62389
2,4-dichlorobenzyl alcohol	1777-82-8	-73.615	10333	9.24672
2,4-dimethyl-6-nitroaniline	1635-84-3	-73.599	11228.5	9.10458
2,4-dimethylaniline	95-68-1	-62.903	8915.09	7.83393
2,4-dimethylphenol	105-67-9	-69.614	9172.6	8.79424
2,5-dichloroaniline	95-82-9	-60.887	8853.31	7.59414
2,5-dichlorophenol	583-78-8	-57.074	8281.28	7.10038
2,5-diethoxyaniline	94-85-9	-90.631	12394.5	11.3962
2,6-dichloroaniline	608-31-1	-74.232	11259.7	9.21265
2,6-dichlorophenol	87-65-0	-60.762	8710.77	7.5854
2,6-dimethylnaphthalene	581-42-0	-65.084	9686.8	8.07716
2,6-di-*tert*-butyl-4-methylphenol	128-37-0	-84.003	11377.1	10.5628
2-chloro-4-nitroaniline	121-87-9	-68.3	11234	8.33326
2-decanone	693-54-9	-70.763	9467.43	8.82637
2-ethylaniline	578-54-1	-67.745	9171.49	8.52856
2-ethylphenol	90-00-6	-70.693	9195.76	8.95073
2-heptanone	110-43-0	-82.065	8703.38	10.7596
2-isopropylaniline	643-28-7	-71.778	9662.26	9.0433
2-isopropylphenol	88-69-7	-74.488	9685.32	9.43064
2-methoxy-5-nitroaniline	99-59-2	-44.083	9994.72	4.85184
2-methyl-2-heptanol	625-25-2	-92.795	9292.03	12.3034
2-methyl-3-nitrophenol	5460-31-1	-74.733	10955.3	9.29712
2-methyl-3-nonanol	26533-33-5	-69.759	9117.31	8.74508
2-methyl-5-nitroaniline	99-55-8	-75.574	11400.3	9.39187
2-methyl-5-nonanol	29843-62-7	-74.011	9324.14	9.35449
2-methyl-6-nitroaniline	570-24-1	-73.304	10805.1	9.14619
2-methylanthracene	0613-12-7	-29.009	8950.7	2.82855
2-methylnaphthalene	91-57-6	-57.506	8831.27	7.07937
2-nitrophenol	88-75-5	-59.49	8454.22	7.42578
2-nonanol	628-99-9	-72.393	9058.94	9.15741
2-nonanone	821-55-6	-74.68	9242.31	9.48227

COMPOUND NAME	CAS NUMBER	TERM A	TERM B	TERM C
2-octanol	123-96-6	-73.647	8662.49	9.44037
2-octanone	111-13-7	-69.955	8554.47	8.88799
2-propylaniline	1821-39-2	-66.843	9431.7	8.3379
2-*tert*-butylphenol	88-18-6	-75.037	9921.14	9.48343
2-tridecanone	593-08-08	-87.719	11655.4	11.0178
3,4,5-trichlorophenol	609-19-8	-77.086	11220.8	9.64518
3,4-dichloraniline	95-76-1	-63.78	9506.75	7.91106
3,4-dimethylaniline	95-64-7	-66.856	9259.86	8.38559
3,4-dimethylphenol	95-65-8	-72.966	9554.41	9.24795
3,5,5-trimethyhexanal	5435-64-3	-77.399	8637.53	10.0729
3,5-dimethoxyphenol	500-99-2	-84.635	11714.9	10.6206
3,5-dimethylaniline	108-69-0	-64.696	9074.32	8.0763
3,5-dimethylphenol	108-68-9	-73.127	9467.65	9.27715
3-bromophenol	591-20-8	-68.611	9573.3	8.61512
3-chlorophenol	108-43-0	-71.091	9367.05	9.01037
3-decyne-1-ol	51721-39-2	-75.095	10101.7	9.40173
3-dodecanone	1534-27-6	-78.576	10680.7	9.79869
3-ethyl-5-methylphenol	698-71-5	-77.395	10116	9.80373
3-nonanol	624-51-1	-75.986	9187.79	9.69934
3-octanone	106-68-3	-74.8	8759.01	9.60467
3-*tert*-butylphenol	585-34-2	-75.443	10117.1	9.5034
4-bromo-2-chloroaniline	38762-41-3	-66.796	9980.98	8.31249
4-bromo-2-chlorophenol	3964-56-5	-56.381	8595.15	6.95674
4-bromo-2-methylaniline	583-75-5	-68.381	10068.5	8.52197
4-chloro-2,6-dinitoaniline	5388-62-5	-34.752	9520.47	3.50252
4-chloro-2-nitroaniline	89-63-4	-72.588	10453.7	9.10094
4-chloro-3-nitroaniline	635-22-3	-62.96	10968	7.56372
4-chloroaniline	106-47-8	-68.266	9372.18	8.60489
4-chlorophenol	106-48-9	-71.398	9435.01	9.0453
4-ethylphenol	123-07-9	-73.449	9478.98	9.32397
4-isopropylaniline	99-88-7	-69.461	9548.46	8.71551
4-methoxy-2-nitroanline	96-96-8	-80.173	11942.6	9.96984
4-methyl-4-nonanol	23418-38-4	-74.871	9214.52	9.51656
4-nitroaniline	100-01-6	-77.046	11586	9.59296
4-nitrophenol	100-02-7	-82.53	11529.6	10.3996
4-nonanol	5932-79-6	-68.966	8792.11	8.68293
4-propylaniline	2696-84-6	-78.338	10173.3	9.96696
4-*sec*-butylphenol	99-71-8	-78.411	10323	9.92774

COMPOUND NAME	CAS NUMBER	TERM A	TERM B	TERM C
4-*tert*-butylphenol	98-54-4	-78.531	10266.7	9.95557
5H-dibenzo[a,d]cyclohepten-5-one	222-33-5	43.9706	4554.24	-7.3677
5-nonanol	623-93-8	-78.067	9275.88	10.0008
7,12-dimethylbenz[a]anthracene	57-97-6	152.621	-2633.2	-22.22
acenaphthylene	208-96-58	-63.427	9719.18	7.87032
aniline	62-53-3	-63.544	8209.14	8.06607
anthracene	120-12-7	-63.131	10797.5	7.67454
benzo[a]pyrene	50-32-8	146.99	-2372.5	-21.36
benzyl alcohol	100-51-6	-62.525	8375.48	7.86413
biphenyl	92-52-4	-67.383	9852.05	8.38856
caffeine	58-08-2	10.5232	6826.14	-2.8412
chrysene	218-01-9	108.343	353.882	-16.191
cis-2-octene	7642-04-8	-77.117	7524.05	10.2904
cyclohexanone	3350-30-9	-66.482	9127.71	8.38077
decanal	112-31-2	-70.964	9502.86	8.85709
decane	124-18-5	-63.686	7736.62	8.08236
docosane	629-97-0	46.1268	5271.06	-8.1758
dodecane	112-40-3	-64.994	8721.99	8.07068
eicosane	112-95-8	-49.338	10804.6	5.30402
fluorene	86-73-7	-68.257	10479.1	8.46913
heptadecane	629-78-7	-87.203	12035.8	10.8498
hexacosane	630-01-3	165.176	-2089	-24.747
hexadecane	544-76-3	-78.681	11148.6	9.70663
m-bromoaniline	591-19-5	-63.004	9395.06	7.81611
m-cresol	108-39-4	-71.461	8972.54	9.11734
m-ethoxyphenol	621-34-1	-85.455	10936.3	10.8731
methyl decanoate	110-42-9	-79.568	10497.5	9.97495
methyl dodecanoate	111-82-0	-93.207	12096.1	11.766
methyl nonanoate	1731-84-6	-76.804	9923.61	9.66141
m-ethylaniline	587-02-0	-67.91	9259.55	8.53398
m-nitrophenol	554-84-7	-76.278	10895.9	9.55271
m-phenylphenol	580-51-8	-74.666	11678.2	9.17994
N,N-diethyl-2,4-dimethylaniline	6287-43-0	-69.968	9466.26	8.77621
N,N-dimethyl-4-nitrosoaniline	138-89-6	-81.318	11852.8	10.1629
N,N-dimethyl-m-nitrosoaniline	1282489-71-7	-77.188	11249.6	9.64216
N,N-dipropylaniline	2217-07-4	-77.002	10572.1	9.63001
naphthalene	91-20-3	-57.558	8414.07	7.16959
N-butylaniline	1126-78-9	-72.878	10132	9.10832

COMPOUND NAME	CAS NUMBER	TERM A	TERM B	TERM C
n-butylbenzene	104-51-8	-59.231	7972.21	7.41496
N-ethylaniline	103-69-5	-66.087	8966.89	8.29163
N-isopentylaniline	103-69-5	-76.806	10577.1	9.62467
nitrobenzene	2051-84-5	-54.292	8048.95	6.70025
nonadecane	629-92-5	-88.971	12909.4	10.9575
nonane	111-84-2	-83.567	8209.83	11.1252
N-propylaniline	622-80-0	-69.957	9562.73	8.76973
n-propylbenzene	103-65-1	-58.197	7467.44	7.36202
o-bromophenol	95-56-7	-53.628	7723.77	6.67976
octacosane	630-02-4	201.451	-4474.7	-29.716
octadecane	593-45-3	-91.75	12698.9	11.4211
octanal	124-13-0	-67.78	8465.62	8.57358
o-fluorophenol	367-12-4	-76.786	8130.96	10.1392
p-bromoaniline	106-40-1	-64.49	9499.01	8.02468
pentachlorophenol	87-86-5	-74.081	11373.3	9.20056
pentadecane	629-62-9	-76.412	10611.4	9.46304
p-ethylaniline	589-16-2	-66.051	9117.97	8.27526
phenanthrene	85-01-8	-63.593	10795.7	7.74578
phenol	108-95-2	-67.565	8350.48	8.63218
p-terphenyl	92-94-4	77.6997	2650.55	-12.168
p-*tert*-pentylphenol	80-46-6	-77.316	10543.3	9.73405
p-xylene	106-42-3	-66.188	7471.61	8.62432
pyrene	129-00-0	31.5105	5197.19	-5.5606
pyridine	110-86-1	-73.323	7474.37	9.75332
tetradecane	629-59-4	-77.144	10237.8	9.64991
tetracosane	646-31-1	115.592	1049.82	-17.886
trans-5-decene	7433-56-9	-61.052	7664.21	7.68872
tributylphosphate	126-73-8	-96.947	13228.8	12.1154
tridecane	629-50-5	-65.343	9173.31	8.03264
trihexylphosphate	2528-39-7	117.804	902.052	-18.186
triisopropylphosphate	513-02-0	-81.929	10408.2	10.3319
trimethylphosphate	512-56-1	-72.463	8860.1	9.22238
trioctylphosphate	1806-54-8	177.439	-2798.9	-26.483
tripentylphosphate	2528-38-3	16.7073	7011.84	-4.0363
triphenylphosphate	115-86-6	146.731	-1623	-21.774
tripropylphosphate	513-08-6	-94.991	12057.9	12.0402
tris-2-ethylhexylphosphate	78-42-2	176.712	-2764.5	-26.377
undecanal	112-44-7	-77.511	10283.7	9.7162

COMPOUND NAME	CAS NUMBER	TERM A	TERM B	TERM C
undecane	1120-21-4	-62.667	8153.48	7.82785
α-bromo-p-tolualdehyde	824-54-4	-71.941	10510.1	8.96883

Table A3-1 Thermodynamic Parameters of the Calibration Mix separated on the 25.3 m reference column, optimized inner diameter =

0.210$_5$ mm

Terms	Thermodynamic Parameters					
	decane	1-octanol	undecane	2,6-dimethylaniline	methyl decanoate	methyl laurate
A (mol)	281.3058	233.3362	234.6506	165.9069	188.9939	173.5277
B (mol K)	-8755.5992	-6305.8873	-6436.7803	-3198.6904	-3977.4551	-3033.03
C (mol)	-42.6836	-35.5893	-35.7106	-25.4716	-28.8409	-26.4505

Table A3-2 Thermodynamic Parameters of Therm. Sample Mix separated on 25.3 m reference column, optimized inner diameter =

0.210$_5$ mm

Terms	Thermodynamic Parameters					
	2-heptanone	trans-5-decene	2-nonanol	methyl nonanoate	undecanal	n-pentadecane
A (mol)	387.1808	283.3943	223.9268	199.7856	178.9601	176.7571
B (mol K)	-13812.5882	-8860.8554	-5845.6965	-4573.6015	-3517.8651	-3233.6979
C (mol)	-58.4646	-42.9966	-34.1673	-30.5088	-27.3743	-26.9303

Table A3-3 Experimental and predicted peak widths of the Thermo. Sample Mix on the target column under the conditions in Table 3-1. Predicted widths are in parentheses (*Italicized widths* were predicted using $\Phi = 1$, $\sigma_{extra}^2 = 0$ s^2, and ***Bold italicized widths*** were predicted using $\Phi = 0.78_7$, $\sigma_{extra}^2 = 0.017_7$ s^2)

Condition Label	Half height widths (s)					
	2-heptanone	trans-5-decene	2-nonanol	methyl nonanoate	undecanal	n-pentadecane
A	1.13 (*0.98*, ***1.15***)	1.14 (*1.03*, ***1.20***)	1.18 (*1.10*, ***1.27***)	1.23 (*1.12*, ***1.30***)	1.25 (*1.14*, ***1.33***)	1.26 (*1.13*, ***1.31***)
B	0.82 (*0.70*, ***0.85***)	0.94 (*0.85*, ***1.01***)	1.04 (*0.92*, ***1.08***)	1.10 (*0.97*, ***1.14***)	1.16 (*1.01*, ***1.18***)	1.25 (*1.05*, ***1.23***)
C	1.00 (*0.79*, ***0.95***)	1.20 (*1.04*, ***1.21***)	1.38 (*1.18*, ***1.37***)	1.49 (*1.28*, ***1.48***)	1.53 (*1.33*, ***1.54***)	1.67 (*1.41*, ***1.62***)
D	1.05 (*0.89*, ***1.05***)	1.04 (*0.90*, ***1.06***)	1.07 (*0.94*, ***1.11***)	1.05 (*0.95*, ***1.12***)	1.02 (*0.97*, ***1.13***)	1.01 (*0.95*, ***1.11***)

Table A3-4 Errors in predicted peak widths of Thermo. Sample Mix on the target column under the conditions in Table 3-1, $\Phi = 1$, $\sigma_{extra}^2 = 0$ s^2

Condition Label	Prediction errors (s)					
	2-heptanone	trans-5-decene	2-nonanol	methyl nonanoate	undecanal	n-pentadecane
A	*-0.15*	*-0.11*	*-0.09*	*-0.11*	*-0.11*	*-0.12*
B	*-0.12*	*-0.09*	*-0.12*	*-0.13*	*-0.15*	*-0.20*
C	*-0.20*	*-0.16*	*-0.20*	*-0.20*	*-0.20*	*-0.26*
D	*-0.16*	*-0.14*	*-0.12*	*-0.10*	*-0.05*	*-0.06*

Table A3-5 Experimental variance of components of the calibration mixture separated on the target column. This data was collected on the same day the PAHs were separated on the target column

| Oven ramp rates (°C min^{-1}) | $\sigma_{experimental}^2$ (s^2) | | | | | |
	decane	1-octanol	undecane	2,6-dimethylaniline	methyl decanoate	methyl laurate
5	0.406	0.472	0.529	0.595	0.738	0.832
8	0.250	0.255	0.289	0.309	0.328	0.383
10	0.188	0.205	0.210	0.221	0.233	0.276
16	0.099	0.106	0.106	0.112	0.116	0.141
20	0.083	0.086	0.085	0.091	0.093	0.099

Table A3-6 Calculated on-column variance of components of the calibration mixture separated on the target column.

| Oven ramp rates (°C min^{-1}) | σ_c^2 (s^2) | | | | | |
	decane	1-octanol	undecane	2,6-dimethylaniline	methyl decanoate	methyl laurate
5	0.287	0.368	0.421	0.478	0.564	0.629
8	0.158	0.186	0.206	0.231	0.252	0.276
10	0.118	0.135	0.147	0.164	0.174	0.189
16	0.064	0.070	0.074	0.083	0.083	0.089
20	0.048	0.052	0.055	0.062	0.061	0.064

Table A3-7 Experimentally determined retention times of the Thermo Sample Mix on the target column under the conditions in Table 3-1.

Condition Label	Experimental retention time, t_{Re} (s)					
	2-heptanone	trans-5-decene	2-nonanol	methyl nonanoate	undecanal	n-pentadecane
A	228.90	303.26	389.65	490.63	555.96	696.42
B	133.43	187.97	261.42	355.63	418.42	557.98
C	178.70	266.06	379.24	517.76	607.46	807.25
D	225.96	288.93	358.53	437.79	488.91	597.38

Table A3-8 Predicted retention times of Thermo Sample Mix on the target column under the conditions in Table 3-1

Condition Label	Predicted retention times, t_{Rp} (s)					
	2-heptanone	trans-5-decene	2-nonanol	methyl nonanoate	undecanal	n-pentadecane
A	226.84	303.15	389.46	490.84	556.40	697.52
B	132.60	189.47	263.35	357.85	420.59	560.23
C	177.76	267.31	379.84	518.36	608.03	808.19
D	223.65	288.18	357.73	437.43	488.79	597.87

Table A3-9 Errors in predicted retention times of Thermo. Sample Mix on the target column under the conditions in Table 3-1

Condition Label	Retention time prediction errors (s)					
	2-heptanone	trans-5-decene	2-nonanol	methyl nonanoate	undecanal	n-pentadecane
A	-2.06	-0.12	-0.19	0.21	0.43	1.10
B	-0.84	1.50	1.92	2.22	2.17	2.25
C	-0.93	1.25	0.60	0.61	0.58	0.94
D	-2.31	-0.76	-0.80	-0.36	-0.12	0.49

Table A3-10 Experimentally determined retention times of the Thermo Sample Mix on the target column under the same conditions as the PAHs

Oven ramp rate (°C min⁻¹)	Experimental retention time, t_{Re} (s)					
	2-heptanone	trans-5-decene	2-nonanol	methyl nonanoate	undecanal	n-pentadecane
5	193.42	302.18	451.45	639.59	762.15	1039.56
8	172.55	252.11	353.10	475.56	554.73	730.11
10	162.25	229.81	312.94	412.41	476.66	617.63
16	140.74	187.28	241.68	305.43	346.71	435.53
20	131.00	169.52	213.73	265.20	298.61	369.88

Table A3-11 Predicted retention times of Thermo Sample Mix on the target column under the same conditions as the PAHs

Oven ramp rate (°C min⁻¹)	Predicted retention times, t_{Rp} (s)					
	2-heptanone	trans-5-decene	2-nonanol	methyl nonanoate	undecanal	n-pentadecane
5	191.97	302.71	450.18	637.49	759.70	1037.02
8	171.80	253.52	354.13	476.73	555.96	731.71
10	161.60	231.14	314.15	413.88	478.23	619.57
16	139.96	187.97	242.43	306.46	347.84	436.92
20	130.08	169.86	214.16	265.86	299.37	370.82

Table A3-12 Errors in predicted retention times of Thermo. Sample Mix on the target column under the same conditions as the PAHs

Oven ramp rate (°C min^{-1})	Retention time rediction errors (s)					
	2-heptanone	trans-5-decene	2-nonanol	methyl nonanoate	undecanal	n-pentadecane
5	-1.45	0.53	-1.27	-2.10	-2.46	-2.54
8	-0.75	1.40	1.03	1.18	1.22	1.60
10	-0.65	1.33	1.22	1.48	1.57	1.94
16	-0.79	0.69	0.75	1.02	1.14	1.38
20	-0.92	0.34	0.43	0.67	0.76	0.94

Table A3-13 Experimentally determined retention times of PAHs on the target column

Oven ramp rate (°C min⁻¹)	Experimental retention time, t_{Re} (s)						
	Naphthalene	Acenaphthylene	Acenaphthene	Fluorene	Fluoranthene	Pyrene	Benzo[a]pyrene
5	561.05	946.32	996.46	1128.33	1683.47	1735.32	2400.75
8	429.86	678.39	710.07	793.84	1147.56	1181.26	1603.73
10	377.46	578.95	604.42	671.91	957.58	985.03	1325.61
16	286.14	415.23	431.29	474.08	656.12	673.98	890.25
20	250.87	355.19	368.06	402.54	549.51	564.09	738.50

Table A3-14 Predicted retention times of PAHs on the target column

Oven ramp rate (°C min⁻¹)	Predicted retention time, t_{Rp} (s)						
	Naphthalene	Acenaphthylene	Acenaphthene	Fluorene	Fluoranthene	Pyrene	Benzo[a]pyrene
5	560.73	945.22	995.55	1127.12	1681.50	1732.53	2390.20
8	431.04	679.99	711.83	795.56	1148.98	1182.41	1602.37
10	378.52	580.55	606.14	673.65	959.08	986.42	1325.48
16	286.13	415.78	431.91	474.75	656.74	674.60	890.11
20	250.28	355.14	368.08	402.58	549.54	564.12	737.69

Table A3-15 Prediction errors in retention times of PAHs on the target column

Oven ramp rate (°C min⁻¹)	Prediction error, $(t_{Rp} - t_{Re})$ (s)						
	Naphthalene	Acenaphthylene	Acenaphthene	Fluorene	Fluoranthene	Pyrene	Benzo[a]pyrene
5	-0.32	-1.10	-0.91	-1.21	-1.96	-2.79	-10.55
8	1.18	1.60	1.77	1.72	1.42	1.15	-1.35
10	1.06	1.60	1.72	1.75	1.51	1.39	-0.13
16	-0.01	0.55	0.62	0.67	0.62	0.62	-0.14
20	-0.58	-0.05	0.02	0.04	0.03	0.02	-0.81

…Till the morning we dream so long

Anybody ever wonder

When they would see the sun up

Just remember when you come up

The show goes on!

-Lupe Fiasco. "The Show Goes On." Lasers. By Jaco, Isaac Brock, N. Naanai, Jonathon Brown, Dann Gallucci, Daniel Johnson, Eric Judy. Produced by Kane Beatz. 2010